Supported Metal Oxides on Monoliths for Paraffin Oxidation

by

Sandeeran Govender

BSc. Applied Chemistry, University of KwaZulu-Natal

BSc. Honours Chemistry, University of KwaZulu-Natal

Submitted in fulfilment of the academic requirements for the degree of **BSc Masters Chemistry**

In the School of Chemistry and Physics, University of KwaZulu-Natal, Westville, South Africa

February 2015

Note: This thesis has been prepared according to Format 3 (MR9c) as outlined in the guidelines from the College of Agriculture, Engineering and Science, which states:

"A dissertation may comprise of one or more papers of which the student is the prime author, published or in press peer-reviewed journals approved by the relevant college academic affairs board or in manuscripts written in paper format, accompanied by introductory and concluding integrative material."

As the candidate's supervisor, I have approved this dissertation for submission.

Name: Prof. Holger B. Friedrich Signed: _____ Date: _____

Preface

The experimental work described in this thesis was carried out in the School of Chemistry, University of KwaZulu-Natal, Westville Campus, from February 2013 to December 2014, under the supervision of Prof. Holger B. Friedrich.

These studies represent original work by the author and have not otherwise been submitted in any form, for any degree or diploma to another tertiary institution. Where use has been made of the work of others, it is duly acknowledged in the text.

Declaration 1

Plagiarism

I, Sandeeran Govender, declare that

1. The research reported in this thesis, except where otherwise indicated, is my original research.
2. This thesis has not been submitted for any degree or examination at another university.
3. This thesis does not contain other persons' data, pictures, graphs or other information, unless specifically acknowledged as being sourced from other persons'.
4. This thesis does not contain other persons' writing, unless specifically acknowledged as being sourced from other researchers. Where other written sources have been quoted, then:
a. Their words have been re-written but the general information attributed to them has been referenced
b. Where their exact words have been used, then their writing has been placed in italics and inside quotation marks, and referenced.
5. This thesis does not contain text, graphics or tables copied and pasted from the Internet, unless specifically acknowledged, and the source being detailed in the thesis and in the references sections.

Declaration 2

Conference contributions and publications

Conference contributions

2013

Catalysis Society of South Africa conference, held at the Wild Coast Sun, South Africa

Poster presentation: A New Synthesis and Approach to Supporting Iron Molybdate

2014

97th Canadian Chemistry Conference and Exhibition, held at the Vancouver Convention Centre, Vancouver, British Columbia

Oral presentation: The Effect of Supporting Iron Molybdate on Monoliths in the Oxidation of *n*-Octane

Publications

1.

Title: Monoliths: A review of the basics, preparation methods and applications
Authors: Sandeeran Govender, Holger B. Friedrich
Status: Manuscript drafted for submission to Catalysis Today
Contribution: I carried out all literature research and manuscript preparation was under supervision of Prof. Holger B. Friedrich

2.

Title: Homogeneous gas phase reactions in the oxidation of *n*-octane in a monolith reactor system
Authors: Sandeeran Govender, Holger B. Friedrich
Status: Manuscript in preparation
Contribution: I carried out all experimental work and manuscript preparation was under supervision of Prof. Holger B. Friedrich

Acknowledgements

I would like to firstly thank the University of KwaZulu-Natal, my supervisor Prof. Holger B. Friedrich and my parents for this opportunity to pursue my Masters degree. Also, I would like to acknowledge the financial support from the NRF, SASOL and THRIP. I am grateful for being allowed this opportunity to grow as a person, student and future scientist.

I would also like to extend my appreciation to the staff at the University of KwaZulu-Natal. Particularly, I would like to acknowledge and sincerely thank Mr Danasegran Padayachee who helped in the preparation of the heating block for my reactor and Mr Enock Checkure for assisting with the wiring of the reactor setup. Also, Mr Vishal Bharuth who spent numerous hours assisting me at the electron microscopy unit with SEM images taken for this project. As a result, I have gained significant insight and experience in electron microscopy imaging and reactor building.

I wish to also extend my gratitude to the members of the Catalysis Research Group. I have learnt a considerable amount since joining this group from Honours level. To Mohamed Fadlalla and Ajij Golandaj, I would like to thank you both for the guidance, support as mentors and for the assistance provided at any point at which I needed it, during my research project. To Venkata Dasireddy, thank you for the assistance and help throughout this project. To Narainamah Gounden and Majid Faharani, thank you for the fruitful discussions, sound opinions and advice when needed. Also, thank you Shivania for the discussions, support, opinions and ever willing to assist with proof reading. To Prof. Holger B. Friedrich, I sincerely thank you for allowing me to conduct my research in this group. I will carry the experience and knowledge I have gained into my future endeavours, as I intend to continue learning and growing as an individual.

Lastly, to my mum, dad, grandmothers, my uncle and my friends, I appreciate all that you have done for me and for the support you have provided to me all these years. To Merushka Lalla, a special thank you for love, encouragement and support you have provided me with during my research. Finally, to person I cannot thank in person, but I will always be forever grateful to, my grandfather. If I could be half the person you were, then I have accomplished a lot in this journey of life.

Thesis overview

This thesis is written as a series of four chapters.

Foremost an overall abstract is provided for this dissertation.

- Chapter 1 provides an overall introduction to the heterogeneous oxidation of alkanes, outlining the fundamental principles and reasoning for alkane oxidation. Also, the influence of molybdates and molybdenum trioxide in selective oxidation is discussed. Concluding, a brief motivation for the use of monoliths is provided, as well as an outline for Chapter 2 and Chapter 3.

- Chapter 2 contains the first paper, which is a review of monoliths, from the basics to preparation methods and finally focusing on applications in the oxidation of alkanes. A perspective leading into Chapter 3 is also provided.

- Chapter 3 contains the second paper, which discusses the contribution of homogeneous gas phase reactions in the oxidation of *n*-octane. This chapter consists of the main experimental and research work for this thesis.

- Chapter 4 provides an overall summary and conclusion for the research work conducted for this thesis.

Appendices 1, 2 and 3 follow Chapter 4.

Abstract

Over the years, monolithic catalysts have proven useful since their initial incorporation in environmental catalytic applications. Apart from the success of the use of monoliths in exhaust gas treatment and the automobile catalytic converter, research has also expanded into the use of these catalysts in the oxidation of alkanes.

The use of monolithic catalysts is therefore an attempt at improving the yield of value-added products. As an example, synthesis gas can be produced in high selectivity, using platinum group metals coated on monoliths, in the oxidation of alkanes. The conversion of alkanes into alkenes and oxygenates in high selectivities over monoliths, however, is suggested to occur via homogeneous gas phase reactions. Although catalysis results employing monoliths in the oxidation of alkanes may at first glance appear promising, they need to be better understood, especially the contribution of homogeneous gas phase reactions to the overall process. The aim of this study therefore involves preliminary testing of monoliths in the oxidation of *n*-octane. Bare cordierite and coated monoliths were tested in this respect, in an attempt to better understand the role of monoliths in the oxidation of *n*-octane, under continuous flow fixed-bed reactor conditions. Experimental reaction conditions were kept constant, maintaining a GHSV of 1000 h^{-1} (71.7 ml/min air, 45 ml/min nitrogen, 0.10 ml/min C_8H_{18}), isothermally at 400 °C and a C:O ratio of 8:2, with a reactant to total feed ratio of 11.43 %. Characterization techniques included XRD, ICP-OES, BET, TEM, FTIR, Raman spectroscopy and SEM.

The oxidation of *n*-octane over the bare cordierite monolith produced cracked products, octenes, octadienes, C_8 oxygenates and carbon oxides. In particular, a high selectivity to cyclic ethers was observed. Coating the bare monolith with an iron-molybdenum active layer retarded the suggested free radical mechanism, however, not as effectively as coating the monolith with gamma-alumina. A drastic change in the mechanism was observed when the iron-molybdenum active layer was supported over the gamma-alumina coated monolith. Carbon oxides dominated the product profile, whilst octadienes and C_8 oxygenates were suppressed, over the iron-molybdenum supported on gamma-alumina coated monolith.

List of Abbreviations and Symbols

GHSV	Gas hourly space velocity
C:O	Carbon to oxygen
XRD	X-ray diffraction
ICP-OES	Inductively coupled plasma-optical emission spectroscopy
BET	Brunauer-Emmet-Teller
TEM	Transmission electron microscopy
FTIR	Fourier transform infrared
SEM	Scanning electron microscopy
C-H	Carbon-hydrogen
TPR	Temperature programmed reduction
TPD	Temperature programmed desorption
XPS	X-ray photoelectron spectroscopy
XAS	X-ray absorption spectroscopy
nm	Nanometre
µm	Micrometre
NO_x	Nitrogen oxides
EPR	Electron paramagnetic resonance

List of Figures

Page

Chapter 2

Chapter 3

List of Schemes

List of Tables

Page

Chapter 3

Table of Contents

Chapter 1

Principles and applications in the heterogeneous oxidation of alkanes: Comprehending the mechanisms involved and the role of molybdates

Overview

Heterogeneous catalysis is a prominent and the industrially dominant form of applied catalysis. Various reactions are performed heterogeneously, with a significant contribution from oxidation catalysis. Industrially, there is a growing interest in selective heterogeneous oxidation. Research has been focused on selective oxidation chemistry due to continually changing environmental legislations as well as economic imperatives. Significant research has therefore been directed at converting alkanes to value-added functionalized products. Molybdates and molybdenum trioxide have played an important role in the selective oxidation of alkanes. In order to completely understand the role of molybdates, an overview of the fundamental principles is required. The background of heterogeneous oxidation catalysis will be introduced, differentiating between dehydrogenation and oxidative dehydrogenation processes. Activation of the hydrocarbon and the oxygen species formed will be discussed. Special attention will also be given to the influence of molybdates and molybdenum trioxide in selective alkane oxidation. In this manuscript relevant applications will be reviewed, whilst emphasis will be placed on the oxidation of alkanes. Silica and alumina supported molybdenum catalysts will also be discussed. Lastly a conclusion and perspective as an entirety is provided.

1.1 Introduction

Catalysis is a branch of chemistry whereby a catalyst is used to increase the rate of a chemical reaction to reach equilibrium. The majority of applications in catalysis are found in the petrochemical, fine chemical and environmental sectors of industries, with approximately 80 % of industries using catalytic processes [1, 2]. This lucrative branch of chemistry is therefore extremely influential in science and to a greater extent, petrochemical science. Catalysis has played an important role in the refining and petrochemical industries in the past, and is predicted to contribute even more significantly into the twenty-first century [3]. Industrially, heterogenized catalysts are favoured over homogeneous and enzymatic catalysts.

Heterogeneous catalysis, in simple terms, is usually described as the form of catalysis when the catalyst is in a different phase to the reactants, for example, a solid catalyst and gaseous or liquid reactant. Some of the most successful industrial processes, such as the contact process, catalytic cracking and catalytic converters involve the use of heterogeneous catalysts. The industrial revolution and growth of technology brought about the demand for petrochemical products, which reinforced the use of heterogeneous catalysts. These catalysts have thus become crucial in the production of fine and bulk chemicals, especially with respect to minimization of waste as compared to non-catalytic processes [4, 5]. Economically and environmentally, heterogeneous catalysis is a far more viable form of industrial chemistry as opposed to homogeneous catalysis, in the twenty-first century [6]. Heterogeneous catalysis has also been highlighted as an important technology for society [7].

Oxidation catalysis was one of the first applications of heterogeneous catalysis, discovered when Faraday experimented with using platinum in oxidation reactions [8]. The initial successes lead to further developments, such as the oxidation of hydrocarbons using noble metals and the realization of the importance of metal oxides in heterogeneous oxidation [9]. A further emphasis of the importance of these catalysts is the value of oxidation catalysts in 1993, which was estimated to be $ 200 – 250 million [10]. Also, selective oxidation significantly contributes to the production of bulk and fine chemicals [11], with approximately 50 % of bulk chemicals produced from hydrocarbons [12] and 25 % of important organic chemicals [13]. Efforts into selective heterogeneous oxidation have, over the years, been reflected in the quantity and quality of research in this area. Oxidation catalysts represent approximately 41 % of the catalysts used and sold in industry [14]. The motivation for further research is due to possible improvements in processes, the increasing demand for olefins and oxygenated products, enhancing the economic value of industrial processes and reducing environmental impact on society [11, 15].

Alkanes are commonly found in fossil fuel feedstocks, such as natural gas and crude oil [16, 17] or produced in chemical processes such as the Fischer-Tropsch process [18, 19] and catalytic cracking [20]. In 2003, the reported global energy production from fossil fuels was 88 % [21]. Petroleum and fine chemical products are in high demand, increasing annually, and the quantity of alkanes produced has increased proportionally. These saturated hydrocarbons are relatively stable and are thought to be inefficiently used by industry [22], as they are most often combusted at high temperatures for the generation of energy [23]. A

more lucrative approach, however, may be to convert alkanes to olefins, aromatics or oxygenates via oxidation reactions [24]. There is a need for the conversion of alkanes to more valuable products, such as olefins and oxygenates, in order to lower the carbon footprint and promote industrial growth [25, 26]. The problem associated with heterogeneous oxidation catalysis is the lack of control over selectivity [27], which has created an opportunity and motivation for further research.

This chapter, therefore, discusses the theoretical aspects of heterogeneous catalysis as a foundation for application in selective oxidation reactions. The focus is on the theory and understanding of the chemistry involved in oxidation catalysis, in particular that associated with the selective oxidation of alkanes. An attempt has been made to highlight the significance of molybdates and molybdenum trioxide in the heterogeneous oxidation of alkanes. Supported molybdenum oxidation catalysts will also be discussed briefly.

1.2 The theoretical aspects and chemistry of heterogeneous oxidation of alkanes

In most heterogeneous catalysis applications, particularly the oxidation of alkanes, a solid catalyst is used and the surface reactions are commonly gas-solid or liquid-solid interactions. The interaction whereby the substrate attaches to the surface, adsorption, and when the substrate detaches, desorption, are both key factors when designing heterogeneous catalysts. Physisorption and chemisorption onto the catalytic surface also play important roles in the catalytic process. The attractive and repulsive forces of physisorption are usually weak, with the formation of a physical bond due to van der Waals or intermolecular forces. This results in a decrease in adsorption with an increase in temperature and an increase in adsorption as pressure increases. Physisorption is therefore not significantly influential in oxidation catalysis, since typical reaction conditions involve atmospheric pressure and high temperatures. The formation of a chemical bond on the surface of the catalyst is termed chemisorption. In order to relate the catalysis to the surface chemistry, chemisorption studies may prove valuable. Activation energy barriers are thus conceptually important when designing heterogeneous catalysts, due to bond formation and bond breaking. The forces of adsorption and desorption are therefore also critically important in catalysis, since the ideal catalyst allows for a molecule to adsorb, react and hence form the desired product and desorb with ease to prevent side reactions. The effect on the catalyst surface, when unable to desorb molecules, is a subsequent agglomeration of adsorbed molecules on the surface. The

agglomeration results in poisoning of the catalyst, which in the case of an oxidation catalyst, is typically coking from carbonaceous products.

The surface characteristics and nature of the materials used play distinct roles in heterogeneous catalysis. Properties such as defects, pores, surface area, morphology and the type of transition metal used, as well as catalyst preparation method, will impact the catalysis. In heterogeneous catalysis, transition metals are seen as being superior to other metals. Transition metals offer amongst others, favourable properties, such as various oxidation states and the ability to form metal oxide species which can be used in a numerous reactions [28], for example, oxidation reactions [29-31]. The advantages of having s, p and d orbitals allow for transition metals to lose or gain electrons easily, which can result in good reducing or oxidizing properties [28, 32]. The various oxidation states, in particular of transition metal oxides, relate to different electronic and structural properties [33]. These properties may be used manipulate the type of chemical reaction that can be performed. Transition metal oxides are generally favoured in oxidation catalysis, particularly the oxidation of alkanes. Transition metal oxides can play functional roles in oxidation, reduction and dehydrogenation [34], which can be advantageous in studying the oxidation of alkanes.

1.2.1. Differentiating between dehydrogenation and oxidative dehydrogenation

Alkanes are known to be relatively unreactive due their electronic structure and strong C-H bonds [35, 36]. The C-H bond decreases in strength from a primary carbon to a secondary carbon [35]. Longer chain linear alkanes are more reactive than shorter chain alkanes. A longer chain corresponds to an increase in the number of secondary carbon sites available, which results in an increase in the number of C-H bonds of weaker strength. Considering the need for the conversion of these unreactive alkanes to valuable products, such as olefins and oxygenates, productive research typically revolves around dehydrogenation and oxidative dehydrogenation, in heterogeneous catalytic applications.

Oxidative dehydrogenation is an attempt at overcoming the limitations of dehydrogenation. Where dehydrogenation reactions proceed without the presence of an oxidant, they require substantially higher temperatures due to the reaction being endothermic. Higher temperatures may result in an increase in the formation of cracked products, from thermal cracking. Lower pressures could also drive the reaction forward [37]. Reactor design is thus more capital intensive when attempting to achieve high conversion. Another limitation of the

dehydrogenation of alkanes is the formation of coke from the products of cracking and the reversibility of the reaction. Despite the limitations, patents [38, 39] and published literature [40-42] do exist and dehydrogenation reactions are used industrially. Oxidative dehydrogenation of alkanes is thus superior in terms of the limitations of dehydrogenation reactions. Introducing an oxidant, such as molecular oxygen, results in an exothermic reaction, driving the reaction forward. The reaction becomes exothermic by introducing an electronegative species [43], which in this case is oxygen. This ideally forms olefins or olefins and water from the oxidative dehydrogenation of alkanes.

The oxidative dehydrogenation reaction, however, does not proceed ideally and a range of products, such as olefins, oxygenates, aromatics and carbon oxides can be expected, depending on the catalyst used as well as the reaction conditions employed. Products formed from oxidative dehydrogenation can be more reactive than the original alkane introduced into the system [44]. These products can thus react further with the oxidant and/or catalyst, producing undesired products. The selectivity of oxidative dehydrogenation, as compared to dehydrogenation, is therefore questionable. This, however, has provided for an opportunity to conduct innovative research. In particular, our research group has made contributions to the oxidative dehydrogenation of *n*-butane [29], *n*-hexane [30, 45] and *n*-octane [31, 46-48], respectively.

Research in oxidative dehydrogenation on the laboratory scale is typically done in a continuous flow fixed-bed reactor [44], as it is a cheaper design compared to other reactor options. In a common lab scale fixed-bed reactor, the catalyst is suspended between glass or quartz wool at the hottest point in a reactor tube. The reactor tube is also packed with inert particles, such as carborundum, to fill void space and quench radical reactions. The paraffin mixes with the oxidant and diluent gas, which are heated prior to passing through the catalytic bed. Conditions such as gas hourly space velocity, carbon to oxygen ratio, upper or lower flammability limit and total feed to hydrocarbon ratio may thus be easily controlled.

1.2.2 Selective oxidation of alkanes

Selective oxidation catalysis is a large branch of heterogeneous catalysis, in which researchers attempt to produce highly active and selective catalysts for the activation of alkanes to products, such as olefins and oxygenates. Factors which need to be considered in selective oxidation include activation of the hydrocarbon, the nature of the oxidant and the

influence of competing mechanisms. These factors can impact considerably on the selectivity and activity of a catalytic system. It is thus imperative that one collates and understands the knowledge already available, as this may assist in improving approaches to selective oxidation processes.

In most applications, the commonly used oxidant is molecular oxygen, in the form of air. There has also been interest in using carbon dioxide as an alternative oxidant to oxygen, which has been covered in a review by Wang and Zhu [49]. The use of carbon dioxide as an oxidant generates interest for reasons such as the abundance of carbon dioxide and the need to utilize this potentially valuable chemical. Carbon dioxide replacing molecular oxygen is advantageous in that flammability limits would not need to be considered in reactions, however, it is limited, as it is not as reactive as oxygen and it also the forms carbon monoxide when used [50]. A lab scale reactor operating carbon dioxide as the oxidant may therefore require an appropriate venting system or a scrubbing approach for the carbon monoxide formed.

Changing the oxidant may have a combination of advantages and disadvantages, however, this may be an aspect of improving target selectivity. The use of nitrous oxide has gained interest since applications such as the oxidation of methane over silica supported MoO_3, in which high selectivity to methanol and formaldehyde was observed [51, 52]. Considering factors such as the abundance of air, affordability and since it is the most widely used oxidant, the focus shall remain on air as an oxidant in most of the applications discussed. Molecular oxygen, in the form of air, is also used in heterogeneous oxidation due to ease of use and low environmental impact. The success of molecular oxygen as an oxidant stems from the formation of the required oxygen species on the surface of the transition metal oxide catalyst. Several reactions, such as activation of the hydrocarbon, formation of surface oxygen species, homogeneous gas phase reactions and other competing reactions may impact on the products formed during heterogeneous oxidation of hydrocarbons.

1.2.2.1 Activating the hydrocarbon and the role of the surface oxygen species

In heterogeneous oxidation catalysis, saturated hydrocarbons may be activated on the surface of the catalyst and by the oxygen species produced from the interaction of molecular oxygen with the metal oxide. The ability of the catalytic surface to adsorb and desorb the saturated hydrocarbon is therefore important and can be directly related to the acidic and basic strength

of the active site. Adsorption and hence activation of the hydrocarbon is thus crucial, since it is rate determining [53]. The mechanisms involved in activation of the hydrocarbon are not entirely known and continue to cause controversy. Understanding how the activation may possibly proceed is important, as the overall oxidation reaction mechanism still requires further elucidation. These mechanisms may also assist in the clarification of the selectivity to the various complex products observed in most oxidation reactions. The alkane molecule, when adsorbed, may undergo homolytic cleavage or heterolytic cleavage [54]. Thermal cracking may be associated with homolytic cleavage, whilst highly acidic catalytic sites may perhaps be responsible for heterolytic cleavage. There are two mechanisms that can occur in heterolytic cleavage, forming either a carboanion or carbocation species, as shown in Scheme 1.1 and Scheme 1.2, respectively.

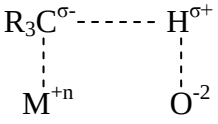

R= hydrogen or carbon

M= transition metal, n= oxidation state

Scheme 1.1: Heterolytic cleavage forming a carboanion species

Scheme 1.1 shows the heterolytic cleavage of the C-H bond that occurs when there is interaction of the carbon with the transition metal cation, whilst the hydrogen interacts with the basic oxygen from the lattice of the transition metal oxide, resulting in the formation of a carboanion [55, 56].

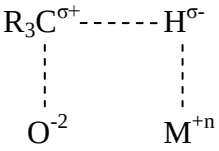

Scheme 1.2: Heterolytic cleavage forming a carbocation species

Scheme 1.2 depicts the heterolytic cleavage of the C-H bond which may occur when there is interaction of the carbon with the lattice oxygen and interaction of the hydrogen with the transition metal cation, resulting in the formation of a carbocation and hydride species [55, 56].

Three mechanisms may occur in homolytic cleavage resulting in the formation of a centred bond between C-H and the transition metal, as shown in Scheme 1.3, or formation of alkyl radicals via two mechanisms, shown in Schemes 1.4 and 1.5, respectively.

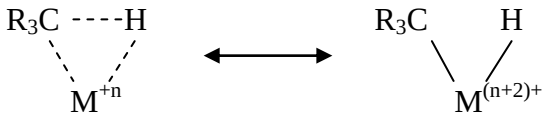

Scheme 1.3: Homolytic cleavage forming a transition metal centre bond with C-H

An electron deficient transition metal cation having a vacant coordination site may form a centre bond with carbon and hydrogen [53, 57, 58], as depicted in Scheme 1.3. The contribution of an electron each from carbon and hydrogen results in a higher oxidation state of the transition metal cation.

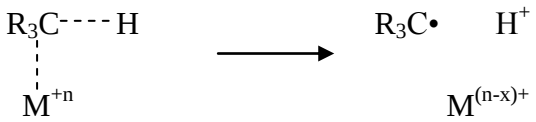

x= number of electrons gained

Scheme 1.4: Homolytic cleavage forming an alkyl radical and proton

In Scheme 1.4, a basic and reducible transition metal cation can facilitate C-H bond cleavage, producing an akyl radical and proton, whilst itself gaining electrons and, hence, undergoing reduction [53, 57, 58].

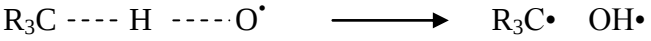

Scheme 1.5: Homolytic cleavage forming an alkyl radical and hydroxyl radical

Oxygen radicals present on the surface of the catalyst abstract a hydrogen from the hydrocarbon, producing an alkyl radical and a hydroxyl radical [53, 57, 58], as shown in Scheme 1.5.

Oxidation of hydrocarbons via the generated oxygen species can be performed by electrophilic or nucleophilic oxidation [54]. The oxygen species adsorbed and formed, either molecular or atomic and neutral or charged [59], are dependent on the reducibility of the surface, as well as the structure or phase of the catalyst [60]. The availability of the active sites through the basal planes, the redox properties of the transition metal, the defects on the

surface or in the lattice and also the transition metal oxygen bond strength, contribute to the relative ease of formation of the oxygen species. In terms of the transition metal oxygen bond strength, a strong bond may result in fewer reactions, a very weak bond may correlate to complete oxidation or non-selective reactions, whilst an intermediate bond strength may result in more selective reactions [13, 61]. Conditions such as carbon to oxygen ratio, upper and lower flammability limits and hydrocarbon to total feed ratio may also play a role in the nature of the species formed.

$$O_{2ads} \rightarrow O_2^- \rightarrow O_2^{-2} \rightarrow O^- \rightarrow O^{-2}{}_{lattice}$$

Scheme 1.6: Transformation of absorbed molecular oxygen [62].

Scheme 1.6 shows the change in oxygen species as molecular oxygen adsorbs onto the surface of a catalyst. Molecular oxygen when adsorbed onto the catalyst surface, gains electrons from the transition metal oxide surface, becoming more electron rich and hence nucleophilic. The final transformation ideally results in lattice oxygen, which may replenish the M-O-M oxide vacancy in the transition metal oxide structure.

The oxygen species involved in electrophilic oxidation are the super oxide O_2^-, peroxide O_2^{-2} and oxide O^- anions, whilst O^{-2} is associated with nucleophilic oxidation [54, 63, 64]. Adsorbed oxygen on the surface can be completely reduced to the O^{-2} form [59]. Non-selective oxidation reactions are generally accepted to proceed via the electrophilic route, whereas lattice oxygen is widely accepted by many researchers to be the key oxygen specie involved in the selective oxidation of alkanes. Super oxide O_2^- and oxide O^- species are paramagnetic, therefore, can be examined by electron paramagnetic resonance [61], whilst peroxide O_2^{-2} and lattice oxygen O^{-2} are non paramagnetic [65]. Successful identification of the super oxide and oxide species, by electron paramagnetic resonance, enabled researchers to elucidate the mechanisms involved when these species react with the hydrocarbon.

Aika and Lunsford suggested, from studying the activation of C_1 to C_4 alkanes, that O^- ions are actively involved in the oxidative dehydrogenation of alkanes on MgO, even in the absence of an oxidant [66]. The authors attributed hydrogen abstraction to be the initial step resulting in the formation of alkenes and alkyl radicals, which rapidly react with O^{-2} ions, yielding alkoxide species [66]. Driscoll and Lunsford also proved gas phase radical formation from the oxidation of methane and ethane, using EPR matrix spectroscopy [67].

Driscoll *et al.* further assigned O^- ions as being responsible for methyl radical formation over MgO [68]. Cavani and Trifiro attribute homogeneous gas phase reactions as being with O_2^- ions in respect to the oxidation of alkanes [69].

The mechanism of homogeneous radical reactions are thought to proceed via initial formation of alkyl radicals by hydrogen abstraction at the surface of the transitional metal oxide, followed by β-elimination of the hydrogen, yielding the corresponding alkene, which further reacts to produce oxygenated products [70, 71]. In the case of homogeneous gas phase reactions, olefins are usually formed as the minor product [69]. In the oxidative dehydrogenation of propane, Nguyen and Kung have highlighted that propagation of the *n*-propyl radical may result in the formation of ethylene and a methyl radical or peroxy species [72]. Radical reactions may produce numerous products, which may include hydrogen, methane, olefins, oxygenates, carbon oxides and water.

A more interesting group of products formed from gas phase reactions is that of cyclic ethers. The formation of cyclic ethers is usually associated with the autoignition of alkanes [73-75]. Mechanistically, hydrogen abstraction occurs on the surface of the catalyst, yielding an alkyl radical, followed by oxygen insertion to produce a peroxy radical [73]. The peroxy radical then reacts by isomerization to give a hydroperoxy alkyl radical, which may further react to finally produce stable cyclic ether rings [76]. Mechanisms involved in gas phase reactions are undoubtedly complex and non-selective, producing a wide range of products and, therefore, may be difficult to control in selective oxidation chemistry.

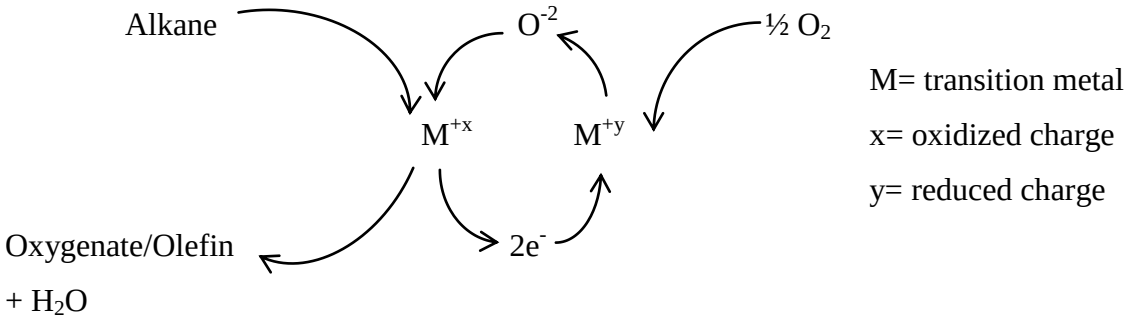

Scheme 1.7: Mars and van Krevelen mechanism for alkane oxidation [77, 78].

The idealistic redox mechanism accepted in alkane oxidation is the Mars and van Krevelen mechanism, shown in Scheme 1.7. Mechanistically, initial reduction of the transition metal

oxide catalyst by the hydrocarbon occurs, removing the lattice oxygen, resulting in the formation of selective products and a reduced transition metal ion and water [62]. Loss of lattice oxygen correlates to reduction of the transition metal ion by two electrons. Molecular oxygen adsorbed and transformed to lattice oxygen is taken up by the transition metal. The transition metal oxide is then re-oxidized by lattice oxygen, returning to the original oxidized state. Continuation of this cycle is termed a selective oxidation process via the Mars and van Krevelen mechanism.

1.2.2.2 Competing mechanisms

Competing mechanisms in the oxidation of alkanes can be problematic. Reporting on the oxidative dehydrogenation of propane, Kondratenko and Sinev attribute formation of carbon oxides predominantly from the oxidation of propene [79]. Alkenes undergo C-H bond dissociation when there is interaction between the Lewis acid metal cation and the pi bonding system of the alkene. Propene undergoes C-H bond dissociation, forming a π-allyl species on the transition metal cation [80]. The allylic species may then react with the generated oxygen species and result in non-selective products. A further example is the oxidation of *n*-octane, in which octenes are suggested as the precursors to carbon oxides [81]. Alkenes are far more reactive than alkanes due to the π bonding system and may, hence, be exposed to complete oxidation to carbon oxides and other non-valued products. Another possibility of olefin reactivity is the suggested diene formation from further hydrogen abstraction [82, 83]. Isomerization of the alkenes, once formed, should also be considered, since the target selectivity may be compromised. Heterocyclics may be associated with homogeneous gas phase reactions from the formation of alkoxide species, followed by cyclization to a stable furan or pyran structure.

Blank reactor studies [31] prior to catalytic testing may provide an indication of the impact of void space [30] and homogeneous gas phase reactions. This may further be used to determine operating reaction conditions in which radical reactions are minimal. Bruckman *et al.* associate heterocycle formation with a concerted two hydrogen abstraction [84], whereas Stoylkova *et al.* suggest formation of heterocycles from dehydration of diols [85]. Strong adsorption in selective oxidation processes are non-ideal, since it can result combustion of the alkane [86]. The Langmuir-Hinshelwood mechanism usually applies to the complete

oxidation of saturated hydrocarbons to carbon oxides, in particular to the formation of carbon dioxide [87].

The transition metal oxide species used, therefore, plays a critical role in the formation of products, such as olefins, oxygenated products, cracked products and carbon oxides. The ability of a catalyst to be selective is important, as a non-selective catalyst may produce undesired products. The design and structure of a catalyst material is thus important. Oxygen activity, the acid and basic surface characteristics, as well as the ability of the reactant to diffuse through the lattice is crucial [60]. Carbon oxides, resulting from total oxidation, are undesired products in most selective oxidation applications. A selective catalyst should possess the optimum characteristics of oxygen capacity and acid-basic sites to perform selective reactions. An ideal selective oxidation catalyst should, therefore, be able to convert the paraffin to the desired product, such as an olefin, and desorb the product rapidly, ensuring fewer side reactions.

Frequently studied oxide catalysts in hydrocarbon oxidation include oxides of vanadium and molybdenum [63]. Molybdates and molybdenum trioxide have provided researchers with ample ideas and indications of mechanistic details that may be summarized and prove informative to the scientific community. This discussion of selective oxidation will consequently include applications of molybdates and molybdenum trioxide, whilst including aspects of the catalytic results.

1.2.2.3 Molybdates and molybdenum trioxide

Molybdates are transition metal oxide species of the form $AMoO_4$ or $A_2(MoO_4)_3$, where A can be another transition metal such as iron. The interest in the use of molybdates for paraffin oxidation has stemmed from their successes in the oxidation of propane [88, 89], as dehydrogenation catalysts [90, 91] and in selective olefin ammoxidation [92, 93]. Another particularly successful oxidation application, was that of methanol to formaldehyde using iron molybdate [94]. Numerous molybdates and modifications thereof have been introduced, since the realization that metal compositions can be tailored to improve selectivity and yield in desired applications [95]. An example of such is the doping of iron, stabilized as Fe^{+2}, serving as a redox couple and allowing for lattice oxygen to replenish the Bi-O-Mo site, in propylene activation to acrylonitrile [95]. Metal ratios can, therefore, be very important in the catalysis based on molybdates and molybdenum trioxide. Characterization, the role of

structure, phase segregation, the catalytic oxidation of alkanes and supported catalysts will also be discussed. An attempt will be made at summarizing relevant applications and highlighting the implications of such.

1.2.2.3.1 Synthetic methodology

Molybdates can be prepared by methods such as co-precipitation [45], hydrothermal synthesis [96] and the citric acid method [97], amongst others. Co-precipitation is by far the most common approach of synthesis. A typical co-precipitation procedure involves the precipitation of two mixed aqueous nitrate solutions, maintaining the required pH for the synthesis, aging the mixture, separating the precipitate, followed by drying and calcinations [98]. Synthesis methods can also influence the catalytic activity of molybdates. Beale *et al.* were able to improve the activity of an iron molybdate catalyst for the oxidation of methanol to formaldehyde by hydrothermal synthesis [99]. Sodium molybdate and chloride salts can also be used to synthesize molybdates, however, most researchers prefer to avoid possible contamination from the chloride and sodium ions. Contamination of the molybdate surface may result in changes to the surface acidity, rendering the active sites non-selective or even decrease activity.

A study of the addition of sodium to iron molybdenum catalysts for methanol oxidation showed an immediate decrease in activity and a decrease in selectivity of the supported iron molybdenum catalyst [100]. Molybdate synthesis can be quite sensitive toward several factors, such as the polymeric species of molybdenum, temperature, concentration of molybdenum and pH [101]. An example requiring considerable pH stability is the synthesis of nickel molybdate, in which the co-precipitation procedure was maintained at pH 5.7, monitored by a pH controller and adjusted with ammonium hydroxide and nitric acid [102]. Co-precipitation, however, remains the most reproducible approach since pH, polymeric species, temperature and the required metal ratio can effectively be controlled.

1.2.2.3.2 Influence of excess molybdenum trioxide and effect of alkali metal promotion on molybdates

Synthetic factors involved in molybdate catalyst design, such as molybdenum content, may also influence the catalysis. In particular, cobalt molybdate with excess molybdenum was reported as more active than the pure molybdate phase in the oxidation of propane to olefins

[103]. Researchers claim this to be a synergistic cooperation between the molybdate and molybdenum trioxide in the oxidation of propane [104, 105]. The importance of molybdenum trioxide can be further emphasized with applications, such as the selective oxidation of 1-butene with nickel molybdate, in which MoO_3 was attributed as the most selective component [106]. This was confirmed in a report of a pure cobalt molybdate system, in which the oxidation of 1-butene to maleic anhydride was reported as non-selective, however, in the presence of excess molybdenum trioxide, enhanced selectivity to maleic anhydride was observed [107]. Trifiro *et al.* attribute the mechanical strength of the iron molybdate catalyst and the ease re-oxidation of β-$FeMoO_4$ to $Fe_2(MoO_4)_3$, to excess MoO_3, in the oxidation of methanol and olefins [108]. A molybdate catalyst incorporated with molybdenum trioxide may, therefore, be imperative in enhancing activity, selectivity, mechanical strength and phase stability when used in the oxidation of alkanes.

In an attempt to improve previously designed catalytic systems, researchers continue to target the effect of promotion on these systems. In the oxidative coupling of methane, manganese molybdate promoted by alkali metals, such as Na, K and Li showed an increase in activity and selectivity [109]. Further characterization revealed no change to the molybdate catalyst, whilst isotopic labeling studies, TPR and TPD indicated a different interaction of the methane molecule with the promoted surface [109, 110]. In a study of the effect of alkali metal promoters on nickel molybdate towards the oxidation of *n*-butane, Martin-Aranda *et al.* confirmed no structural change to the bulk molybdate, however, addition of alkali metals decreased the activity of the catalyst and improved selectivity in the direction of butenes and butadiene [111]. The authors claimed the greater basicity was responsible for the higher selectivity to butenes and butadiene, but also acknowledged that the optimum loading to enhance yields required small amounts of homogeneously spread alkali metals on the surface of the catalyst. In contrast to these authors, Portela *et al.* noted an improvement in the activity of nickel molybdate doped with potassium and calcium, respectively [112]. Both studies attribute the surface basicity as a significant trait in the improved selectivity to butenes and butadiene, along with a decrease in carbon oxides. Kaddouri *et al.* corroborated the improved selectivity to alkenes with promoted nickel molybdate catalysts in the oxidative dehydrogenation of propane and isobutane [113]. The authors also associated prevention of the decomposition of propene and isobutene with the use of promoters. Thus, the use of barium as a promoter was reported to increase the selectivity to propene from the oxidation of

propane, using a nickel molybdate catalyst, due to an increase in the number of basic sites and the synergistic interaction between barium oxide and molybdenum trioxide [114].

The role of excess molybdenum in molybdate catalysts may be difficult to comprehend, however, it is apparent that surface acidity and basicity may be more influential in molybdate catalytic systems than anticipated. Attempting to understand the structure, redox and surface properties involved with these catalytic systems may enlighten our perceptions of the mechanisms in hydrocarbon oxidation.

1.2.2.3.3 Structure-catalytic properties

Molybdates with the metal cation in the +3 oxidation state exists as $A_2(MoO_4)_3$ and in the +2 oxidation state as $AMoO_4$, where A is the metal cation. Iron molybdate for example, $Fe_2(MoO_4)_3$, is monoclinic with tetrahedrally situated MoO_4 and octahedral FeO_6 [115], whereas in a system such as $MnMoO_4$, both the manganese cation and molybdenum are octahedrally co-ordinated [116]. The monoclinic structure has eight $Fe_2(MoO_4)_3$ molecules per unit cell, with sixteen FeO_6 octahedra and twenty four MoO_4 tetrahedra [117]. In the case of the structure-catalytic relationship of molybdates amongst other selective oxidation catalysts, the intrigue involves lattice oxygen.

The role of terminal M=O and bridging M-O-M bonds in the generation of lattice oxygen remains unclear. Experimental work conducted by Callahan and Grasselli revealed the lattice oxygen bond should be of intermediate strength in order to give good selectivity to desired products [118]. Grasselli, much later, went on to conclude that a strong metal oxygen bond may result in no reaction occurring, whilst a weak metal oxygen bond may result in non-desired products [13].

A very different postulation with regard to structure-catalytic relationship was that by Fagherazzi and Pernicone, who suggested that a small excess of molybdenum in iron molybdate enlarges the monoclinic structure, whereby Mo^{+6} substitutes Fe^{+3} in the octahedral sites and the charge is balanced by O^{-2} ions in the lattice [119]. This distorted unit cell with defect sites, due to the substitution of molybdenum, was recognized as the active component in the oxidation of methanol by the authors [119]. Lattice insertion, however, may be sensitive and for this postulation to hold, other metal molybdates with a slight excess of molybdenum should ideally show the same behavior.

Orthorhombic crystal structured MoO_3 exists in an octahedral co-ordination, as established by characterization using techniques such as infrared and Raman spectroscopy [120] and electron spin resonance spectroscopy [121, 122]. In terms of structure-catalytic relationships, one may need to consider the effects of metal oxygen-bonds and facets of crystal structure. The initial study of the correlation of the crystalline structure of MoO_3 to specificity was conducted by Volta and Moraweck, in the oxidation of propene [123]. Results from this study revealed that acrolein formation was favoured by the 020 plane of molybdenum trioxide. Research involving structure-function relationships and oxidation reactions subsequent to this study grew considerably and was summarized by Volta and Portefaix in a review [124]. In the mild oxidation of propene, Volta and Tatibouet attributed the side (100) plane with allylic oxidation and the basal (010) plane with deep oxidation [125]. Contradictory to this work, Haber and Serwicka suggested the basal (010) plane responsible for selection oxidation by lattice oxygen [126]. In support, Bruckman *et al.* found a proportional dependence of surface area of the basal plane to the acrolein yield from propene, which further suggested selective oxidation via the basal plane [127].

Since initial studies mainly focused on propene activation, researchers sought understanding of structure relationships through other hydrocarbon molecules. In studies of the partial oxidation of methane to formaldehyde, Smith and Ozkan suggested that the formation of formaldehyde was dependent on lattice oxygen via the M=O side plane, whilst oxygen from the M-O-M basal planes appeared to direct reactions toward complete oxidation [128, 129]. In the oxidation of 1-butene, Haber and Lalik claimed the side (100) and apical (101) planes of MoO_3 may be associated with C-H bond activation, whilst the basal (110) plane containing O^{-2} ions may be responsible for nucleophilic attack, forming an oxygenated product [130]. The authors were able to perform these studies using relative exposed amounts of the planes of MoO_3 and isotopic labeling, under steady state reactions.

Summarizing the information provided thus far, it is clear that complete oxidation may occur on all facets. This may be correlated with the fact that over oxidation mechanistically applies to alkanes, alkenes and intermediate products. Analogous to this, is the evidence provided by Hernandez and Ozkan, suggesting the possibility of complete and selective oxidation on all facets of molybdenum trioxide [131].

1.2.2.3.4 Redox and surface properties

Molybdates are known to perform as redox catalysts, existing in multiple oxidation states. Molybdates, when reduced, may form MoO_3 and suboxides such as Mo_4O_{11} and MoO_2. Due to the capability of molybdenum to exist in several oxidation states, there may be co-existence of several suboxides in small quantities. Research [132, 133] suggests Mo_4O_{11} is an intermediate to the formation of MoO_2. An XPS study showed the simultaneous existence of Mo^{+5} and Mo^{+3} species, upon the reduction of molybdenum trioxide with hydrogen [134]. A possible explanation for this may be the greater stability of the suboxides of Mo^{+4} and Mo^{+2} as opposed to other suboxides, hence these species may be detectable in small quantities. The mechanism by which suboxide formation occurs continues to be controversial. In view of this, in situ XAS and XRD studies confirmed the formation of MoO_2 in a one step process from MoO_3, with Mo_4O_{11} not identified as an intermediate product and instead suggested to form simultaneously from the reduction of MoO_3 and MoO_2 [135]. Among the suggested mechanisms and confirmed suboxide phases, one may also need to consider the environment in which the reduction takes place. Lalik *et al.* suggest the formation of Mo_4O_{11} may be dependent on the catalytic material and conditions used [136]. In heterogeneous gas phase oxidation catalysis, for example, the hydrocarbon, oxidant and molybdate used may impact on the molybdenum species formed via the reduction oxidation cycle. There may be competing reduction oxidation capabilities, thus limiting perhaps the formation of Mo_4O_{11} and therefore leading to the reduction of Mo^{+4} to Mo^{+2}.

High oxidation state metals such as Mo^{+6} are Lewis acids and may perform as acidic oxides, following the mechanism of carbocation formation or an alkoxide intermediate in olefin oxidation [92, 137]. Reduction and hence gain of electrons by the oxide of Mo^{+6} may result in an ionic character [53]. The reduced form or phase may therefore act as a basic oxide, forming a carboanion, followed by attack of lattice oxygen [92, 137]. Ueda *et al.* report the highest rate of propene formation from the oxidation of propane due to a very acidic magnesium molybdate catalyst [138]. Graselli *et al.* explained the higher rate of oxidation of propene by Bi_2O_3•$2MoO_3$ compared to Bi_2O_3•$3MoO_3$, as a optimum balance of Mo^{+6} sites and bismuth cation sites for hydrogen abstraction [92]. Considering the acidic nature of MoO_3 [139], a slight excess of molybdenum may balance the acidic and basic sites on the surface of the molybdate [95], resulting in a fairly active and selective oxidation catalyst. Excessive molybdenum may lead to a highly acidic surface, which may influence the activity

and selectivity of the molybdate catalyst. The strength of acidity on the surface is therefore fundamental, as it may impact the rate of hydrogen abstraction from a saturated hydrocarbon. Successful oxidative dehydrogenation catalysts, such as molybdates, typically exhibit good redox capability and can facilitate bond breaking and desorption due to acid and basic character.

1.2.2.3.5 The effect of supporting molybdenum

In an attempt to improve the properties mentioned above, catalysts are often supported, since this may enhance the catalytic behavior and facilitate a different mechanism for the catalysis. It is important to note that the type of support strongly influences the catalytic properties exhibited by molybdenum oxide species, especially in the oxidative dehydrogenation of alkanes [140, 141]. It may therefore be concluded that the interaction between the surface of the support and the respective molybdenum species is dissimilar for different supports. For example, oxygen chemisorption of silica supported molybdenum trioxide revealed weak interaction between MoO_3 and SiO_2 and hence poor dispersion [142]. In the case of Mo^{+6} supported on silica, the metal cation is believed to replace hydrogen from the Si-OH bond thus forming a bridging bond through oxygen with the support [35, 143]. If one were to consider the acidity of Mo^{+6} and MoO_3 as mentioned in Section *1.2.2.3.4* and the acidic nature of silica, we may conclude that the weak interaction is a consequence of these species.

Silica, itself as a support, has been shown to be active in oxidation catalysis [144]. Silica has also been attributed with the formation of oxygen species responsible gas phase reactions in heterogeneous oxidation catalysis [145]. In the partial oxidation of ethane, Mendelovici and Lunsford proposed hydrogen abstraction by O^- ions responsible for the formation of ethyl radicals, which further react to produce ethylene and acetaldehyde over silica supported molybdenum [146]. Song *et al*. suggested gas phase radicals were formed over MoO_3/SiO_2 as opposed to lattice oxygen insertion, in the epoxidation of propylene to propylene oxide [147]. In contrast to the activity of silica and silica supported molybdenum, Stern and Graselli, concluded from their results of the oxidative dehydrogenation of propane via silica supported divalent molybdates, that propylene yield was catalytically dependent and not initiated by gas phase reactions [88]. Also, Maione and Devillers, have shown that active cobalt, nickel and mixed cobalt-nickel molybdates supported on silica resulted in a greater intrinsic propene activity, in the oxidative dehydrogenation of propane [148]. Dias *et al*.

showed that supporting nickel molybdate on silica proves beneficial, since the oxidative dehydrogenation of isobutane over the unsupported catalyst results in higher amounts of carbon oxides and coke, compared to the molybdate supported on silica [149]. Similarly in the oxidative dehydrogenation of isotubane over silica supported nickel molybdate catalysts, the catalyst supported on silica with a higher surface area shows a higher conversion of isobutane, highest isobutene selectivity and lowest selectivity to carbon oxides [150]. The authors attribute the stabilization of the beta-phase of nickel molybdate, responsible for the improvement in the catalytic results. This stabilization is suggested to occur due to the interaction of the molybdenum species and the silanol groups on silica, ultimately resulting in a higher level of the beta-phase of nickel molybdate and an improvement in the acidic-basic character of the supported catalyst [148-150].

Gamma-alumina, compared to silica, is an amphoteric support. The dissimilarity in the surface acidic-basic properties of gamma-alumina compared to silica, result in different metal-support interactions, leading to mechanistic differences during reactions. In particular, characterization and catalytic testing of an iron-molybdenum catalyst supported on gamma-alumina revealed insertion of iron and molybdenum into the lattice, resulting in the formation of an Fe-Al-Mo bond [151]. Upon methanol oxidation with this catalyst, formaldehyde was not produced, instead dimethyl ether was the major product due to acidic-basic properties, as concluded by the authors [151]. A stronger interaction between the surface of alumina and molybdenum was suggested to have occurred. This has been corroborated in the study of propylene oxidation via supported molybdenum, undertaken by Desikan and coworkers, in which a good correlation of the interaction between support acidic-basic properties and molybdenum oxide is provided [152]. The authors showed that catalytic activity decreased in the order $TiO_2 > Al_2O_3 > SiO_2$ via Arrhenius plots of propylene oxidation using catalysts with low and high loadings of MoO_3. A better dispersion of molybdenum trioxide was observed on TiO_2 and Al_2O_3 as confirmed by oxygen uptake through chemisorption studies [152]. Considering that titania and alumina are both amphoteric, whilst silica is more acidic in nature, the superior interaction of supported acidic molybdenum trioxide on TiO_2 and Al_2O_3 may be related to the ideal combination of acid and base properties. Gamma-alumina may be advantageous as a support for molybdenum trioxide, as an increase in molybdenum loading increases the Brønsted acidity [153]. This may favour the production of olefins over alkanes, however, basic sites may be required to desorb the olefin molecules, to prevent over-

oxidation. A study by Heracleous *et al.*, in the oxidative dehydrogenation of ethane, showed that gamma-alumina supported molybdenum oxide produced mainly carbon oxides [154]. The authors suggested that the ethene formed probably adheres strongly to the surface of the catalyst, due to the acidity and therefore undergoing further oxidation to carbon oxides.

1.3 Conclusion and perspective

Heterogeneous gas phase oxidation catalysis continually inspires researchers to develop new research methodologies and target the formation of value-added products from feeds such as alkanes. A clear understanding of catalytic oxidation may therefore be required for new researchers in the field and a reiteration for the experienced scientific community. A fundamental approach may, hence, be constructive prior to catalytic design and experimental work. It is undoubtedly clear that several mechanisms may be involved in the oxidation of hydrocarbons and consequently alkane activation.

In summary, the properties of an oxidation catalyst may vary, however, a good selective oxidation catalyst should possess optimum redox properties to facilitate the transfer of lattice oxygen and acidic/basic surface properties to encourage the ideal adsorption of the reactant and desorption of valued products, such as olefins or oxygenates.

Molybdates in particular can be functional selective oxidation catalysts. An excess of molybdenum trioxide in a molybdate catalyst plays a vital role, which may be a synergistic interaction, as well a combination of surface acidity and basicity. A supported molybdenum catalyst may perform better on alumina as opposed to silica due to the amphoteric nature of the former surface, encouraging stronger interaction of the molybdenum species with the support. Further research should, for example, be conducted on a support containing both alumina and silica, such as cordierite monoliths, allowing for a superior combination of acidic and basic sites.

1.4 Aim and motivation for this research

The aim of this work is to therefore support a molybdenum based catalyst such as iron molybdate on cordierite monoliths, to determine if monoliths may be used as a suitable support for iron molybdate in the oxidation of *n*-octane.

Bare and coated monoliths will be studied in the oxidation of *n*-octane. The cordierite monoliths can be coated with a secondary support such as gamma-alumina to improve the

interaction of the active catalyst and support. The iron-molybdenum catalyst is of higher molybdenum content, since excess molybdenum has proven to be beneficial to molybdate catalysts, as discussed in this chapter. In order to understand the role of monoliths as supports a review of monoliths is therefore provided in Chapter 2, covering the basics, preparation methods and applications of monolithic catalysts. Chapter 2 also leads on to the main study in Chapter 3, which involves the oxidation of *n*-octane over bare and coated monoliths.

The overall study will therefore provide insight into the efficacy of monoliths as supports in the conversion of alkanes to value-added products. Ultimately, this research study will contribute to the collaborative research effort toward the heterogeneous oxidation of alkanes, within the Catalysis Research Group.

1.5 References

[1] A.M. Thayer, Chemical & Engineering News Archive 70 (1992) 27-49.

[2] F. Zaera, Surface Science 500 (2002) 947-965.

[3] C. Marcilly, Journal of Catalysis (2003) 47-62.

[4] H.-U. Blaser, M. Studer, Applied Catalysis A: General 189 (1999) 191-204.

[5] H.-U. Blaser, Catalysis Today 60 (2000) 161-165.

[6] G. Somorjai, C. Kliewer, Reaction Kinetics and Catalysis Letters 96 (2009) 191-208.

[7] M. Bowker, The Basis and Applications of Heterogeneous Catalysis, Oxford University Press Incorporated, New York, 1998.

[8] S.M. George, Chemical Reviews 95 (1995) 475-476.

[9] L. Hiam, H. Wise, S. Chaikin, Journal of Catalysis 10 (1968) 272-276.

[10] G. Centi, Catalysis Letters 22 (1993) 53-66.

[11] F. Cavani, Journal of Chemical Technology & Biotechnology 85 (2010) 1175-1183.

[12] E. Bordes, Comptes Rendus de l'Académie des Sciences - Series IIC - Chemistry 3 (2000) 725-733.

[13] R.K. Grasselli, Topics in Catalysis 21 (2002) 79-88.

[14] B. Delmon, The future of industrial oxidation catalysis spurred by fundamental advances, in: R.K. Grasselli, S.T. Oyama , A.M. Gaffney, J.E. Lyons, (Eds.), Studies in Surface Science and Catalysis, Elsevier, 1997, 43-59.

[15] F. Cavani, Catalysis Today 157 (2010) 8-15.

[16] A.E. Shilov, G.B. Shul'pin, Chemical Reviews 97 (1997) 2879-2932.

[17] R.A. Periana, D.J. Taube, S. Gamble, H. Taube, T. Satoh, H. Fujii, Science 280 (1998) 560-564.

[18] M.E. Dry, Applied Catalysis A: General 189 (1999) 185-190.

[19] M.E. Dry, Catalysis Today 71 (2002) 227-241.

[20] J.S. Jung, J.W. Park, G. Seo, Applied Catalysis A: General 288 (2005) 149-157.

[21] J.R. Rostrup-Nielsen, Catalysis Reviews 46 (2004) 247-270.

[22] R.G. Bergman, Nature 446 (2007) 391-393.

[23] T.V. Choudhary, S. Banerjee, V.R. Choudhary, Applied Catalysis A: General 234 (2002) 1-23.

[24] J. Brazdil, Topics in Catalysis 38 (2006) 289-294.

[25] F. Cavani, F. Trifirò, Catalysis Today 24 (1995) 307-313.

[26] H.J. Curran, P. Gaffuri, W.J. Pitz, C.K. Westbrook, Combustion and Flame 114 (1998) 149-177.

[27] J.A. Labinger, J.E. Bercaw, Nature 417 (2002) 507-514.

[28] E.M. Larsen, Transitional Elements, W.A. Benjamin Incorporated, New York, 1965.

[29] N. Govender, H.B. Friedrich, M.J. van Vuuren, Catalysis Today 97 (2004) 315-324.

[30] H.B. Friedrich, N. Govender, M.R. Mathebula, Applied Catalysis A: General 297 (2006) 81-89.

[31] H.B. Friedrich, A.S. Mahomed, Applied Catalysis A: General 347 (2008) 11-22.

[32] C. Masters, Homogeneous Transitional-Metal Catalysis-A Gentle Art, Chapman and Hall Limited, London, 1981.

[33] P.A. Cox, Transition Metal Oxides - An Introduction to their Electronic Structure and Properties, Clarendon Press, Oxford, 1992.

[34] G.C. Bond, Catalysis by Metals, Academic Press Incorporated, London, 1962.

[35] M.A. Bañares, Catalysis Today 51 (1999) 319-348.

[36] R.H. Crabtree, Chemical Reviews 85 (1985) 245-269.

[37] M.M. Bhasin, J.H. McCain, B.V. Vora, T. Imai, P.R. Pujadó, Applied Catalysis A: General 221 (2001) 397-419.

[38] P.A. Agaskar, R.K. Grasselli, J.N. Michaels, P.T. Reischman, D.L. Stern, J.G. Tsikoyiannis, U.S. Patent 5530171 (1996).

[39] G. Mul, M.F. Asaro, A.S. Hirschon, R.B. Wilson Jr., U.S. Patent 6509485 (2003).

[40] T.F. Narbeshuber, A. Brait, K. Seshan, J.A. Lercher, Journal of Catalysis 172 (1997) 127-136.

[41] S. Taubmann, H.G. Alt, Journal of Molecular Catalysis A: Chemical 287 (2008) 102-109.

[42] D. Sanfilippo, I. Miracca, Catalysis Today 111 (2006) 133-139.

[43] R.H. Crabtree, Journal of the Chemical Society, Dalton Transactions (2001) 2437-2450.

[44] F. Cavani, F. Trifirò, Catalysis Today 36 (1997) 431-439.

[45] B. Pillay, M.R. Mathebula, H.B. Friedrich, Applied Catalysis A: General 361 (2009) 57-64.

[46] E.A. Elkhalifa, H.B. Friedrich, Applied Catalysis A: General 373 (2010) 122-131.

[47] E.A. Elkhalifa, H.B. Friedrich, Catalysis Letters 141 (2011) 554-564.

[48] M. Narayanappa, V.D.B.C. Dasireddy, H.B. Friedrich, Applied Catalysis A: General 447–448 (2012) 135-143.

[49] S. Wang, Z.H. Zhu, Energy & Fuels 18 (2004) 1126-1139.

[50] V.C. Corberán, Catalysis Today 99 (2005) 33-41.

[51] R.S. Liu, M. Iwamoto, J.H. Lunsford, Journal of the Chemical Society, Chemical Communications (1982) 78-79.

[52] M.M. Khan, G.A. Somorjai, Journal of Catalysis 91 (1985) 263-271.

[53] J.C. Védrine, Topics in Catalysis 21 (2002) 97-106.

[54] J. Haber, M. Witko, Journal of Catalysis 216 (2003) 416-424.

[55] R. Burch, M.J. Hayes, Journal of Molecular Catalysis A: Chemical 100 (1995) 13-33.

[56] E. Brocławik, J. Haber, W. Piskorz, Chemical Physics Letters 333 (2001) 332-336.

[57] J. Haber, Molecular mechanism of heterogeneous oxidation — organic and solid state chemists' views, in: R.K. Grasselli, S.T. Oyama, A.M. Gaffney, J.E. Lyons, (Eds.), Studies in Surface Science and Catalysis, Elsevier, 1997, 1-17.

[58] J. Haber, M. Witko, Accounts of Chemical Research 14 (1981) 1-7.

[59] G.I. Panov, A.K. Uriarte, M.A. Rodkin, V.I. Sobolev, Catalysis Today 41 (1998) 365-385.

[60] U.S. Ozkan, R.B. Watson, Catalysis Today 100 (2005) 101-114.

[61] R. Schlögl, Concepts in Selective Oxidation of Small Alkane Molecules, Modern Heterogeneous Oxidation Catalysis, Wiley-VCH Verlag GmbH & Co. KGaA, 2009, 1-42.

[62] B. Grzybowska-Świerkosz, Topics in Catalysis 11-12 (2000) 23-42.

[63] G.I. Panov, K.A. Dubkov, E.V. Starokon, Catalysis Today 117 (2006) 148-155.

[64] J. Haber, W. Turek, Journal of Catalysis 190 (2000) 320-326.

[65] G.K. Boreskov, Catalytic Activation of Dioxygen, in: J.R. Anderson, M. Boudart, (Eds.), Catalysis - Science and Technology, Springer-Verlag, Berlin, 1982, 40-137.

[66] K. Aika, J.H. Lunsford, The Journal of Physical Chemistry 81 (1977) 1393-1398.

[67] D.J. Driscoll, J.H. Lunsford, The Journal of Physical Chemistry 89 (1985) 4415-4418.

[68] D.J. Driscoll, W. Martir, J.X. Wang, J.H. Lunsford, Journal of the American Chemical Society 107 (1985) 58-63.

[69] F. Cavani, F. Trifirò, Catalysis Today 51 (1999) 561-580.

[70] I.R. Slagle, D. Sarzynski, D. Gutman, J.A. Miller, C.F. Melius, Journal of the Chemical Society, Faraday Transactions 2: Molecular and Chemical Physics 84 (1988) 491-503.

[71] M.Y. Sinev, Catalysis Today 24 (1995) 389-393.

[72] K.T. Nguyen, H.H. Kung, Industrial & Engineering Chemistry Research 30 (1991) 352-361.

[73] R. Minetti, M. Carlier, M. Ribaucour, E. Therssen, L.R. Sochet, Combustion and Flame 102 (1995) 298-309.

[74] F. Buda, R. Bounaceur, V. Warth, P.A. Glaude, R. Fournet, F. Battin-Leclerc, Combustion and Flame 142 (2005) 170-186.

[75] O. Herbinet, W.J. Pitz, C.K. Westbrook, Combustion and Flame 154 (2008) 507-528.

[76] O. Herbinet, S. Bax, P.-A. Glaude, V. Carré, F. Battin-Leclerc, Fuel 90 (2011) 528-535.

[77] J.C. Vedrine, G. Coudurier, J.-M.M. Millet, Catalysis Today 33 (1997) 3-13.

[78] M. Misono, Topics in Catalysis 21 (2002) 89-96.

[79] E.V. Kondratenko, M.Y. Sinev, Applied Catalysis A: General 325 (2007) 353-361.

[80] H.H. Kung, Industrial & Engineering Chemistry Product Research and Development 25 (1986) 171-178.

[81] V.D.B.C. Dasireddy, H.B. Friedrich, S. Singh, Applied Catalysis A: General 467 (2013) 142-153.

[82] G. Centi, F. Trifiro, Catalysis Today 3 (1988) 151-162.

[83] G. Centi, F. Trifiro, J.R. Ebner, V.M. Franchetti, Chemical Reviews 88 (1988) 55-80.

[84] K. Bruckman, J. Haber, E.M. Serwicka, Faraday Discussions of the Chemical Society 87 (1989) 173-187.

[85] T.Y. Stoylkova, C.D. Chanev, H.T. Lechert, C.P. Bezouhanova, Applied Catalysis A: General 203 (2000) 121-126.

[86] R. Burch, D.J. Crittle, M.J. Hayes, Catalysis Today 47 (1999) 229-234.

[87] F. Cavani, F. Trifiró, Catalysis Today 34 (1997) 269-279.

[88] D.L. Stern, R.K. Grasselli, Journal of Catalysis 167 (1997) 550-559.

[89] C. Mazzocchia, E. Tempesti, C. Aboumrad, U.S. Patent 5086032 (1992).

[90] H.F. Hardman, U.S. Patent 4131631 (1978).

[91] H.F. Hardman, U.S. Patent 4255284 (1981).

[92] R.K. Grasselli, J.D. Burrington, J.F. Brazdil, Faraday Discussions of the Chemical Society 72 (1981) 203-223.

[93] R.K. Grasselli, Journal of Chemical Education 63 (1986) 216-221.

[94] H. Adkins, W.R. Peterson, Journal of American Chemical Society 53 (1931) 1512-1520.

[95] R.K. Grasselli, Catalysis Today 49 (1999) 141-153.

[96] J. Guo, P. Zavalij, M.S. Whittingham, Journal of Solid State Chemistry 117 (1995) 323-332.

[97] W. Kuang, Y. Fan, K. Chen, Y. Chen, Journal of Chemical Research, Synopses (1997) 366-367.

[98] S. Pradhan, J.K. Bartley, D. Bethell, A.F. Carley, M. Conte, S. Golunski, M.P. House, R.L. Jenkins, R. Lloyd, G.J. Hutchings, Nature Chemistry 4 (2012) 134-139.

[99] A.M. Beale, S.D.M. Jacques, E. Sacaliuc-Parvalescu, M.G. O'Brien, P. Barnes, B.M. Weckhuysen, Applied Catalysis A: General 363 (2009) 143-152.

[100] B.I. Popov, L.N. Shkuratova, N.G. Skorokhova, Reaction Kinetics and Catalysis Letters 3 (1975) 463-469.

[101] F. Trifirò, Catalysis Today 41 (1998) 21-35.

[102] B. Pillay, University of KwaZulu-Natal, 2009.

[103] Y.S. Yoon, N. Fujikawa, W. Ueda, Y. Moro-oka, K.W. Lee, Catalysis Today 24 (1995) 327-333.

[104] L.E. Cadus, M.C. Abello, M.F. Gomez, J.B. Rivarola, Industrial & Engineering Chemistry Research 35 (1996) 14-18.

[105] L.E. Cadus, M.F. Gomez, M.C. Abello, Catalysis Letters 43 (1997) 229-233.

[106] U. Ozkan, G.L. Schrader, Journal of Catalysis 95 (1985) 137-146.

[107] U. Ozkan, G.L. Schrader, Applied Catalysis 23 (1986) 327-338.

[108] F. Trifirò, M. Carbucicchio, P.L. Villa, Hyperfine Interactions 111 (1998) 17-22.

[109] S.A. Driscoll, U.S. Ozkan, Isotopic Labeling Studies on Oxidative Coupling of Methane over Alkali Promoted Molybdate Catalysts, in: V.C. Corberán, S.V. Bellón, (Eds.), Studies in Surface Science and Catalysis, Elsevier, 1994, 367-375.

[110] S.A. Driscoll, D.K. Gardner, U.S. Ozkan, Journal of Catalysis 147 (1994) 379-392.

[111] R.M. Martin-Aranda, M.F. Portela, L.M. Madeira, F. Freire, M. Oliveira, Applied Catalysis A: General 127 (1995) 201-217.

[112] M.F. Portela, R.M. Aranda, M. Madeira, M. Oliveira, F. Freire, R. Anouchinsky, A. Kaddouri, C. Mazzocchia, Chemical Communications (1996) 501-502.

[113] A. Kaddouri, C. Mazzocchia, E. Tempesti, Applied Catalysis A: General 169 (1998) L3-L7.

[114] Y. Liu, J. Wang, G. Zhou, M. Xian, Y. Bi, K. Zhen, Reaction Kinetics and Catalysis Letters 73 (2001) 199-208.

[115] W.T.A. Harrison, Materials Research Bulletin 30 (1995) 1325-1331.

[116] A. Clearfield, A. Moini, P.R. Rudolf, Inorganic Chemistry 24 (1985) 4606-4609.

[117] H.-y. Chen, Materials Research Bulletin 14 (1979) 1583-1590.

[118] J.L. Callahan, R.K. Grasselli, AIChE Journal 9 (1963) 755-760.

[119] G. Fagherazzi, N. Pernicone, Journal of Catalysis 16 (1970) 321-325.

[120] G.A. Nazri, C. Julien, Solid State Ionics 53–56, Part 1 (1992) 376-382.

[121] G. Mestl, N.F.D. Verbruggen, H. Knoezinger, Langmuir 11 (1995) 3035-3041.

[122] M. Labanowska, Physical Chemistry Chemical Physics 1 (1999) 5385-5392.

[123] J.-C. Volta, B. Moraweck, Journal of the Chemical Society, Chemical Communications (1980) 338-339.

[124] J.C. Volta, J.L. Portefaix, Applied Catalysis 18 (1985) 1-32.

[125] J.C. Volta, J.M. Tatibouet, Journal of Catalysis 93 (1985) 467-470.

[126] J. Haber, E. Serwicka, Polyhedron 5 (1986) 107-109.

[127] K. Brückman, R. Grabowski, J. Haber, A. Mazurkiewicz, J. Słoczyński, T. Wiltowski, Journal of Catalysis 104 (1987) 71-79.

[128] M.R. Smith, U.S. Ozkan, Journal of Catalysis 141 (1993) 124-139.

[129] M.R. Smith, U.S. Ozkan, Journal of Catalysis 142 (1993) 226-236.

[130] J. Haber, E. Lalik, Catalysis Today 33 (1997) 119-137.

[131] R.A. Hernandez, U.S. Ozkan, Industrial & Engineering Chemistry Research 29 (1990) 1454-1459.

[132] J. Słoczyński, Journal of Solid State Chemistry 118 (1995) 84-92.

[133] W.V. Schulmeyer, H.M. Ortner, International Journal of Refractory Metals and Hard Materials 20 (2002) 261-269.

[134] J.G. Choi, L.T. Thompson, Applied Surface Science 93 (1996) 143-149.

[135] T. Ressler, R.E. Jentoft, J. Wienold, M.M. Günter, O. Timpe, The Journal of Physical Chemistry B 104 (2000) 6360-6370.

[136] E. Lalik, W.I.F. David, P. Barnes, J.F.C. Turner, The Journal of Physical Chemistry B 105 (2001) 9153-9156.

[137] G. Busca, E. Finocchio, G. Ramis, G. Ricchiardi, Catalysis Today 32 (1996) 133-143.

[138] W. Ueda, Y.-S. Yoon, K.-H. Lee, Y. Moro-oka, Korean Journal of Chemical Engineering 14 (1997) 474-478.

[139] Y. Moro-oka, Applied Catalysis A: General 181 (1999) 323-329.

[140] F.C. Meunier, A. Yasmeen, J.R.H. Ross, Catalysis Today 37 (1997) 33-42.

[141] G. Tsilomelekis, A. Christodoulakis, S. Boghosian, Catalysis Today 127 (2007) 139-147.

[142] A.N. Desikan, L. Huang, S.T. Oyama, The Journal of Physical Chemistry 95 (1991) 10050-10056.

[143] R.D. Roark, S.D. Kohler, J.G. Ekerdt, Catalysis Letters 16 (1992) 71-76.

[144] J.N. Armor, P.M. Zambri, Journal of Catalysis 73 (1982) 57-65.

[145] Y. Barbaux, D. Bouqueniaux, G. Fornasari, F. Trifirò, Applied Catalysis A: General 125 (1995) 303-312.

[146] L. Mendelovici, J.H. Lunsford, Journal of Catalysis 94 (1985) 37-50.

[147] Z. Song, N. Mimura, J.J. Bravo-Suárez, T. Akita, S. Tsubota, S.T. Oyama, Applied Catalysis A: General 316 (2007) 142-151.

[148] A. Maione, M. Devillers, Journal of Solid State Chemistry 177 (2004) 2339-2349.

[149] C.R. Dias, R. Zavoianu, M.F. Portela, Catalysis Communications 3 (2002) 85-90.

[150] R. Zăvoianu, C.R. Dias, A.P.V. Soares, M.F. Portela, Applied Catalysis A: General 298 (2006) 40-49.

[151] M. Carbucicchio, F. Trifirò, A. Vaccari, Journal of Catalysis 75 (1982) 207-218.

[152] A.N. Desikan, W.M. Zhang, S.T. Oyama, Journal of Catalysis 157 (1995) 740-748.

[153] M.C. Abello, M.F. Gomez, O. Ferretti, Applied Catalysis A: General 207 (2001) 421-431.

[154] E. Heracleous, A.F. Lee, I.A. Vasalos, A.A. Lemonidou, Catalysis Letters 88 (2003) 47-53.

Chapter 2

Monoliths: A review of the basics, preparation methods and applications

Abstract

The use of monolithic catalysts has extended from initial environmental applications to various other catalytic applications through the years. Here the preparation, from monoliths to monolithic catalysts is summarised. Also, a concise description of the manufacturing of ceramic and metallic monoliths is provided. Coating of gamma-alumina as a secondary support, coating active catalysts, high surface area monoliths and extruded monolithic catalysts are discussed herein, as are the coating of carbon and zeolites. The main foci are on understanding the methodology to produce monolithic systems and to relate these to appropriate applications. Ideas and concerns are also addressed herein to encourage better approaches to designing monolithic catalysts. A historical background, brief insight into hydrogenation and detailed development in oxidation are reviewed.

2.1 Introduction

Catalysis is one of the most important developments of the industrial age [1], with research growing rapidly as an ever demanding economy prospers. Heterogeneous catalysis is the most applied approach to catalysis, industrially, as compared to homogeneous catalysis and has seen major developments since large scale implication [1]. Heterogeneous catalysis covers several processes, such as catalytic combustion, hydrogenation, partial oxidation and oxidative dehydrogenation amongst many others. In addition, developments have involved the supporting of catalysts on appropriate supports, allowing for better dispersion of the catalytically active phase, improving mechanical strength and allowing for efficient use of the catalyst species. Examples of such catalyst supports are monoliths. Monolithic catalysts have had large commercial success in environmental applications since their incorporation in catalytic converters for automobiles [2]. Research has thus expanded to investigate the possible benefits of monoliths in various other catalytic applications. Monolithic catalysts offer several benefits over catalysts commonly in the pellet form, for use in fixed-bed reactors. Preparative methods, engineering aspects and uses of monolithic catalysts have been discussed previously in the literature [3, 4]. Published reviews include methods of depositing the active catalyst on the monolith surface [5], monolith reactors in heterogeneous

catalysis [6], the use of monoliths in multiphase reactors [7] and a brief introduction to monoliths in general [8]. An overall view of monoliths and the advancement in economically relevant applications have not yet been presented. The basic properties, the understanding of the preparation of monoliths and monolithic catalysts, uses and developments in applications have, hence, been summarised and are discussed herein.

2.2 Monoliths

2.2.1 Monolith basics

Monoliths are uniform blocks available in different shapes and sizes, sold primarily in ceramic or metallic forms [9]. The major manufacturers of ceramic and metallic monoliths include Corning and Johnson Matthey, amongst others mentioned by Tomasic and Jovic [9].

Monoliths are most commonly used in heterogeneous catalysis as catalytic support materials, whereby the active catalyst is coated onto the monolith surface and the reactant particles interact with the active phase within the channels, that are parallel throughout the body of the monolith [10]. The type of flow through the channels of the monolith is referred to as Taylor flow or bubble train flow, which involves the reactants moving through the channels in a circular type pattern or slugs, resulting in the formation of a thin film over the catalytic layer [11, 12]. The thin layer on the catalyst surface and the circular pattern results in an increase in the mass transfer and radial mass transfer, respectively, hence, a large rate of mass transfer and better selectivity toward a desired product [11, 12].

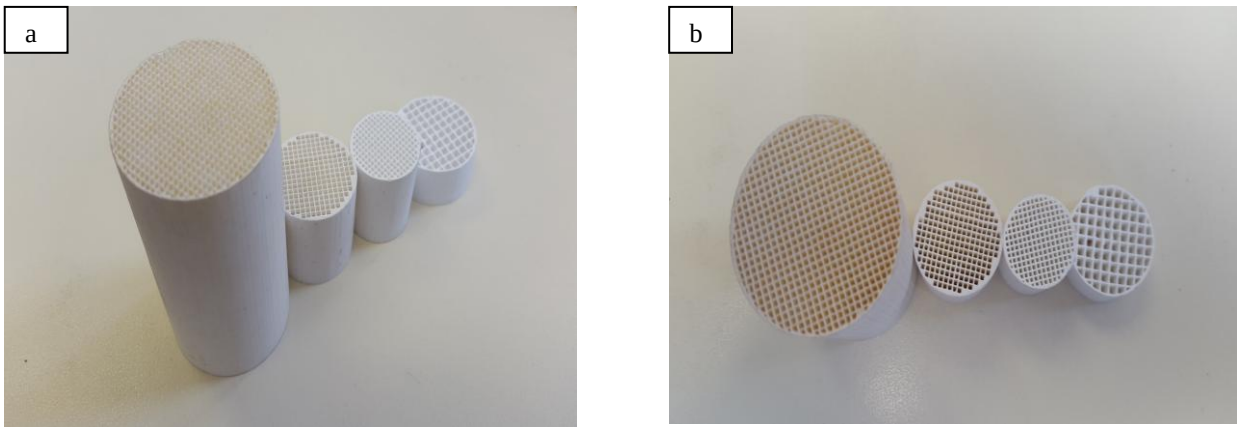

Figure 2.1: Monoliths with different cell densities/sizes, (a) side view (b) top view

Figure 2.1 shows different sizes of ceramic monoliths from a side and top view. As shown in both images, the lengths, diameters and channel widths may be different. The physical dimensions of a monolith are usually expressed by cell density, equation (1), in cells per square inch (cpsi), which is determined by the width of the channels [10, 13]. The geometric model of a monolith structure is discussed with a schematic representation and relevant equations (1) to (4) by Roy *et al.* [14] and Williams [4].

$$\text{Cell density} = 1/(l)^2 \quad (1)$$

$$\text{Open Frontal Area} = (l - t_w)/(l)^2 \quad (2)$$

$$\text{Geometric Surface Area} = 4\,(l - t_w)/(l)^2 \quad (3)$$

$$\text{Hydraulic diameter} = 4\,(\text{Open Frontal Area})/(\text{Geometric surface area}) \quad (4)$$

Where l = width/length of channel in inches and t_w = thickness of the wall in inches

Geometric surface area, Equation (3), is an important concept, such that a higher conversion of exhaust gases in catalytic converters can be achieved with a higher geometric surface area [10]. The hydraulic diameter, Equation (4), can be used to determine the effect on the hydrodynamics from the size of channels [14]. Monolithic catalysts have a large open frontal area, determined by Equation (4), as compared to catalyst pellets. They, hence, have a low pressure drop compared to geometric surface area, due to little resistance of flow through the channels [10, 13]. The lower resistance to flow allows for significantly higher gas hourly space velocities, as compared to conventional catalyst pellets. Higher gas hourly space velocities result in shorter contact times, which may result in greater yield of product, in a shorter time.

A secondary support, commonly gamma-alumina [10], is usually coated onto the monolith surface prior to the coating of the active catalyst due to the monolith having a low BET surface area. The adherence of the active phase to the monolith and the interaction between the active phase and secondary support may play an important role in the reaction occurring within the channels. Catalysts in the form of pellets and coated onto monoliths show different diffusion profiles of reactants through the catalyst bed, due to the variation in the size of channels exposed to the reactants. This may consequently result in a different product

profile to that of catalyst pellets. Kolaczkowski discusses in detail diffusivity of gases on a catalytic washcoat over a monolith [15]. In summary, the author provides evidence for researchers to improve monolith catalytic systems, by emphasising the importance of intra-phase diffusion and representative material size in diffusivity measurements.

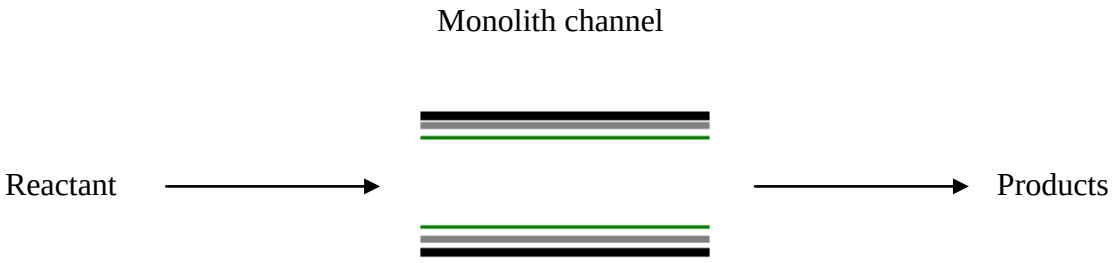

Where monolith wall = black, for example cordierite, secondary support = grey, for example gamma-alumina and catalyst layer = green, for example platinum

Figure 2.2: Reactant passing through a single monolith channel converting to products

A simple representation of a reactant, passing through a single monolith channel coated with a secondary support and active layer, interacting with the coated catalyst and, hence, forming products which exit through the end of the channel, is shown in Figure 2.2.

The chemical engineering principles of a monolith reactor are the same as those of a fixed bed/plug flow reactor, as discussed with kinetic expressions by Heck *et al.* [10] The significantly lower pressure drop offered by monolith reactors are explained by Boger and Sorensen [13] and Heck *et al.* [10], relating the pressure drop to surface area, respectively. Vergunst *et al.* have summarized equations for the monolithic reactor with respect to mass balances, mass transfer, gas phase reactions and catalytic effectiveness of the thickness of the active layer, in the application to hydrogenation [16]. These equations were used to aid the authors in indentifying the impact of cell density and coating thickness in the selective hydrogenation of phenylacetylene. Apparent from the study, was the definite effect of cell density and coating thickness, which concluded in the authors recommending a high cell density and thinner coating. It may thus be helpful to note that a higher cell density, hence, smaller channel width, would be the best approach for a lab scale reactor. A thinner coating, however, may result in a larger void space volume, thus creating volume for gas phase reactions. Further insight on mass transfer characteristics of monoliths with experimental data correlating to this has been provided by West *et al.* [17]. These principles and equations

with their relevant applications may assist in the understanding of the monolith reactor model.

2.2.2 Preparation of monoliths

Monoliths are commonly produced in ceramic or metallic forms. Ceramic and metallic monoliths differ greatly in physical and chemical properties, each having their respective advantages and disadvantages, which can prove important in a specific application. Ceramic monoliths have been used in many applications, such as automotive emission control, ozone abatement, water filtration and combustion processes amongst others [4]. Cordierite monoliths are used primarily in combustion processes due to their thermal stability over large temperature intervals [6]. It is important to consider the type of application and the catalyst when using ceramic and metallic monoliths, respectively. Adherence of the catalyst to the monolith surface will differ when using ceramic or metallic monoliths, since the material make up of these monoliths is completely different. Ceramic monoliths are advantageous over metallic monoliths due to superior properties, such as better porosity, hence good coating adherence, and thermal stability, whilst metallic monoliths offer advantages with respect to heat transfer, pressure drop, mechanical stability, wall thickness and overall volume [9]. Ceramic monoliths have good thermal stability due to a low thermal expansion coefficient, however, they can still crack under significant changes in temperature [3, 10, 12]. Also, metallic monoliths are becoming popular, despite the difficulty of catalyst adherence to the surface of the monolith. An example of this is the use of metallic monoliths in catalytic combustion, due to a lower pressure drop over the metallic monolith, than in ceramic monoliths, as well as a higher cell density that can be obtained with a thinner wall thickness [18]. However, despite the increase in the use of metallic monoliths, ceramic monoliths currently still dominate.

2.2.2.1 Ceramic monoliths

Ceramic monoliths are obtained by extrusion or corrugation with a variety of starting materials dependant on the application, with cordierite ($2MgO{\cdot}2Al_2O_3{\cdot}5SiO_2$), which can be confirmed by X-ray diffraction [19], being used extensively [9, 12]. Due to the cordierite structure of monoliths, a low surface area of less than 1 m^2/g is usually obtained [20]. Ceramic monoliths, as mentioned, are usually extruded with specially designed extruders, using the required starting materials and additives for the type of application, which are

commonly used for environmental applications [3, 9, 12, 21]. The process of extruding ceramic monoliths generally involves five basic steps. These are mixing of the dry solid oxides, adding the required plasticizers or other organic/inorganic additives, using the appropriate dies to extrude a particular shape needed, drying to obtain a uniform structure without cracking and finally firing the structure, thus forming ceramic cordierite and removing binders [21-23].

Corrugation involves adding inorganic oxides or salts to a mixture of starting materials, then the required additives, binders and plasticizers, using fibres for reinforcement, rolling and stacking and lastly calcining at the relevant temperature [6]. A more detailed account of the processes involved in extrudation and corrugation of ceramic monoliths has been provided by Avila *et al*. [22].

Another form of ceramic monoliths is that of ceramic foams. Ceramic foam monoliths are prepared by impregnating a polymeric foam with the required inorganic additives [24]. The foam monolith offers advantages such as improved radial transport and availability of different shapes made possible by the preparation method of the ceramic foam [24]. Reviews by De Luca and Campbell [25], followed by Lachman *et al.* [26-29] provide further summarized literature of preparative methods for ceramic monoliths.

Preparative methods for ceramic monoliths are also available in the patent literature [30, 31]. Forzatti *et al.* discuss in detail the rheological characterization of the paste when extruding, mixing and plasticizing, paste composition and drying and calcining in preparation of cordierite monoliths [21]. The importance and difference in the steps involved with the preparation methods for ceramic monoliths is highlighted extensively in the literature [4, 9, 21, 22] and patent work [32-35].

2.2.2.2 Metallic monoliths

Metallic monoliths are obtained through corrugation, and usually contain iron, chromium, aluminium and rare earth metals [9, 10, 36]. The corrugated sheets can be prepared in several ways and are then cut to obtain the required shapes, for example parallel or spiral type structures [6, 22]. The iron and aluminium are used to facilitate the monoliths reaching relatively high operating temperatures, whilst other metals are included to help with the adherence of the active catalyst layer onto the metallic monolith [6, 18]. Avila *et al*. discuss

the innovation involving the different alloys used for metallic monoliths, as well as the history of the design types [22]. There were several types of layered metallic monoliths developed between 1968 and 1991, with the major innovator being EMITEC [22, 37-39]. Figure 2.3 is an example of a metallic monolith designed by EMITEC.

Figure 2.3: EMITEC metallic monolith (reproduced with permission from Elsevier [9]).

Preparation of ceramic and metallic monolith structures may thus be an intensive process and a skilled art, requiring specialised equipment. Most researchers therefore resort to purchasing these monolith structures, as opposed to designing them from the starting materials. The unavoidable task, however, may be that of the preparation of the actual monolithic catalyst.

2.2.3 Preparation of monolithic catalysts

Monolithic catalysts may be prepared by coating an inert monolith support with the required secondary support followed by coating the active phase, impregnating the active phase onto an extruded high surface area monolith structure or incorporating the active phase into the monolith structure [9, 21, 22]. Ceramic and metallic monoliths as primary supports have low BET surface areas, as mentioned in Section *2.2.1*, therefore a secondary support is usually applied. The technique involved in the application of the secondary support onto the monolith is referred to as washcoating [15]. The secondary support layer is usually an inorganic oxide, which has a high surface area, is porous and can allow for efficient dispersion of the catalytically active phase. Ceramic monoliths have a macroporous structure, allowing for a porous secondary support to adhere to the monolith surface [3, 12]. Coating of metallic monoliths can be problematic due to a weaker adherence of the coat layer than on ceramic monoliths, however, a method such as anodisation of aluminium has been developed to attain a good secondary support and active phase coating [40]. The most

common secondary support applied to a monolith structure is gamma-alumina. Gamma-alumina allows for good dispersion of metal oxide species with differences in physical and chemical properties as opposed to the bulk oxide species [41]. Apart from the use of gamma-alumina as a secondary support for monoliths in the oxidation of alkanes, secondary support coating of gamma-alumina on monoliths has also been used in the wet oxidation of acetic acid [42] and for three way catalysts [43]. The coating methods and advantages of gamma-alumina on monoliths are outlined in the literature [44-47] and in several patents [48-51].

2.2.3.1 Gamma-alumina

Gamma-alumina is one of the most widely used catalytic supports, predominantly employed in the petrochemical and automobile industries, due to properties such as Lewis acidic and basic sites, good porosity and high surface area [52-54]. Gamma-alumina is generally formed from the heat treatment of boehmite above 450°C [54, 55]. The formation of the gamma-alumina phase from aluminium hydroxides or oxohydroxides is strongly dependant on temperature, and temperatures used, range between 450°C to 700°C [54, 55]. Paglia *et al.* have shown a gamma-prime-alumina phase at temperatures above 750°C from boehmite, which forms a triple cell structure of gamma-alumina [55]. Characterization of gamma-alumina can be done firstly by confirming the gamma phase using X-Ray diffraction, confirming high surface area by BET, comparison of micro images to literature by SEM and TEM, and infrared spectroscopy confirming the appropriate vibrational modes. Gamma-alumina has a spinel structure similar to that of the AB_2X_4 ($MgAl_2O_4$) structure [56], where in gamma-alumina magnesium is replaced by aluminium in the ideal $MgAl_2O_4$ structure [54, 57]. The defect in the structure due to the lack of a divalent cation and the presence of trivalent aluminium cations results in the formation of a cubic close packing of the oxygen lattice, as well as octahedrally and tetrahedrally situated aluminium atoms in the spinel structure [54, 57]. The macrostructure and acid/base properties of the surface of gamma-alumina were reported in detail by Trueba and Trasatti [54]. These properties exhibited by gamma-alumina may, therefore, be particularly useful as a secondary support coated over monoliths.

2.2.3.2 Coating methods for the gamma-alumina secondary support

In general, the coating procedure involves the repeated dipping of the monolith in a solution or slurry mixture, allowing it to soak for a few minutes, removing excess liquid from the

channels with compressed air, followed by calcination. This finally allows for the formation of the required secondary support layer, upon each repetitive coating cycle. Adaptations to the coating method can be easily made according to preference, such as continued dipping then drying and finally calcining, or constant rotation of the monolith upon repeated calcination. Repeated dipping, rotating, drying and final calcination may result in a more uniform coating across the channels [3]. The amount of coat layer on the monolith is usually expressed in weight percent. The weight percent coated may vary according to application and how active the catalyst may be. Successful coating of monoliths with gamma-alumina of up to 15 weight % has been reported [44], as well as coating up to 20 weight % using the sol-gel approach [58]. The thickness of the coating is thus an important factor when considering the application of the catalytic system, since open frontal area, geometric surface area and hydraulic diameter will be affected. A thicker coating may result in a decreased open frontal area, which could prove limiting to higher gas hourly space velocities or even diffusion of larger reactant molecules through the monolith channels. There are several important factors that need to be taken into consideration when applying a washcoat to a monolith structure. These factors may include pH, slurry concentration, appropriate calcination, drying or specific techniques for a required application.

The techniques for coating result in pore filling or deposition of a coated layer on the support [3]. Pore filling occurs when using sol-gel or colloidal suspensions which allows for the pores within the monolith structure to be mostly filled with the washcoat, whereas deposition of a layer can be achieved with slurry coating, allowing for the coat layer to adhere to the pores [3]. An advantage of the pore filling technique would be a smaller decrease in the open frontal area of the monolith, as opposed to slurry coating, and strong adherence of the coat layer with the monolith structure. The disadvantage, however, would be the limitation of macropore volume of the structure [3]. The disadvantage of slurry coating would be a larger decrease in open frontal area of the monolith. An advantage of a higher loading of washcoat [3, 59] is that a higher loading of active catalyst may be achieved with slurry coating. The pore filling technique may be best suited for a highly active catalyst, since a low loading of catalyst will be sufficient, whereas for a less active catalyst more catalyst may be coated onto a slurry coated monolith.

2.2.3.2.1 Colloidal coating

Colloidal coating is a pore filling technique, using particles of the nano scale size to allow for strong adherence to the monolith surface. Colloidal particles may be produced via different methods. Beauseigneur *et al*. report an average particle size between 1 to 100 nm in the colloidal coating of monoliths for exhaust gas treatment [60]. Larsson *et al*. used boehmite powder with hydrochloric acid to produce the required colloidal solution, followed by calcination producing the gamma-alumina coating onto the monolith [61]. Colloidal alumina can also be prepared successfully from commercial boehmite peptized in acidic solution [62]. The gamma-alumina phase is produced by calcination between 500 °C to 700 °C of the peptized boehmite [63]. Colloidal alumina is now easily available and water can be used in the dispersion technique, thus, Özdemir *et al.* use colloidal alumina dispersed in water to coat monoliths for carbon monoxide oxidation [64], while Barbero *et al.* reported successful coating of their metallic monoliths with the use of colloidal alumina as a primer and a suitable stabiliser [65]. Perhaps for the ease of convenience purchasing colloidal alumina may be the better option, unless researchers intend on approaching new methods of colloidal coating.

2.2.3.2.2 Sol-gel

A sol refers to the dispersed form of a colloidal solution and in which gelation occurs when an interlinked network is formed between the particles, therefore sol-gel is a dispersed form of the interlinked particles [66]. The sol-gel method for coating monoliths involves the secondary support being in the dissolved form, therefore, forming gamma-alumina upon calcination after dipping of the monolith in the solution. This results in better pore filling of the monolith as compared to colloidal coating [3]. A sol can be prepared via a hydrolytic route or non-hydrolytic route as shown in Equations (5) and (6) [36].

$$M(OR)_n + nH_2O \longrightarrow M(OH)_n + nROH \quad (5)$$

$$\text{-M-OH} + \text{HO-M'-} \longrightarrow \text{-M-O-M'-} + H_2O \quad (6)$$

Where M = metal, for example aluminium

Equation (5) shows the hydrolysis reaction of the metal alkoxide using a suitable acid or base and water [36]. During the sol preparation with heat treatment and time, condensation

occurs, as shown in Equation (6) [67]. A more detailed description of the sol-gel process is presented by Schmidt [67]. Xiaoding *et al.* reported a study of sol-gel coating of monoliths via three types of aluminium sols, namely pseudoboehemite with urea and nitric acid, hydrolysis of aluminium chloride and aluminium powder, and hydrolysis of tri-sec-butoxide aluminium [68]. It was concluded that sols prepared via pseudoboehimite with urea and nitric acid and hydrolysis of tri-sec-butoxide are most suitable for sol-gel alumina coating of monoliths [68]. A typical sol-gel method of coating involves dipping the monolith in a sol from pseudoboehimite, urea and 0.3M nitric acid in a weight ratio of 2:1:5, followed by emptying the channels, drying and finally calcination [69]. The sol-gel method for coating may thus be advantageous over colloidal coating, however, the maximum capacity for sol-gel coating on the monolith structure has not been reported.

2.2.3.2.3 Slurry coating

Slurry coating involves using a gamma-alumina suspension, usually with a larger particle size as compared to colloidal coating, preferably between 2 µm and 5 µm for strong adherence to the monolith surface [59]. The general procedure uses an acid to disperse the alumina, the monolith is then dipped in the slurry, after which excess liquid is removed by blowing compressed air through the channels, followed by drying and calcination or direct calcination [45, 70]. Wet milling of the gamma-alumina to attain a required particle size is very important, as factors such as pH and viscosity play a key role in adhesion to the monolith surface [70]. The particles inside a typical stirred mill are highly influenced by stress energy, number of stress events and specific energy [71]. Milling can be a tedious process to attain a required particle size, however, gamma-alumina is available commercially with an average particle size less than 5 µm.

The most effective acid in slurry coating is nitric acid which helps to stabilise the slurry and allows for a better washcoat uptake [72]. The percentage solids in the slurry also plays an important role in the efficacy and homogeneity of the coating [45]. Important to note is that with the technique of slurry coating, monoliths need to be coated in batches, since continued coating may result in an increase in the viscosity of the slurry mixture. This increase in viscosity may seriously impact on the homogeneity of the coating. Capillary forces allow for water to be drawn into the pores of the monolith structure which creates competition for adherence of the slurry [73]. An intermediate prewetting step discussed by Mogalicherla and

Kunzru allowed for a high washcoat loading to be achieved [73]. Agrafiotis and Tsetsekou have reported an optimum slurry concentration of 45 weight % solids and viscosity between 50 and 150 mPa·s [45]. Villegas *et al.* reported homogeneous gamma-alumina coating with 25 weight % solids [44], revealing that a high weight percent coating may be achieved via slurry coating.

Dispersible powders of boehmite or aluminium hydroxide can be used to produce gamma-alumina on the monolith surface after calcination [44, 59]. It was reported, however, that an average particle size of alumina of 3 μm allowed for a higher loading of alumina to be achieved, as well as good adhesion properties as compared to boehmite type powders [44]. Slurry coating may, therefore, be ideal for a high weight percent coating and the particle size of the alumina being coated may be controlled. The method of slurry coating may, therefore, offer less coating repetitions and good adherence of gamma-alumina. Considering advantages such as these, slurry coating may be more practical and less time consuming than the other coating approaches mentioned.

Characterization of the secondary support coating is usually performed by SEM, which may be used to show the coating inside the channels of the monolith as compared to a bare monolith. This characterization technique can further be used to assess the homogeneity of the coating and also aid in measuring the coating thickness. Figures 2.4 (a) and (b) show sectioned ceramic monoliths prior and after coating with 10 weight % gamma-alumina, by method of slurry coating. After coating of the secondary support, a layer is obtained within the monolith channels, which may provide for better interaction with the active layer as compared to the bare monolith.

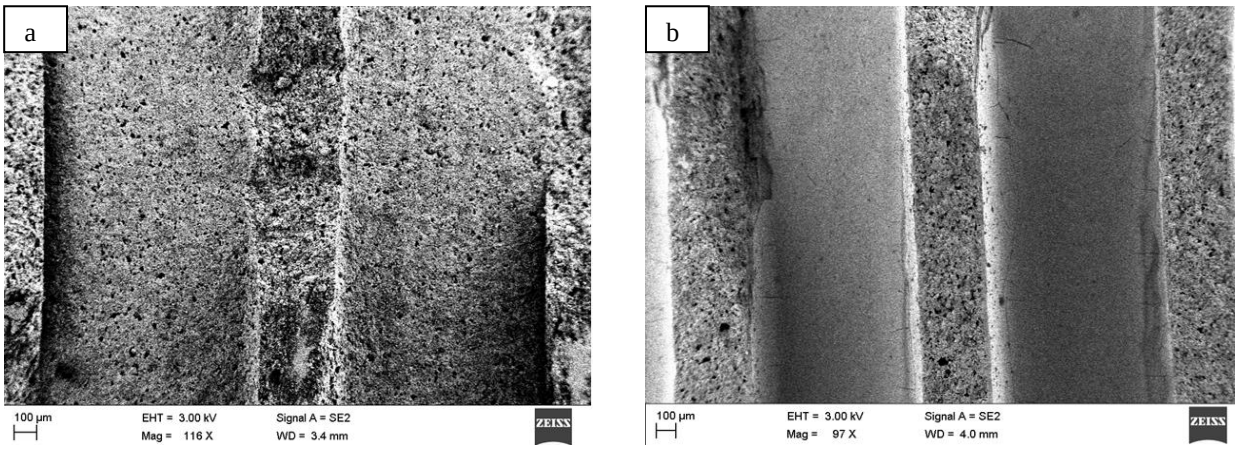

Figure 2.4 SEM images of channels of monolith: (a) uncoated (b) coated with 10 weight % gamma-alumina

2.2.3.3 Coating of the active catalyst

The active component can be incorporated onto the monolith surface with the washcoat layer of the high surface area oxide or it can be coated onto the washcoat layer by impregnation, deposition precipitation, ion-exchange, sol-gel and growth of the active components in situ [74]. Impregnation and deposition precipitation are the most common methods used to coat the active layer. Coating of the active phase on the monolith is just as important as the washcoat layer of the high surface area oxide. The metals should be distributed uniformly on the washcoat layer or on the bare monolith. A general procedure for coating of the active phase involves dipping of the monolith in the solution or mixture, blowing out excess liquid from the channels, drying and calcination at the required temperature. Factors that should be considered include, type of application, active species required, amount of catalyst species required and method of coating of active phase. Coating of the active phase similarly may impact the geometric properties, as in washcoating of the secondary support. Considering a highly active catalyst, less catalyst should be used and vice versa, since a high selectivity to desirable products may be achievable from fine tuning the appropriate gas hourly space velocities. An appropriate example would be coating noble metal catalysts, which are expensive, however, highly active when coated on monoliths [75, 76].

2.2.3.3.1 Impregnation

Impregnation usually involves preparing a solution of the active metals or components which can be easily drawn up the monolith surface by capillary forces. Klinghoffer *et al.* describe the coating of platinum onto alumina coated monoliths by dissolving the platinum catalyst, originally prepared via incipient wetness, in double distilled water followed by dipping of the

monoliths, drying and lastly calcining [42]. The impregnation procedure can be applied across monoliths with different material make up, such as silica monoliths as reported by Xiaodong *et al.*, who describe coating an iron/copper catalyst using mixed solutions of iron nitrate and copper nitrate [77], and ceramic monoliths as reported by Thimmaraju *et al.*, describing coating of molybdenum(VI) onto ceramic monoliths with suitable characterization [78]. Impregnation may prove useful dependent on the application. An example of this, is the use of impregnation in enhancing the performance of noble metal coated three way catalysts [79]. The technique of impregnating the active catalyst can also be applied to coating metallic monoliths [18]. The successful coating of monoliths by impregnation has also been reported in several patents [80-83]. Impregnation usually results in non-uniform distribution of metals and is not a reproducible method [84]. Methods of microwave heating or freeze drying can be used to solve this problem [84] or, alternatively, deposition precipitation may be used upon preference.

2.2.3.3.2 Deposition precipitation

Deposition precipitation involves the precipitation of a metal salt with a base [85], however, applying this to a monolithic support may be more difficult and an inhomogeneous coating may often be obtained. Barrio *et al.*, conversely, reported a homogeneous coating achieved by redox deposition precipitation, in which acetone is used as a solvent to coat the monoliths with manganese oxide [86]. The most common approach to deposition precipitation coating of monoliths involves the use of urea as the precipitating agent, where for example Carnö *et al*. supported manganese and platinum onto monoliths [87]. The metal salt and precipitating agent are in the liquid phase, therefore, the monolith can be dipped into this solution and calcined. During calcination, the urea decomposes, allowing for an increase in pH and hence precipitation of the required active phase [3, 87]. Deposition precipitation can also be used to coat metallic monoliths. Frias *et al*. use the basis of deposition precipitation for coating of monoliths as being more energetically favourable when the active phase is formed over the monolith surface [88]. Monolithic catalyst preparation by deposition precipitation has been used in diverse applications such as biomass gasification [89], methane combustion [90], oxidation [86, 87] and selective catalytic reduction [91].

Concerning active phase coating, it may be important to note that not all catalysts may be coated via impregnation or deposition precipitation. Adapting the original preparation

method of a powder catalyst for coating on monoliths may impact on the surface properties. Thus variations of coating procedures may be required and approaches such as sol-gel coating [92] or solution-combustion [93] may, hence, be of interest. The preparation of monolithic catalysts by these techniques require the preparation of a precursor sol or solution, followed by repeated dip coating and calcination to form the active layer. These methods may be used to obtain smaller particle sizes and, therefore, better interaction between the active layer and monolith or secondary support.

2.2.3.4 Coating of metallic monoliths

Metallic monoliths, similarly to ceramic monoliths, have a low surface area, hence, a washcoat of a secondary support is required. The main problem associated with coating metallic monoliths is the adhesion of the secondary support layer, however, using higher aluminium content in the preparation of the metallic structure may allow for better adhesion [18, 94]. The coating method may also influence the adhesion properties of the high surface area oxide on the metallic surface, therefore, coating methods such as oxidation of bulk aluminium [95], slurry coating [2], chemical vapour deposition [96] and anodisation of aluminium [40, 97] have been developed and used. The preparation procedure for coating can significantly influence the activity of the catalysts, as shown by Zwinkels *et al*., when preparing metallic monoliths for combustion catalysis [98]. Coating of the active phase after coating with a secondary support may be achieved similarly as for ceramic monoliths. An example of such is the impregnation of palladium after sol-gel coating of gamma-alumina [99], whilst a further example is the washcoating of Pt-ZSM5 [100]. Coated metallic monoliths are, hence, being used as catalysts in several fields, such as combustion [65, 101], Fischer-Tropsch [102, 103] and oxidation [104], due to a better understanding of coating and the benefits thereof.

2.2.3.5 Coating zeolites and carbon onto monoliths

Zeolites are known to be highly selective and can produce high yields in numerous reactions, hence, coating different zeolites onto monoliths, as reported [105], can prove useful. The use of zeolites on monoliths is advantageous due to the possibility of coating smaller zeolite particles, which would not cause problems with pressure drop [106]. Selectivity can also be tuned with the high gas space velocities attainable with monoliths. Zeolites can be coated directly onto monoliths via two methods, namely hydrothermal synthesis or slurry coating

[107]. Coating of zeolites onto the ceramic monolith surface is possible due the macroporous structure of the monoliths allowing for adherence of the zeolite layer [107]. Hydrothermal synthesis results in a stronger interaction between the zeolite coating and the surface of the monolith, when compared to slurry coating [107, 108]. A more detailed understanding has been provided by Ulla *et al.*, discussing direct hydrothermal synthesis and secondary hydrothermal synthesis of ZSM-5 zeolites on cordierite monoliths, highlighting the properties of zeolites on the monoliths [108]. Li *et al.* report a different approach via an in situ hydrothermal method for the coating of zeolites on cordierite monoliths [106]. The authors focus on how preparative factors influence the growth of zeolites on monoliths. In contrast to common methods of coating zeolites, dip coating may also be used via a mixture containing BEA zeolite crystals, a suitable solvent, binder and surfactant [109].

Carbon coated monoliths are typically used in environmental applications, for example in selective catalytic reduction systems [110]. The main advantage of using carbon as a support is the stability in acidic or basic media [111], which may possibly prove useful in the presence of corrosive gases. Another advantage is the ability to recover the active phase, such as precious metals used in environmental applications [111, 112]. Carbon coating may usually be achieved by dip coating a monolith into a liquid polymer that has been crosslinked and carbonised, followed by curing to the required temperature [113]. A review of the preparation of carbon coated monoliths and applications in catalytic and adsorptions processes thereof has been presented by Vergunst *et al.* [114]. In particular, they also describe in detail the preparation of carbon coated monoliths via furfuryl alcohol based polymers [115]. The authors underlined the problem associated with carbon coating, which is shrinkage of the polymer coating resulting in incomplete coverage of the monolith with the coating. In comparison, Garcia-Bordeje and co-workers were able to optimize carbon coating of monoliths via Novolac and furan resins [112]. These authors raised fundamental factors that impact on the coating, which are the viscosity of the dip coating mixture and the individual properties of the resins. An example of such an impact is that the yield of each resin was established as being different [112]. The potential of carbon monoliths are being realised, especially with regard to lowering the environmental impact of catalytic processes and it may be fitting to suggest that we may see numerous research efforts dedicated to this aspect in the future.

Coating monoliths with carbon nanotubes is also being studied. Carbon nanotubes are used predominantly as supports in catalysis and have proven effective, as such, in hydrogenation [116], ammonia synthesis [117] and Fischer-Tropsch synthesis [118] amongst other applications. Monoliths offer a favourable characteristic of high geometric surface area for growth of carbon nanotubes as compared to the powder form of carbon nanotubes [117]. Carbon nanofibres have also been successfully grown onto gamma-alumina coated cordierite monoliths [69, 119].

2.2.3.6 High surface area monoliths

High surface area monoliths are extruded similarly to ceramic monoliths using the relevant materials required as indicated by Avila *et al.* [22] and Forzatti *et al.* [21] Materials used are generally alumina powder, organic binders and precursors required to hold the monolith structure together [4]. Lower firing temperatures are also required to allow for good porosity and to maintain high surface area [4, 120]. Significantly higher surface areas are attainable, compared to ceramic cordierite monolith extrusion, with the compromise of added agglomerants which remain in the monolith structure [22]. Pillared clays have been used to produce monoliths with a surface area above 220 m^2/g [23]. Xiaodong *et al.* reported the preparation of a silica monolith via a sol-gel reaction of tetramethoxysilane, producing a monolith with surface area 648 m^2/g, having mesopores and macropores [121].

High surface area monoliths are used predominantly in environmental applications, such as in selective catalytic reduction [122] and mineralization of volatile organic compounds [123]. The properties of these monoliths differ significantly compared to ceramic and metallic monoliths, since they are more porous and contain acidic and basic sites. The thermal stability of the structure, however, may be questionable. Considering the improved porosity and more acidic and basic sites, high surface area monoliths may be seen as advantageous in some environmental applications as opposed to ceramic or carbon coated monoliths.

The disadvantages of high surface monoliths may include lower mechanical strength of the structure and a more complex understanding of catalyst interaction with the high surface area material used to produce the monolith. Another disadvantage may include the use of these structures in applications other than environmental, since the monolith itself may be highly active due to the properties mentioned herein. Despite this, however, diversity of the use of high surface monoliths is currently under investigation with applications in selective carbon

dioxide adsorption [124], separation of molecules [125], gas storage [126] and biocatalysis [127].

2.2.3.7 Extruded/Integral monolithic catalysts

Extruded monoliths or integral monoliths, as they are termed, contain the catalytically active component within the monolith structure. The entire monolith is, therefore, made of the catalyst, by extruding it through specialised equipment. Disadvantages of the preparation methods for integral monolithic catalysts generally outweigh the advantages. The main advantages, however, may include fewer steps required in the preparation, as well as a non questionable active coating homogeneity, due to the monolith being extruded. Extrudation of these monolith structures on the contrary are quite complex. Intensive thought into the design may be needed, as maintaining the active species will be imperative. A matter of concern, with regard to the entirety of the structure, may be the mechanical strength of the monolith. The extruded monolith may also not offer the most efficient use of the catalyst species, especially when using noble metal catalysts. The general steps involved in extrudation of the monolith would need to be adjusted according to preference, so as not to destroy the catalytic species during preparation.

Forzatti *et al.* highlight that the high surface area support becomes the predominant component and the active phase the minor component, in an extruded monolithic catalyst system [21]. The preparation methods for extruded monolithic catalysts are thus more expensive and specialised than the coated monolithic catalysts. Extruded monolithic catalysts are mainly used in environmental applications, such as selective catalytic reduction, as discussed by Lachman and Williams [29]. The advantage of using extruded monolithic catalysts in these environmental applications is the resistance to deactivation, as compared to applying an active layer over a secondary support [22].

2.2.4 Historical applications and new developments

Industrial application of monolithic catalysts began in 1966 with the clean up of nitric acid tail gases, using a ceramic catalyst coated with palladium, which removed oxides of nitrogen [6, 128]. The initial success intrigued many researchers and industries, which allowed for large platform onto which ideas could be built. Monolithic catalysts were later used in car exhausts as three way catalysts for emission control [6].

The era of research into catalytic converters containing monolithic catalysts developed due the benefit of a lower pressure drop, which lead to automobiles being equipped with catalytic converters in 1975 [129]. These catalytic converters contained a cordierite ceramic monolith structure, developed by Corning Incorporated, washcoated with an alumina support and a mixture of a low loading of platinum group metals, such as platinum, rhodium and palladium, as the catalytically active layer [9, 129]. Research into the use platinum group metals was primarily due to factors such as higher activity, high throughput with high concentration of sulphur in the reactant gas, thermal stability and durability [130]. Catalytic converters gained significant attention due to the increase in the production of automobiles and stringent regulations with respect to emissions. Farrauto and Heck have published their perspective of catalytic converters in combustion engines, which describes the understanding and design of catalytic converters through to the possible challenges [131]. Several other informative publications are available on automotive catalysis, discussing the successes and future challenges [132-135]. Numerous valuable innovations using monoliths in catalytic converters over the past years have been patented [136-140].

The large scale implication and success of monoliths in exhaust gas clean up also lead to further interest and development, resulting in environmental industrial applications such as flue gas treatment [9, 10]. Research expanded from this initial application to catalytic combustion, oxidation catalysis and hydrogenation, amongst other possible applications. These areas of research possibly show the most promise for the use of monolithic catalysts, due to industrial growth and the need for development. Applications such as these could prove useful in the global concern of environmental issues and offer more sustainable economic expansion.

2.2.4.1 Environmental applications and catalytic combustion

A main development in the use of monolithic catalysts is that of combustion of volatile organic compounds. Catalytic combustion processes are usually operated at high temperatures and have a high gas throughput, therefore temperature control and pressure drop are important factors when designing reactor systems [141]. The advantages of using monoliths in catalytic combustion are thus understandable. Volatile organic compounds are known to contribute significantly to air pollution and hence global warming, therefore the designs of efficient combustion systems for eliminating these compounds are continually

being improved. The use of monoliths in the destruction of these volatile organic compounds has resulted in lower costs and better efficiency over the conventional catalysts used initially [142].

Tomasic provides a detailed insight into using monoliths in $DeNO_x$ catalysis, including exhaust gas clean up and modelling of monolith reactors for NO_x environmental treatment [143]. In environmental applications, typically noble metals are used due to a high activity and improved efficiency when coated on monoliths [144]. The most successful example of this would be the catalytic converter used in automobiles as a three way catalyst system. The problems encountered in these systems are emissions during cold start, thermal stability and deactivation [72]. A more informative view of the role and attempts to improve monoliths as three way catalytic converters is provided by Gokalp, where new developments are also discussed [145]. Combustion and three way catalytic systems are undoubtedly central applications of monoliths, but monoliths may prove valuable in other catalytic processes.

2.2.4.2 Hydrogenation

Hydrogenation is typically performed in the pharmaceutical and fine chemical industries, although large scale applications are also common [141]. The former hydrogenation reactions were previously performed in batch reactors, however, this posed several hazards and therefore continuous flow conditions are now a common trend [146]. Continuous flow reactors are commonly operated at high pressures to attain better selectivity to desired products [146]. Hydrogenation reactions have problems with mass transfer characteristics [147], where monoliths may prove advantageous.

Hatziantoniou *et al.* performed a study of mass transfer effects and selectivity for hydrogenation of nitro compounds using a monolithic catalyst, attributing the high activity to the mass transfer steps being rate determining [148]. Xiaoding *et al.* reported nickel coated monoliths for the hydrogenation of benzaldehyde in an attempt to achieve improved selectivity, and showed better selectivity and conversion than conventionally used catalysts [149]. In comparison to a stirred tank and trickle bed reactor in hydrogenation, a monolith reactor showed greater selectivity to the desired product [143]. The diverse applications of monoliths can be seen in the investigation of monolithic catalysts for the hydrogenation of edible oil, where comparing this system to the conventional slurry reactor showed a reduction in cost for monolithic system [147].

Although hydrogenation is a prominent field in industrial catalysis, an area of greater interest may be that oxidation catalysis. The economic and environmental implications of implementing monoliths in the heterogeneous gas phase oxidation of alkanes may certainly outweigh other applications. It is for these reasons that we see significant research conducted in the form of oxidation catalysis using monolithic catalysts.

2.2.4.3 Oxidative dehydrogenation and partial oxidation

Alkanes can be oxidatively dehydrogenated to produce more valuable products such as olefins and oxygenates. Industrially, conversion and selectivity to valuable products should be high, in order to operate efficient reactors and maximise profit. A study performed by Huff and Schmidt on the oxidative dehydrogenation of ethane using monoliths revealed interesting information on the role of coating platinum group metals on monoliths [150]. The platinum coated monolith showed the greatest activity (> 80 %) and selectivity (70 %) towards ethylene formation, whilst rhodium facilitated the production of mainly synthesis gas and the use of palladium encouraged carbon formation. The authors attributed production of ethylene via an initial oxidative dehydrogenation mechanism on platinum followed by β-hydrogen elimination and finally desorption of ethane. Huff and Schmidt claimed this mechanism holds true for longer chain alkanes and isobutane [151-153]. In the partial oxidation of medium length alkanes, Dietz *et al.* observed the formation of oxygenates as well as olefins, which they concluded was a similar product profile to that of thermal pyrolysis [154]. Converse to the mechanism claimed by Huff and Schmidt [150], Beretta and co-workers were able to prove, in a comprehensive study of the oxidative dehydrogenation of propane via a annular reactor, homogeneous gas phase reactions were responsible for the high yield of olefins [155, 156]. The authors performed a series of homogeneous gas phase reaction experiments, which showed high selectivity (> 55 %) toward olefins at a high conversion, similar to that of catalytic testing with the platinum/gamma-alumina coated ceramic support. The increase in olefin selectivity was attributed to short contact times, whilst carbon oxides were confirmed as the terminal products from these radical reactions.

Beretta *et al.* further went on to provide evidence of homogeneous gas phase reactions in the oxidation of propane under autothermal conditions [157]. The platinum catalyst coated on metallic support was suggested as the initiator of the radical reaction process. Radical reactions are initiated by hydrogen abstraction, consequently yielding an akyl radical and

peroxy specie, which can further react to generate numerous non-selective products. The product profile observed in the oxidative dehydrogenation of propane [157] and when extended toward ethane oxidation [158], therefore supported the conclusion of a radical type mechanism.

Promoting the platinum coated monolith system with tin or copper, in autothermal oxidation of ethane, was shown to enhance the yield of ethylene [159]. Hakonsen and co-workers were able to corroborate these results with a platinum-tin impregnated monolith, however, were unable to rule out gas phase reactions [160]. In the cases presented herein, the addition of a promoter may perhaps contribute to an increase in the rate of propagation of the radical mechanism as opposed to a catalytic involvement. Considering that void space may impact significantly on the gas phase reactions, utilizing monoliths with a higher cell density may aid in decreasing void space, hence retarding radical reactions. This concept was applied by Sadykov and co-workers, whereby micromonoliths were used in the oxidative dehydrogenation of propane [76]. The authors were able to fine-tune reaction conditions, implementing aspects such as an excess of hydrocarbon to consume almost all oxygen and the use of promoters, as well as a reactor design enabling rapid quenching of products. A propylene selectivity of up to approximately 30 % at a 63 % conversion was achieved from implementing these aspects.

In contrast to the claim of the formation of carbon oxides via terminal gas phase reactions [155], Silberova and researchers ascribed the contribution of heterogeneous reactions on platinum coated monoliths toward the formation of carbon oxides and hydrogen gas, in the oxidation of ethane and propane [161]. Hickman and Schmidt were the first to report the activity (~ 80 % conversion) of platinum and platinum-rhodium coated monoliths in the oxidation of methane toward syngas [162]. The suggested mechanism was that of methane pyrolysis, forming hydrogen gas and carbon which may be oxidized to carbon monoxide. A continued study in the partial oxidation of methane revealed rhodium coated monoliths as the better catalyst in the formation of CO and H_2 [163]. These co-workers attributed a superior catalytic system by rhodium, with a higher activation energy barrier for the formation of water as compared to that of platinum. The reaction using rhodium may therefore be driven toward the formation of hydrogen and carbon monoxide, as opposed to facing a competing mechanism of hydrolysis. In accordance with these results, Hickman and Schmidt further

published a detailed explanation, involving the mechanistic chemistry and kinetics of syngas formation via platinum and rhodium coated monoliths [164].

The role and impact of the use of monoliths in oxidation catalysis has been not been ignored and has even been suggested [165, 166] and modelled [167] for industrial application of commonly used processes. Numerical and theoretical studies have also been performed in an attempt at improving established monolithic systems [168-170]. For the development of viable catalytic applications of monoliths, it may be of importance to consider factors such as the washcoat, support material and amount of loading, since these factors do influence catalytic results [171, 172]. The trends amongst the latest oxidation applications of monolithic catalysts include using carbon dioxide as an oxidant [173], steering selectivity towards desired products such as ethene from ethane [174], partial oxidation of methane rich mixtures [170] and preferential oxidation of carbon monoxide [175, 176] and the oxidation of longer chain alkanes [172, 177].

2.3 Conclusion and perspective

The inception and success of monoliths in oxidation catalysis may have encouraged the interest in diversifying monolith catalytic systems. Even so, heterogeneous oxidation catalysis remains highly important and further research is needed. A significant number of contributions in literature and patent work have been provided for the novice or experienced scientist concerning the coating of monoliths. In particular, gamma-alumina is shown as the most common high surface area support used and it is applied to several catalytic systems.

Although secondary support coating of monoliths via gamma-alumina may increase surface area and improve interaction of the catalyst species, this may not be the best option for the optimum interaction between the support and various active species. Zirconia and titania may also be other secondary supports to consider. Supplementary research is subsequently being done on high surface area monoliths and extruded monoliths to exploit any advantages possible.

Coating the active phase by commonly used methods, such as impregnation and deposition precipitation, have their respective advantages and disadvantages and are dependent on the application. Relatively new coating methods, however, have been developed such as sol-gel and solution-combustion. Important to consider, may be the catalyst species required, which

will prompt the researcher to approach a combination of coating techniques to produce the desired active layer. The greater speciality an application may require, consequently, may demand a larger investment toward the design technology of the monolithic system. It is our opinion nevertheless, monolithic catalysts may be used more extensively in the future, especially in the oxidation alkanes. Therefore, the work in Chapter 3 will report the oxidation of *n*-octane over a monolithic catalyst. Understanding that homogeneous gas phase reactions may play a role in the oxidation of *n*-octane over monoliths, Chapter 3 will report testing uncoated monoliths and coated monoliths, as preliminary work, which perhaps will provide informative for future rigorous research.

2.4 Acknowledgements

We would like to thank SASOL, the NRF and THRIP for financial support.

2.5 References

[1] M. Bowker, The Basis and Applications of Heterogeneous Catalysis, Oxford University Press Incorporated, New York, 1998.

[2] M. Valentini, G. Groppi, C. Cristiani, M. Levi, E. Tronconi, P. Forzatti, Catalysis Today 69 (2001) 307-314.

[3] T.A. Nijhuis, A.E.W. Beers, T. Vergunst, I. Hoek, F. Kapteijn, J.A. Moulijn, Catalysis Reviews: Science and Engineering 43 (2001) 345-380.

[4] J.L. Williams, Catalysis Today 69 (2001) 3-9.

[5] V. Meille, Applied Catalysis A: General 315 (2006) 1-17.

[6] A. Cybulski, J.A. Moulijn, Catalysis Reviews 36 (1994) 179-270.

[7] S. Roy, T. Bauer, M. Al-Dahhan, P. Lehner, T. Turek, AIChE Journal 50 (2004) 2918-2938.

[8] S.M. Soltani, S. Hosseini, M.R. Malekbala, Journal of Applied Sciences Research 9 (2013) 2548-2560.

[9] V. Tomasic, F. Jovic, Applied Catalysis A: General 311 (2006) 112-121.

[10] R.M. Heck, S. Gulati, R.J. Farruto, Chemical Engineering Journal 82 (2001) 149-156.

[11] T.A. Nijhuis, M.T. Kreutzer, A.C.J. Romijn, F. Kapteijn, J.A. Moulijn, Chemical Engineering Science 56 (2001) 823-829.

[12] F. Kapteijn, T.A. Nijhuis, J.J. Heiszwolf, J.A. Mouljin, Catalysis Today 66 (2001) 133-144.

[13] T. Boger, A.K. Heibel, C.M. Sorensen, Industrial Engineering Chemistry Research 43 (2004) 4602-4611.

[14] S. Roy, A. K. Heibel, W. Liu, T. Boger, Chemical Engineering Science 59 (2004) 957-966.

[15] S.T. Kolaczkowski, Catalysis Today 83 (2003) 85-95.

[16] T. Vergunst, F. Kapteijn, J.A. Moulijn, Industrial Engineering Chemistry Research 40 (2001) 2801-2809.

[17] D.H. West, V. Balakotaiah, Z. Jovanovic, Catalysis Today 88 (2003) 3-16.

[18] F.N. Aguero, B.P. Barbero, O. Sanz, F.J.E. Lozano, M. Montes, L.E. Cadus, Industrial Engineering Chemistry Research 49 (2010) 1663-1668.

[19] F. Zhao, G. Zhang, P. Zeng, X. Yang, S. Ji, Chinese Journal of Catalysis 32 (2011) 821-826.

[20] E. Soghrati, M. Kazemeini, A.M. Rashidi, K.J. Jozani, Procedia Engineering 42 (2012) 1484-1492.

[21] P. Forzatti, D. Ballardini, L. Sighicelli, Catalysis Today 41 (1998) 87-94.

[22] P. Avila, M. Montes, E.E. Miro, Chemical Engineering Journal 109 (2005) 11-36.

[23] F. Mohino, A.B. Martin, P. Salerno, A. Bahamonde, S. Mendioroz, Applied Clay Science 29 (2005) 125-136.

[24] W.M. Carty, P.W. Lednor, Current Opinion in Solid State and Materials Science 1 (1996) 88-95.

[25] J.P. De Luca, L.E. Campbell, Monolithic catalyst supports, in: J.J. Burton, K.L. Garten, (Eds.), Advanced Materials in Catalysis, Academic Press, London, 1977.

[26] I.M. Lachman, R.N. McNally, High-Temperature Monolithic Supports for Automobile Exhaust Catalysis, Second ed., John Wiley and Sons Incorporated, Singapore, 1981.

[27] I.M. Lachman, R.M. McNally, Chemical Engineering Journal 81 (1985) 29-31.

[28] I.M. Lachman, Sprechsaal 119 (1986) 1116-1119.

[29] I.M. Lachman, J.L. Williams, Catalysis Today 14 (1992) 317-329.

[30] T. Matsuhisa, S. Soejima, N. Yamamoto, U.S. Patent 4295892 (1981).

[31] M.J. Murtagh, N.I. Limited, U.S. Patent 5141686 (1992).

[32] C.B. Lundsager, U.S. Patent 3963504 (1976).

[33] C.B. Lundsager, R.M. Murch, U.S. Patent 3985846 (1976).

[34] N.D. Corbin, B.J. Miller, K. Sawicki, J.W. Lucek, J.G. Hannoosh, U.S. Patent 5306565 (1994).

[35] D. Popovic', J.W. Halloran, G.E. Hilmas, G.A. Brady, S. Somers, A. Barda, G. Zywicki, U.S. Patent 5645781 (1997).

[36] X. Xu, J.A. Moulijin, Transformation of a structured carrier into structured catalyst, in: A. Cybulski, J.A. Moulijn, (Eds.), Structured Catalysts and Reactors, Marcel Dekker, New York, 1998.

[37] D.T. Sheller, U.S. Patent 5532453 (1991).

[38] L. Wieres, U.S. Patent 5431330 (1995).

[39] M. Wolfgang, L. Wieres, U.S. Patent 6095406 (2000).

[40] N. Burgos, M. Paulis, M. Montes, Journal of Materials Chemistry 13 (2003) 1458-1467.

[41] Y. Chen, L. Zhang, Catalysis Letters 12 (1992) 51-62.

[42] A.A. Klinghoffer, R.L. Cerro, M.A. Abraham, Catalysis Today 40 (1998) 59-71.

[43] N.D.S. Mohallem, M.M.Viana, R.A. Silva, Automotive Catalysts: Performance, Characterization and Development, in: M. Chiaberge, (Ed.), New Trends and Developments in Automotive Industry, InTech, Croatia, 2011.

[44] L. Villegas, F. Masset, N. Guilhaume, Applied Catalysis A: General 320 (2007) 43-55.

[45] C. Agrafiotis, A. Tsetsekou, Journal of Materials Science 35 (2000) 951-960.

[46] C. Agrafiotis, A. Tsetsekou, A. Ekonomakou, Journal of Materials Science Letters 18 (1999) 1421-1424.

[47] N.R. Peela, A. Mubayi, D. Kunzru, Catalysis Today 147, Supplement (2009) S17-S23.

[48] C.-Z. Wan, J.C. Dettling, U.S. Patent 4727052 (1988).

[49] T. Dupin, U.S. Patent 4529718 (1985).

[50] C.-Z. Wan, J.C. Dettling, U.S. Patent 4677095 (1987).

[51] L.R. Chapman, U.S. Patent 4318828 (1982).

[52] K. Oberlander, Applied Industrial Catalysis, Academic Press, New York, 1984.

[53] K. Wefers, Alumina Chemicals: Science and Technology Handbook, The American Ceramic Society Incorporated, Ohio, 1990.

[54] M. Trueba, S.P. Trasatti, European Journal of Inorganic Chemistry 2005 (2005) 3393-3403.

[55] G. Paglia, C.E. Buckley, A.L. Rohl, R.D. Hart, K. Winter, A.J. Studer, B.A. Hunter, J.V. Hanna, Chemistry of Materials 16 (2003) 220-236.

[56] K.E. Sickafus, J.M. Wills, N.W. Grimes, Journal of the American Ceramic Society 82 (1999) 3279-3292.

[57] A. Ionescu, A. Allouche, J.P. Aycard, M. Rajzmann, F. Hutschka, The Journal of Physical Chemistry B 106 (2002) 9359-9366.

[58] J. Su, Q. Liu, Z. Liu, Z. Huang, Industrial & Engineering Chemistry Research 47 (2008) 4295-4301.

[59] C. Agrafiotis, A. Tsetsekou, Journal of the European Ceramic Society 20 (2000) 815-824.

[60] P.A. Beauseigneur, I.M. Lachman, M.D. Patil, S.H. Swaroop, U.S. Patent 5334570 (1994).

[61] L.B. Larsson, L.O. Löwendahl, J.-E. Otterstedt, The Effect of the Chemical Nature of the Wash-Coat on the Catalytic Performance of CO Oxidation Catalysts of Monolith Type, in: A. Crucq, A. Frennet, (Eds.), Studies in Surface Science and Catalysis, Elsevier, 1987, 333-344.

[62] E. Morgado Jr, Y.L. Lam, S.M.C. Menezes, L.F. Nazar, Journal of Colloid and Interface Science 176 (1995) 432-441.

[63] D. Fauchadour, F. Kolenda, L. Rouleau, L. Barré, L. Normand, Peptization mechanisms of boehmite used as precursors for catalysts, in: E. Gaigneaux, D.E. De Vos, P. Grange, P.A. Jacobs, J.A. Martens, P. Ruiz, G. Poncelet, (Eds.), Studies in Surface Science and Catalysis, Elsevier, Amsterdam, 2000, 453-461.

[64] S. Özdemir, Z.I. Önsan, R. Yildirım, Journal of Chemical Technology & Biotechnology 87 (2012) 58-64.

[65] B.P. Barbero, L. Costa-Almeida, O. Sanz, M.R. Morales, L.E. Cadus, M. Montes, Chemical Engineering Journal 139 (2008) 430-435.

[66] L.L. Hench, J.K. West, Chemcial Reviews 90 (1990) 33-72.

[67] H. Schmidt, Journal of Non-Crystalline Solids 100 (1988) 51-64.

[68] X. Xiaoding, H. Vonk, A. Cybulski, J.A. Moulijn, Alumina washcoating and metal deposition of ceramic monoliths, in: G. Poncelet, J. Martens, B. Delmon, P.A. Jacobs, P. Grange, (Eds.), Studies in Surface Science and Catalysis, Elsevier, Amsterdam, 1995, 1069-1078.

[69] E. García-Bordejé, I. Kvande, D. Chen, M. Rønning, Advanced Materials 18 (2006) 1589-1592.

[70] V. Blachou, D. Goula, C. Phillippopulos, Industrial & Engineering Chemistry Research 31 (1922) 364-369.

[71] S.A. Adegbite, Journal of Materials Science Research 2 (2013) 135 - 147.

[72] J.R. González-Velasco, M.A. Gutiérrez-Ortiz, J.L. Marc, J.A. Botas, M.P. González-Marcos, G. Blanchard, Industrial & Engineering Chemistry Research 42 (2002) 311-317.

[73] A.K. Mogalicherla, D. Kunzru, International Journal of Applied Ceramic Technology 8 (2011) 430-436.

[74] M. Campanati, G. Fornasari, A. Vaccari, Catalysis Today 77 (2003) 299-314.

[75] R.P. O'Connor, E.J. Klein, L.D. Schmidt, Catalysis Letters 70 (2000) 99-107.

[76] V.A. Sadykov, S.N. Pavlova, N.F. Saputina, I.A. Zolotarskii, N.A. Pakhomov, E.M. Moroz, V.A. Kuzmin, A.V. Kalinkin, Catalysis Today 61 (2000) 93-99.

[77] M. Xiaodong, S. Hongwen, S. Quan, G. Hongwen, F. Bo, Z. Shuo, Journal of Natural Gas Chemistry 19 (2010) 589-592.

[78] N. Thimmaraju, S.R. Pratap, M. Senthilkumar, S.Z.M. Shamshuddin, Journal of the Korean Chemial Society 56 (2012) 563-570.

[79] R. van Yperen, D. Lindner, L. Mußmann, E.S. Lox, T. Kreuzer, Novel Pd-based three-way catalysts, in: N. Kruse, A. Frennet, J.M. Bastin, (Eds.), Studies in Surface Science and Catalysis, Elsevier, Amsterdam, 1998, 51-60.

[80] F.J. Bröcker, E. Schwab, U.S. Patent 6436873 (2002).

[81] P. Euzen, E. Tocque, S. Rebours, G. Mabilon, U.S. Patent 6284210 (2001).

[82] I. Guibard, D. Durand, G. Mabilon, N. des Courtils, U.S. Patent 5643543 (1997).

[83] T. Shimrock, R.D. Taylor, J.M. Collins Jr., U.S. Patent 4550034 (1984).

[84] T. Vergunst, F. Kapteijn, J.A. Moulijn, Applied Catalysis A: General 213 (2001) 179-187.

[85] F. Pinna, Catalysis Today 41 (1998) 129-137.

[86] I. Barrio, I. Legórburu, M. Montes, M. Domínguez, M. Centeno, J. Odriozola, Catalysis Letters 101 (2005) 151-157.

[87] J. Carnö, M. Ferrandon, E. Björnbom, S. Järås, Applied Catalysis A: General 155 (1997) 265-281.

[88] D.M. Frías, S. Nousir, I. Barrio, M. Montes, L.M. Martínez T, M.A. Centeno, J.A. Odriozola, Applied Catalysis A: General 325 (2007) 205-212.

[89] J. Li, R. Yan, B. Xiao, D.T. Liang, L. Du, Environmental Science & Technology 42 (2008) 6224-6229.

[90] S. Cimino, L. Lisi, R. Pirone, G. Russo, M. Turco, Catalysis Today 59 (2000) 19-31.

[91] M. Ouzzine, G.A. Cifredo, J.M. Gatica, S. Harti, T. Chafik, H. Vidal, Applied Catalysis A: General 342 (2008) 150-158.

[92] R. Ran, G. Xiong, W. Yang, Journal of Materials Chemistry 12 (2002) 1854-1859.

[93] S. Sharma, M.S. Hegde, Catalysis Letters 112 (2006) 69-75.

[94] L. Dumitrescu, F. Maury, Surface and Coatings Technology 125 (2000) 419-423.

[95] M. Ferrandon, M. Berg, E. Björnbom, Catalysis Today 53 (1999) 647-659.

[96] Z. Ding, X. Hu, P.L. Yue, G.Q. Lu, P.F. Greenfield, Catalysis Today 68 (2001) 173-182.

[97] O. Sanz, L.M. Martínez T, F.J. Echave, M.I. Domínguez, M.A. Centeno, J.A. Odriozola, M. Montes, Chemical Engineering Journal 151 (2009) 324-332.

[98] M.F.M. Zwinkels, S.G. Järs, P. Govind Menon, Preparation of combustion catalysts by wash coating alumina whiskers-covered metal monoliths using a sol-gel method, in: G. Poncelet, J. Martens, B. Delmon, P.A. Jacobs, P. Grange, (Eds.), Studies in Surface Science and Catalysis, Elsevier, Amsterdam, 1995, 85-94.

[99] L. Giani, C. Cristiani, G. Groppi, E. Tronconi, Applied Catalysis B: Environmental 62 (2006) 121 - 131.

[100] O. Sanz, L.C. Almeida, J.M. Zamaro, M.A. Ulla, E.E. Miró, M. Montes, Applied Catalysis B: Environmental 78 (2008) 166-175.

[101] B. Kucharczyk, W. Tylus, L. Kępiński, Applied Catalysis B: Environmental 49 (2004) 27-37.

[102] C.G. Visconti, E. Tronconi, L. Lietti, G. Groppi, P. Forzatti, C. Cristiani, R. Zennaro, S. Rossini, Applied Catalysis A: General 370 (2009) 93-101.

[103] L.C. Almeida, F.J. Echave, O. Sanz, M.A. Centeno, G. Arzamendi, L.M. Gandía, E.F. Sousa-Aguiar, J.A. Odriozola, M. Montes, Chemical Engineering Journal 167 (2011) 536-544.

[104] L.M. Martínez Tejada, M.I. Domínguez, O. Sanz, M.A. Centeno, J.A. Odriozola, Gold Bulletin (2013) 1-11.

[105] B. Mitra, D. Kunzru, Journal of the American Ceramic Society 91 (2008) 64-70.

[106] L. Li, B. Xue, J. Chen, N. Guan, F. Zhang, D. Liu, H. Feng, Applied Catalysis A: General 292 (2005) 312-321.

[107] J.M. Zamaro, M.A. Ulla, E.E. Miró, Chemical Engineering Journal 106 (2005) 25-33.

[108] M.A. Ulla, R. Mallada, J. Coronas, L. Gutierrez, E. Miró, J. Santamaría, Applied Catalysis A: General 253 (2003) 257-269.

[109] A.E.W. Beers, T.A. Nijhuis, N. Aalders, F. Kapteijn, J.A. Moulijn, Applied Catalysis A: General 243 (2003) 237-250.

[110] T. Valdés-Solís, G. Marbán, A.B. Fuertes, Microporous and Mesoporous Materials 43 (2001) 113-126.

[111] F. Rodríguez-reinoso, Carbon 36 (1998) 159-175.

[112] E. García-Bordejé, F. Kapteijn, J.A. Moulijn, Carbon 40 (2002) 1079-1088.

[113] E. García-Bordejé, F. Kapteijn, J.A. Moulijn, Catalysis Today 69 (2001) 357-363.

[114] T. Vergunst, M.J.G. Linders, F. Kapteijn, J.A. Moulijn, Catalysis Reviews 43 (2001) 291-314.

[115] T. Vergunst, F. Kapteijn, J.A. Moulijn, Carbon 40 (2002) 1891-1902.

[116] V. Lordi, N. Yao, J. Wei, Chemistry of Materials 13 (2001) 733-737.

[117] G. Binbin, W. Rong, L. Bingyu, X. Feng, Y. Xiujin, W. Kemei, Catalysis Letters 122 (2008) 287-294.

[118] M. Trépanier, A. Tavasoli, A.K. Dalai, N. Abatzoglou, Fuel Processing Technology 90 (2009) 367-374.

[119] E. García-Bordejé, I. Kvande, D. Chen, M. Rønning, Carbon 45 (2007) 1828-1838.

[120] I.M. Lachman, L.A. Nordlie, U.S. Patent 4631267 (1986).

[121] M. Xiaodong, S. Hongwen, Y. Peng, Journal of Materials Science 43 (2008) 887-891.

[122] B.S. Kim, S.H. Lee, Y.T. Park, S.W. Ham, H.J. Chae, I.S. Nam, Korean Journal of Chemical Engineering 18 (2001) 704-710.

[123] P. Avila, A. Bahamonde, J. Blanco, B. Sánchez, A.I. Cardona, M. Romero, Applied Catalysis B: Environmental 17 (1998) 75-88.

[124] A. Wahby, J.M. Ramos-Fernández, M. Martínez-Escandell, A. Sepúlveda-Escribano, J. Silvestre-Albero, F. Rodríguez-Reinoso, ChemSusChem 3 (2010) 974-981.

[125] J. Urban, F. Svec, J.M.J. Fréchet, Analytical Chemistry 82 (2010) 1621-1623.

[126] J.P. Marco-Lozar, M. Kunowsky, F. Suarez-Garcia, J.D. Carruthers, A. Linares-Solano, Energy & Environmental Science 5 (2012) 9833-9842.

[127] T.Y. Klein, L. Treccani, J. Thoming, K. Rezwan, RSC Advances 3 (2013) 13381-13389.

[128] U.S. Environmental Protection Agency, Air Pollution Aspects of Emission Sources: Nitric Acid Manufacturing - A Bibliography with Abstracts, A.P.C. Office, North Carolina, 1971.

[129] A. Cybulski, J.A. Moulijn, Structured Catalysts and Reactors, Second ed., CRC Press, Taylor and Francis Group, London, 2005.

[130] H.S. Gandhi, G.W. Graham, R.W. McCabe, Journal of Catalysis 216 (2003) 433-442.

[131] R.J. Farrauto, R.M. Heck, Catalysis Today 51 (1999) 351-360.

[132] M. Shelef, R.W. McCabe, Catalysis Today 62 (2000) 35-50.

[133] R.M. Heck, R.J. Farrauto, Applied Catalysis A: General 221 (2001) 443-457.

[134] J. Kašpar, P. Fornasiero, N. Hickey, Catalysis Today 77 (2003) 419-449.

[135] M.V. Twigg, Applied Catalysis B: Environmental 70 (2007) 2-15.

[136] M.R. Foster, J.E. Smith, U.S. Patent 4239733 (1980).

[137] R.P. Merry, U.S. Patent 4617176 (1986).

[138] H. Mizuno, F. Abe, T. Harada, U.S. Patent 5063029 (1991).

[139] G.S. Sims, S.W. Hawes, U.S. Patent 5106588 (1992).

[140] H. Zhang, J. Beer, U.S. Patent 5938715 (1999).

[141] U.K. Singh, M.A. Vannice, Applied Catalysis A: General 213 (2001) 1-24.

[142] I.E. Sungkono, H. Kameyama, T. Koya, Applied Surface Science 121–122 (1997) 425-428.

[143] V. Tomasic, Catalysis Today 119 (2007) 106-113.

[144] L.F. Liotta, Applied Catalysis B: Environmental 100 (2010) 403-412.

[145] B. Gokalp, Journal of Renewable & Sustainable Energy 4 (2012) 1-21.

[146] B. Desai, C.O. Kappe, Journal of Combinatorial Chemistry 7 (2005) 641-643.

[147] T. Boger, M.M.P. Zieverink, M.T. Kreutzer, F. Kapteijn, J.A. Moulijn, W.P. Addiego, Industrial & Engineering Chemistry Research 43 (2004) 2337-2344.

[148] V. Hatziantoniou, B. Andersson, N.H. Schoon, Industrial & Engineering Chemistry Process Design and Development 25 (1986) 964-970.

[149] X. Xiaoding, H. Vonk, A.C.J.M. van de Riet, A. Cybulski, A. Stankiewicz, J.A. Moulijn, Catalysis Today 30 (1996) 91-97.

[150] M. Huff, L.D. Schmidt, Journal of Physical Chemistry 97 (1993) 11815-11822.

[151] M. Huff, P.M. Torniainen, L.D. Schmidt, Catalysis Today 21 (1994) 113-128.

[152] M. Huff, L.D. Schmidt, Journal of Catalysis 155 (1995) 82-94.

[153] M. Huff, L.D. Schmidt, Journal of Catalysis 149 (1994) 127-141.

[154] A.G. Dietz, A.F. Carlsson, L.D. Schmidt, Journal of Catalysis 176 (1996) 459-473.

[155] A. Beretta, L. Piovesan, P. Forzatti, Journal of Catalysis 184 (1999) 455-468.

[156] A. Beretta, E. Ranzi, P. Forzatti, Experimental and theoretical investigation on the roles of heterogeneous and homogeneous phases in the oxidative dehydrogenation of light paraffins in novel short contact time reactors, in: A. Corma, F.V. Melo, S. Mendioroz, J.L.G. Fierro, (Eds.), Studies in Surface Science and Catalysis, Elsevier, 2000, 1913-1918.

[157] A. Beretta, P. Forzatti, E. Ranzi, Journal of Catalysis 184 (1999) 469-478.

[158] A. Beretta, E. Ranzi, P. Forzatti, Catalysis Today 64 (2001) 103-111.

[159] C. Yokoyama, S.S. Bharadwaj, L.D. Schmidt, Catalysis Letters 38 (1996) 181-188.

[160] S.F. Håkonsen, B. Silberova, A. Holmen, Topics in Catalysis 45 (2007) 61-67.

[161] B. Silberova, M. Fathi, A. Holmen, Applied Catalysis A: General 276 (2004) 17 - 28.

[162] D.A. Hickman, L.D. Schmidt, Journal of Catalysis 138 (1992) 267-282.

[163] D.A. Hickman, E.A. Haupfear, L.D. Schmidt, Catalysis Letters 17 (1993) 223-237.

[164] D.A. Hickman, L.D. Schmidt, Science 259 (1993) 343-346.

[165] S.S. Bharadwaj, L.D. Schmidt, Fuel Processing Technology 42 (1995) 109-127.

[166] S.S. Bharadwaj, C. Yokoyama, L.D. Schmidt, Applied Catalysis A: General 140 (1996) 73-97.

[167] O. Deutschmann, L.D. Schmidt, AIChE Journal 44 (1998) 2465-2477.

[168] R. Schwiedernoch, S. Tischer, O. Deutschmann, J. Warnatz, Proceedings of the Combustion Institute 29 (2002) 1005-1011.

[169] R. Schwiedernoch, S. Tischer, C. Correa, O. Deutschmann, Chemical Engineering Science 58 (2003) 633-642.

[170] J.E.P. Navalho, I. Frenzel, A. Loukou, J.M.C. Pereira, D. Trimis, J.C.F. Pereira, International Journal of Hydrogen Energy 38 (2013) 6989-7006.

[171] A.S. Bodke, S.S. Bharadwaj, L.D. Schmidt, Journal of Catalysis 179 (1998) 138-149.

[172] N.J. Degenstein, R. Subramanian, L.D. Schmidt, Applied Catalysis A: General 305 (2006) 146-159.

[173] X. Shi, S. Ji, K. Wang, C. Li, Energy & Fuels 22 (2008) 3631-3638.

[174] S.F. Håkonsen, J.C. Walmsley, A. Holmen, Applied Catalysis A: General 378 (2010) 1-10.

[175] L.E. Gómez, I.S. Tiscornia, A.V. Boix, E.E. Miró, Applied Catalysis A: General 401 (2011) 124-133.

[176] L.E. Gómez, I.S. Tiscornia, A.V. Boix, E.E. Miró, International Journal of Hydrogen Energy 37 (2012) 14812-14819.

[177] J.J. Krummenacher, K.N. West, L.D. Schmidt, Journal of Catalysis 215 (2003) 332-343.

Chapter 3

Homogeneous gas phase reactions in the oxidation of *n*-octane over a monolith reactor system

Abstract

The oxidation of *n*-octane over the bare cordierite monolith produced cyclic ethers in 31.6 % selectivity, under continuous flow fixed bed reactor conditions. Other products formed over the bare monolith included cracked products, octenes, octadienes, C_8 oxygenates and carbon oxides. Coating the monolith with an iron-molybdenum active layer reduced the yields to cracked products and C_8 oxygenates, whilst increasing the yields to octadienes and carbon oxides. The monolith coated with gamma-alumina, compared to the bare monolith, substantially retarded the conversion of *n*-octane, from 27 % to 5 %. An iron-molybdenum active layer supported on the gamma-alumina coated monolith rendered a drastic change to the mechanism, favouring deep oxidation with a selectivity of 64.2 % to carbon dioxide. The iron-molybdenum powder was characterized by XRD, ICP-OES, BET, TEM, FTIR and Raman spectroscopy. The bare and coated monoliths were examined by SEM. Experimental reaction conditions were kept constant, maintaining a GHSV of 1000 h^{-1} (71.7 ml/min air, 45 ml/min nitrogen, 0.10 ml/min C_8H_{18}), isothermally at 400 °C and a C:O ratio of 8:2, for the bare and coated monoliths tested. A homogeneous gas phase mechanism is proposed for the formation of the cyclic ethers over the bare monolith. The results from coating cordierite monoliths suggest that secondary support coating is a better approach, over coating the active layer directly onto the monolith in this work.

3.1 Introduction

Monoliths, since initial use in environmental applications [1], have been successfully incorporated in catalytic oxidation [2, 3]. In particular, monoliths have been well incorporated in the oxidation of alkanes to olefins and synthesis gas, respectively. These applications usually involve coating the ceramic structures with platinum group metals and performing oxidation reactions at high temperatures and high gas flow rates [4, 5]. Initial testing of these monoliths showed excellent selectivity to olefins, however, further investigation pointed to the formation of olefins from monolithic catalysts to occur via homogeneous gas phase reactions [6, 7]. Monoliths, coated with platinum and rhodium, on

the other hand, showed good conversion and selectivity toward the catalytic formation of synthesis gas [2, 4].

Apart from the formation of olefins via homogeneous gas phase reactions, dienes and oxygenated products were also reported from the partial oxidation of C_5 and C_6 alkanes, over platinum coated foam monoliths in short contact time reactors [8]. The production of olefins and oxygenated compounds was also observed in the partial oxidation of C_1 to C_5 alkanes, in single gauze reactors, where the product profile was attributed to homogeneous gas phase reactions [9, 10]. In a single gauze reactor, using *n*-hexane as the feed and a platinum-rhodium gauze, O'Connor and Schmidt reported a high selectivity to oxygenated hydrocarbons [11]. These oxygenated products were mainly C_6 cyclic ethers. Characteristically, cyclic ethers form as a result of free radical reactions [12-14].

Recent applications in oxidative dehydrogenation using monolithic catalysts include the conversion of propane to propylene [15] and a molybdenum-vanadium-niobium coated monolith in the oxidation of ethane to ethylene [16]. Monolithic catalysts may therefore prove valuable in the oxidation of alkanes, however, the contribution of homogeneous gas phase reactions from these catalysts needs to be better understood. The monolithic structure, prior and after active layer coating, should therefore be examined in oxidation reactions. Herein cheaper active components, namely iron-molybdenum, in comparison to platinum group metals, were used. Iron-molybdenum catalysts have been extensively studied in methanol oxidation [17-22] and have been reported in the oxidation of *n*-decane [23].

In this research effort the oxidation of *n*-octane over bare and coated cordierite monoliths was examined. Also, gamma-alumina was used as a secondary support and compared to direct coating of the active layer on the monolith. This preliminary alkane testing over the bare and coated monoliths, in a continuous flow fixed bed reactor system, may provide for a better understanding of the influence of an uncoated monolith compared to when coated with an secondary support and active layer.

3.2 Experimental

3.2.1 Pre-treatment of ceramic monoliths

All monoliths used in the experimental work were sonicated in deionised water for thirty minutes, followed by drying at 110 °C, to ensure removal of any contaminants.

3.2.2. Iron-molybdenum coated on monoliths

An iron-molybdenum precursor solution was prepared by initial co-precipitation [23], followed by addition of oxalyldihydrazide [24]. Ammonium heptamolybdate of 8.76 g (99 %, Merck) was added to 100 ml deionised water with stirring. Concentrated nitric acid (≥ 69 %, Sigma Aldrich) was used to acidify the solution to approximately pH 2, monitored with universal indicator paper. Iron nitrate nonahydrate of 9.11 g (97 %, Merck) was dissolved in deionised water and added dropwise with stirring to the acidified ammonium heptamolybdate solution . The greenish/yellow slurry was aged with stirring at approximately 80 °C for one hour, after which oxalyldihydrazide of 5.82 g (98 %, Sigma Aldrich) was added, forming a solution. Aging was continued for a further four hours to reduce the water content. The dark green liquor was allowed to cool to room temperature with stirring. Cordierite monoliths (20 mm diameter, 25 mm length, 1 mm channel width) were dipped into this liquor, allowed to soak for 15 minutes, after which excess liquid in the channels was removed with compressed air. The coated monoliths were then heated at 600 °C for 15 minutes, in a muffle furnace, under static air. Upon cooling of the monoliths to room temperature, the procedure was repeated to obtain the desired weight percent loading.

3.2.3. Gamma-alumina supported iron-molybdenum coated monoliths

A gamma-alumina washcoat slurry was prepared by adding 20 g (3 µm average particle size gamma-alumina, Alpha-Aesar) and 41 mmol concentrated nitric acid (≥ 69 %, Sigma Aldrich) to 80 g deionised water, with stirring [25]. The slurry was allowed to stir at room temperature for 24 hours. Cordierite monoliths (20 mm diameter, 25 mm length, 1 mm channel width) were dipped in the slurry and allowed to soak for approximately 15 minutes. The excess liquid was removed using compressed air, followed by heating of the monoliths at 600 °C for 15 minutes, in a muffle furnace, under static air. The procedure was repeated until the desired weight percent coating was achieved. The iron-molybdenum active layer was coated over the gamma-alumina coated monoliths similarly as described in Section *3.2.2*.

3.2.4 Characterization techniques

XRD, ICP-OES, Raman spectroscopy, BET, TEM and SEM were used to characterize the coated layer in powder form. SEM was used to characterize the surface of the bare and coated monoliths.

The X-ray diffraction pattern of the iron-molybdenum powder was obtained using a Bruker D8 Advance diffractometer fitted with a graphite monochromator and operated at 40 mA and 40 kV. The radiation source was Cu Kα with a wavelength of 1.5406 Å. The 2θ range was employed from 10 ° to 90 °, at a speed of 1 ° per minute and a step size of 0.02 °.

ICP-OES was used to confirm the metal ratio of Mo:Fe of the iron-molybdenum catalyst formed. Standards were prepared according to the metal ratios present in $Fe_2(MoO_4)_3 \bullet MoO_3$. Active layer powder (~ 0.02 g) was dissolved in 5 ml concentrated hydrochloric acid (32 %, SMM Instruments) and diluted to 100 ml with double distilled water. ICP-OES analysis was completed on a Perkin Elmer Optical Emission Spectrometer Optima 5300DV (radial plasma). Multi-element standards were prepared from 1000 ppm working solutions.

The surface area of the iron-molybdenum catalyst powder was determined by BET surface area measurements. Measurements were completed in duplicate. Samples (~ 0.3 g) were degassed under nitrogen flow at 90 °C for 1 hour, then 200 °C overnight, using a Micrometrics Flow Prep 060 sample degas system. Samples were analyzed using nitrogen adsorption at -196 °C, with a Micrometrics Tristar II Surface Area and Porosity Analyzer. The BET surface area of the gamma-alumina used to coat the monoliths was also determined similarly.

A DeltaNu Advantage 532 instrument equipped with a 532 nm laser source was used to obtain the Raman spectrum of the iron-molybdenum catalyst powder. The best quality spectrum was obtained at an intensity of medium-high and an integration time of five seconds. Peak intensities were observed between 200 cm^{-1} and 1000 cm^{-1}, therefore the spectrum was plotted in this range.

Infrared analyses were performed on a Perkin Elmer Spectrum 100 FTIR Spectrometer equipped with a Universal Attenuated Total Reflectance accessory. A small amount of powder sample was placed over the ATR crystal and a force of 110 gauge was applied to obtain an infrared spectrum. Vibration bands for the sample were observed between 500 cm^{-1} and 1000 cm^{-1}, therefore the spectrum was plotted to show these bands.

Electron microscopy images were acquired using a Jeol JEM 1010 Transmission Electron Microscope at 100 kV. The iron-molybdenum catalyst powder was dispersed in ethanol and sonicated for five minutes, after which a small quantity was suspended on carbon resin and

allowed to dry. Images were then taken to assess the morphology of iron-molybdenum catalyst throughout the surface of the sample.

In comparison to TEM, SEM images were acquired to evaluate the surface morphology. A Carl Zeiss ULTRA PLUS FEG-SEM was used to obtain images of the uncoated and coated monoliths. The bare cordierite monolith and coated monoliths were sectioned in half. Images of the monoliths obtained were focused on the coating within the channels.

3.2.5 Catalytic testing and product analysis

Catalytic testing was performed in a continuous flow fixed bed monolith reactor, specially designed to accommodate the monolith structure as the catalyst bed. A Lab Alliance Series II HPLC pump was used to deliver the *n*-octane to the reactor. The outlet from the pump was 1/16 inch stainless steel tubing which was further connected, via a reducing union, to the main reactor line. The main reactor line consisted of 1/4 inch 316 stainless steel tubing, wrapped with heating tape (400W, 240V). Nitrogen and air were fed to the main reactor line via Bronkhurst mass flow controllers and mixed with the *n*-octane at a 1/4 inch stainless steel "T" piece. One way valves were placed at the beginning of the reactor lines that supplied the gases and *n*-octane in order to prevent back flow of the gases. Nitrogen and air, together with *n*-octane were thus mixed and preheated at 200 °C before reaching the reactor tube. A tubular 316 stainless steel reactor tube (25 mm O.D., 2 mm thickness) was used to load the monolithic catalyst. The monolithic catalyst (7.85 ml) was suspended at the hottest region of the reactor tube, between glass wool, with the remainder reactor space filled with 24 grit carborundum. Glass wool was also placed at the ends of the reactor tube to ensure the carborundum remains firmly packed. Reducing unions were used to reduce the ends of the reactor tube to 1/4 inch. The temperature of the hottest region was measured using a K-type thermocouple, connected to a temperature control unit and placed in a 1/8 inch 316 stainless steel tube in the middle of the reactor tube. Once packed, the reactor tube was placed in the center of a stainless steel block, equipped with six cartridge heaters (12.5 mm diameter, 150 mm length, 230 V/400 W) with fiber-glass nickel stranded leads, connected to a thermocouple and temperature control unit. The exit gas from the reactor tube entered a catch pot which was cooled using a water chiller to approximately 2 °C. Liquid samples were collected from the catch pot via a one way needle valve, while gas samples were collected through a glass bomb fitted with a septum. The quantity of gas which exited the

reactor after the catch pot was measured with a Ritter Drum-Type (TGI-model 5) wet gas flow meter. The reactor setup is shown in Figure 1, in Appendix 2.

The oxidation of *n*-octane was investigated isothermally (400 °C) in the gas phase at a space velocity of 1000 h^{-1}, with a carbon to oxygen ratio of 8:2. Air and nitrogen (diluent) were passed through the reactor using Bronkhurst mass flow controllers. The gas hourly space velocity was maintained by flowing 71.7 ml/min air (Peak Scientific, Zero Air Generator), 45 ml/min nitrogen (Afrox, Instrument Grade) and 0.10 ml/min *n*-octane (99 %, Merck), over a catalyst volume of 7.85 ml (monolith volume, $\pi r^2 h$). A constant *n*-octane to total feed ratio of approximately 11.43 % was used for the reactor work. All reactions in this study were performed in duplicate.

The products from catalytic testing were analyzed off line by GC-FID and GC-TCD, whilst GC-MS was used for product identification. A Shimadzu GC-2025 Gas Chromatograph, equipped with a Restek Rtx-1 PONA column (48 m length, 0.25 mm I.D., 0.5 μm thickness), was used for liquid and gaseous hydrocarbon analysis. Carbon oxides were analyzed using a Perkin Elmer Clarus 400 Gas Chromatograph, fitted with a SUPELCO Carboxen 1010 PLOT column (30 m length, 0.53 mm I.D., 30 μm thickness). Hydrocarbon products were identified using a Perkin Elmer Precisely Clarus 500 Gas Chromatograph, with a SGE forte BP1 PONA GC capillary column (50 m length, 0.15 mm I.D., 0.5 μm thickness) and Perkin Elmer precisely Clarus 560S Mass Spectrometer. The detailed method parameters are shown in Appendix 3.

The percentage water in both organic and aqueous samples was analyzed via a Mettler Toledo Easy KFV titrator.

3.3 Results and discussion

3.3.1 Characterization of iron-molybdenum powder and coated monoliths

Monolithic catalysts are difficult to characterize, however, the coating within the channels can be assessed by SEM and the active layer in powder form can also be characterized. The active layer in powder form was therefore also characterized as mentioned in Section *3.2.4*. The iron-molybdenum powder was prepared by heating a small amount of liquid, used to coat the monolith, in the same heat treatment procedure as in Section *3.2.2*. Slurry coating was chosen for coating the gamma-alumina secondary support over the monolith, to allow for

strong adherence of the coating to the monolith surface. The repeated dipping and calcining procedure was chosen to reduce the number of coating cycles required, as compared to repeated dipping and drying and final calcination. The active layer was coated similarly.

3.3.1.1 Powder X-Ray diffraction

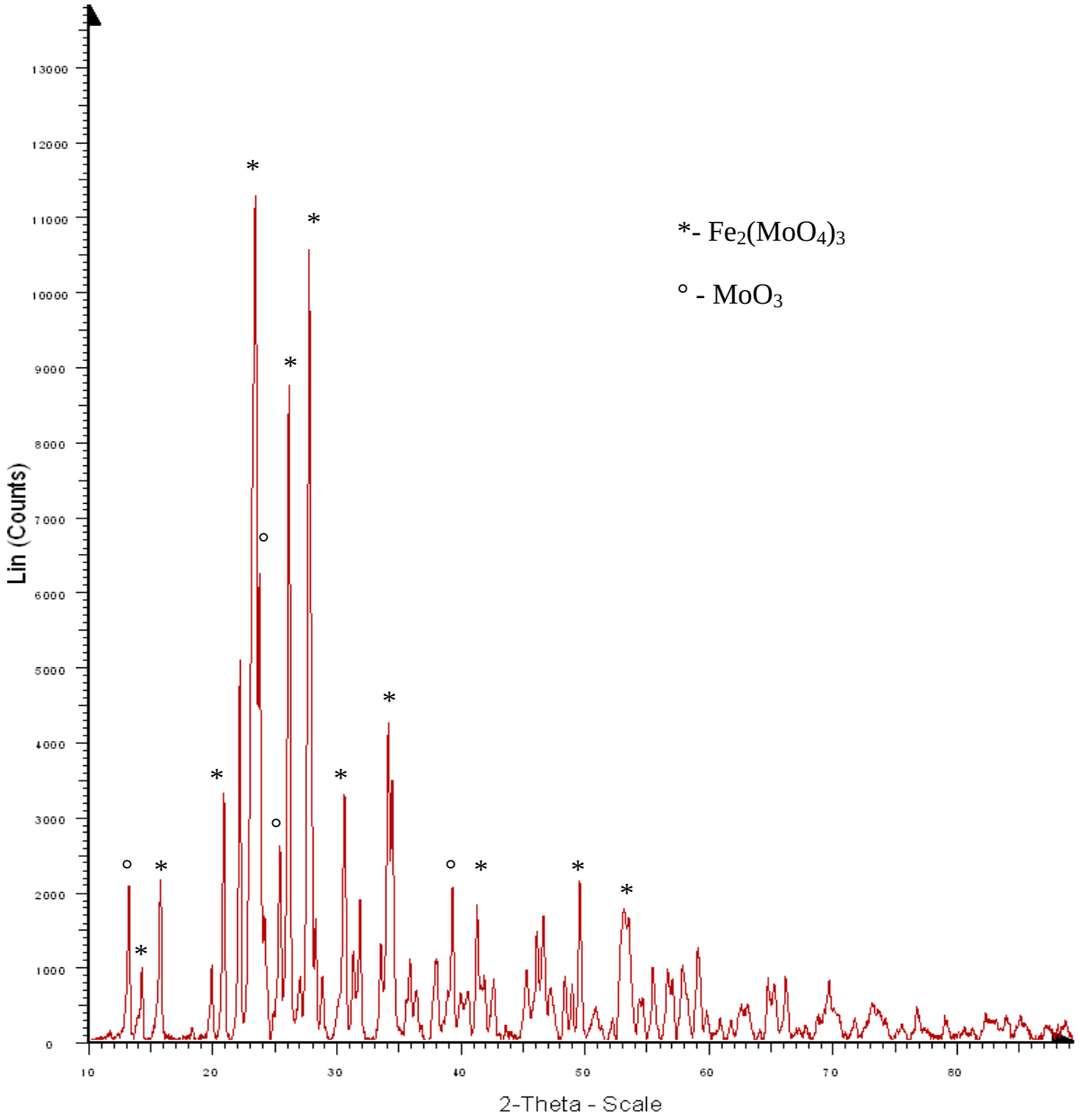

Figure 3.1: XRD diffractogram of the iron-molybdenum powder

Figure 3.1 shows the diffraction pattern of a characteristic crystalline iron-molybdenum catalyst with excess molybdenum, resulting in diffraction lines corresponding to $Fe_2(MoO_4)_3$ and MoO_3. The major peaks corresponding to iron molybdate and molybdenum trioxide have been assigned, whilst the smaller unassigned peaks are due to iron molybdate. The iron

molybdate phase can be indexed to ICDD card number 01-083-1701, corresponding to monoclinic $Fe_2(MoO_4)_3$ and molybdenum trioxide present can be indexed to ICDD card number 01-085-2405. This light green powder is consistent with the monoclinic iron molybdate structure, typically formed at approximately pH 2 [26] and Mo:Fe ratio of 2.2:1 [27]. The active iron-molybdenum layer cannot be seen clearly, in XRD, whilst coated over the monolith. Major peaks due to cordierite, shown in Appendix 1, are in the theta range 15 to 60 °, which coincide with the major peaks for iron molybdate and molybdenum trioxide.

3.3.1.2 ICP-OES and BET surface area

Table 3.1: BET surface area measurement results

	BET surface area (m^2/g)
Bare monolith	< 1
$Fe_2(MoO_4)_3$•MoO_3	2
Gamma-alumina	85

The iron-molybdenum active layer was prepared in a 2.2:1 Mo:Fe ratio, confirmed by ICP-OES. Detailed calculations of ratio of metals are shown in Appendix 1. The BET surface area of the iron-molybdenum powder obtained was 2 m^2/g, shown in Table 3.1, which is the expected for the ratio of molybdenum:iron synthesized [28]. Molybdates usually exhibit BET surface areas less than 10 m^2/g, however, these are dependent on the preparation method, the counter ion to the molybdate and the ratio of molybdenum to the metal [22, 29, 30].

The cordierite monolith has a BET surface area of less than 1 m^2/g, which may not necessarily allow for good adherence of an active layer to this support, therefore gamma-alumina with a surface area of 85 m^2/g was coated onto the monolith and investigated, prior and after active layer coating.

3.3.1.3 Raman spectroscopy and Fourier transform-infrared spectroscopy

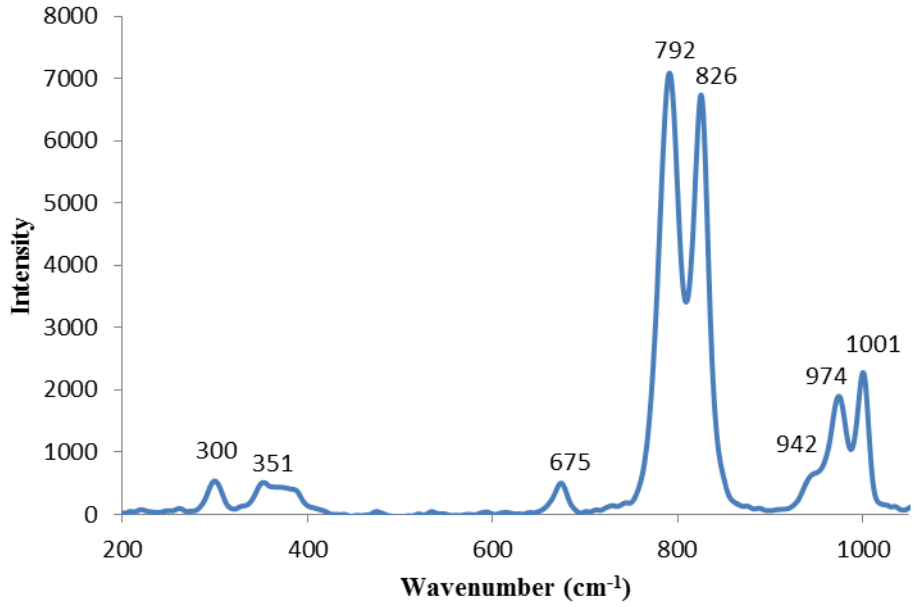

Figure 3.2: Raman spectrum of the iron-molybdenum powder

The Raman spectrum of the iron-molybdenum powder, shown in Figure 3.2, depicts the expected peaks, due to the molybdenum to iron ratio of 2.2:1, corresponding to iron molybdate and molybdenum trioxide. The Raman bands at 351, 792, 942 and 974 cm^{-1}, in Figure 3.2, correspond to $Fe_2(MoO_4)_3$ [20, 31]. The bands at 300, 675, 826 and 1001 cm^{-1} are due to vibrations of MoO_3 [31]. The weak band exhibited at 351 cm^{-1} is probably due to the wagging of Mo=O in MoO_4 of $Fe_2(MoO_4)_3$ [20, 32]. This weak band contains a low intensity, wide shoulder, extending toward 400 cm^{-1}, possibly due to stretching modes of MoO_3 [27]. Pure iron molybdate usually exhibits asymmetric stretching modes of Mo-O-Mo in $Fe_2(MoO_4)_3$, represented by an intense band at 792 cm^{-1} and a shoulder peak at approximately 820 cm^{-1} [32], as well as symmetric stretches of Mo=O in MoO_4 at 942, 974 and approximately 990 cm^{-1} [20, 33]. In this spectrum obtained, however, the shoulder peak at 820 cm^{-1} and the symmetric stretch at 990 cm^{-1} may be masked by the MoO_3 bands. The vibrational modes of MoO_3 present were those of Mo=O bending, symmetric stretching of Mo-O-Mo, asymmetric stretching of Mo-O-Mo and stretching of Mo=O at 300, 675, 826 and 1001 cm^{-1}, respectively.

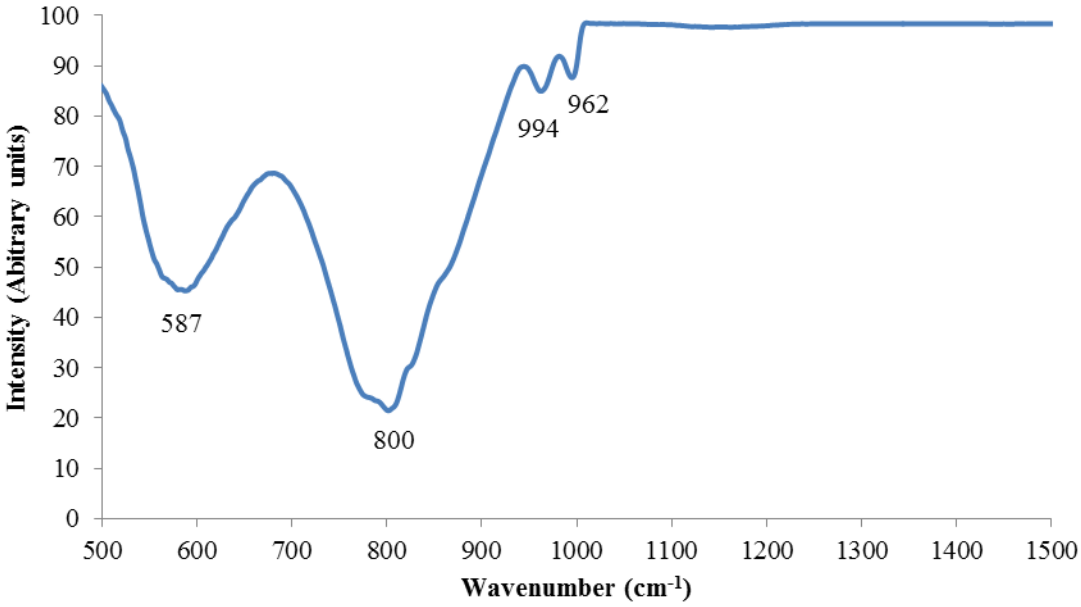

Figure 3.3: FT-IR spectrum of the iron-molybdenum powder

The infrared spectrum, shown in Figure 3.3, is characteristic of an $Fe_2(MoO_4)_3$-MoO_3 catalyst. Four absorption bands were observed between 500 and 1000 cm^{-1}. The absorption band at approximately 587 cm^{-1} is due to the vibration of Mo-O in MoO_3 [34], whilst the weak band at 994 cm^{-1} is ascribed to the terminal vibration of Mo=O in MoO_3 [35]. Vibrations from the Mo-O bonds, in the MoO_4 units of $Fe_2(MoO_4)_3$, are responsible for the intense and broad band at 800 cm^{-1} [20, 34, 35]. A weak band due to the Fe-O-Mo vibration was observed at 962 cm^{-1} [34, 35].

3.3.1.4 Transmission electron microscopy

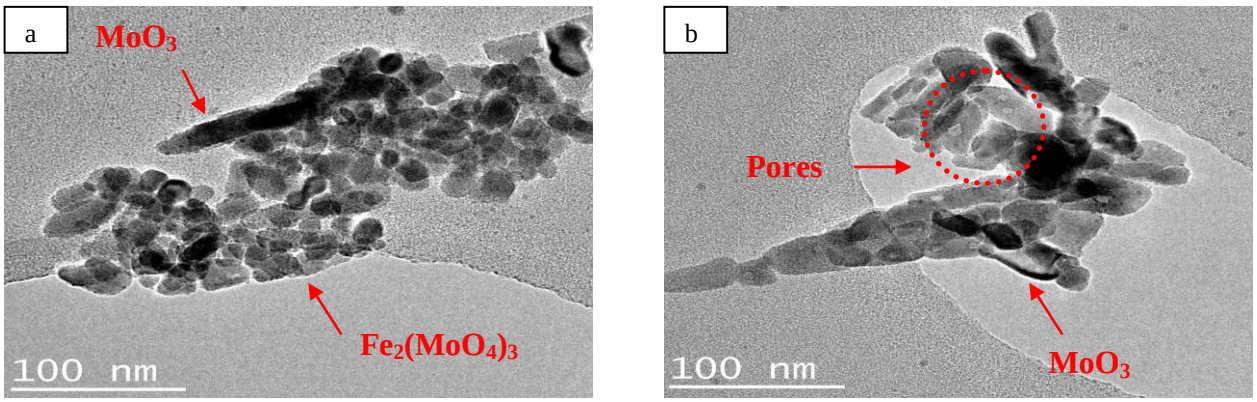

Figure 3.4: TEM images of the iron-molybdenum powder, (a) bulk iron molybdate (b) molybdenum trioxide plates

TEM micrographs of the iron-molybdenum powder are represented in Figures 3. 4 (a) and 3.4 (b). The images show the presence of the two distinct morphologies, that is, bulk spherical iron molybdate and rod/plate-like molybdenum trioxide. Bulk iron molybdate particles were in the 10 - 80 nm range, whilst molybdenum trioxide plates varied in size from 50 - 150 nm. The small, almost circular, lighter regions in Figure 3.4 (b) may be pores or voids in the bulk iron molybdate clusters [31].

3.3.1.5 Scanning electron microscopy

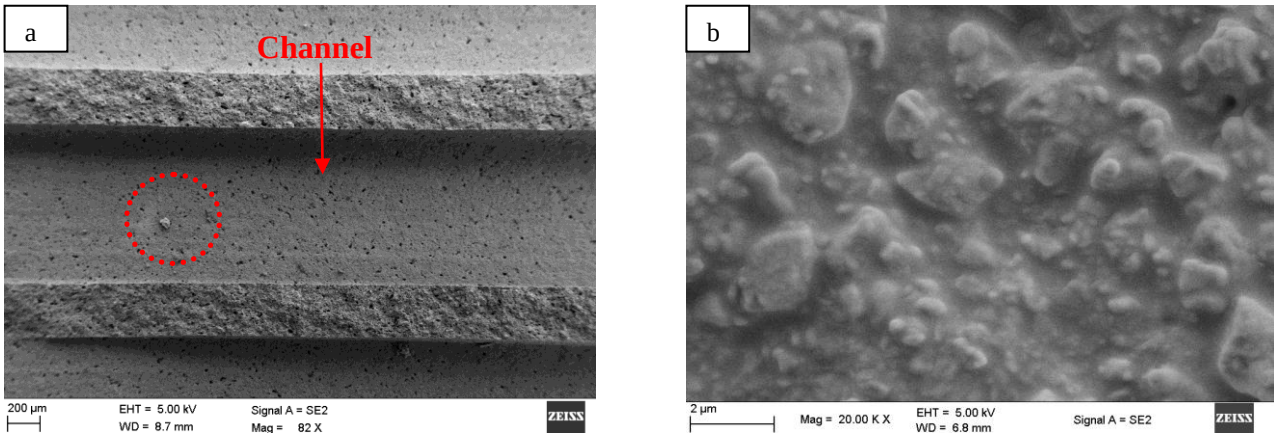

Figure 3.5: SEM images of the bare monolith, (a) within channels (b) 20 000 times magnification

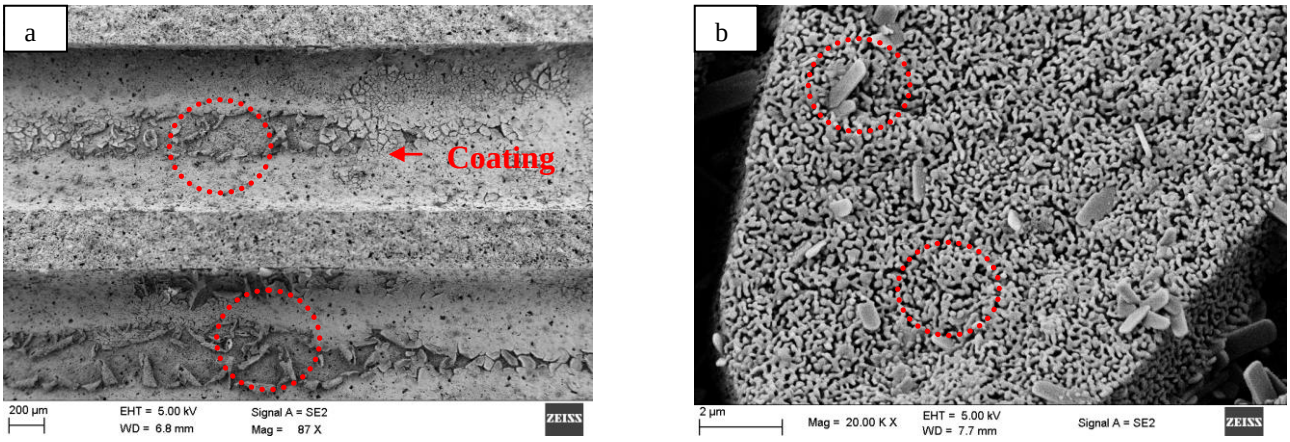

Figure 3.6: SEM images of the 5 weight % iron-molybdenum coated monolith, (a) coating within channels (b) 20 000 times magnification

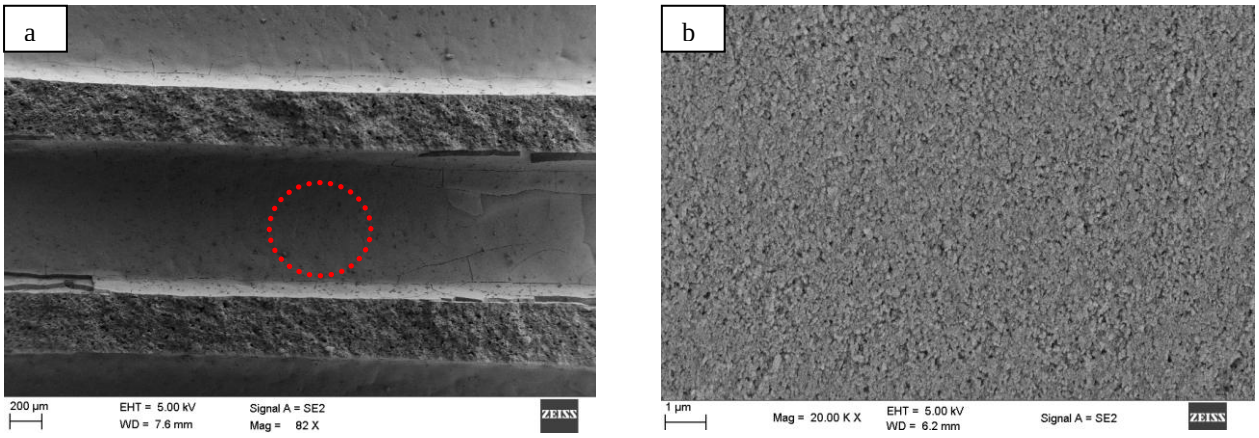

Figure 3.7: SEM images of the 10 weight % gamma-alumina coated monolith, (a) coating within channels (b) 20 000 times magnification

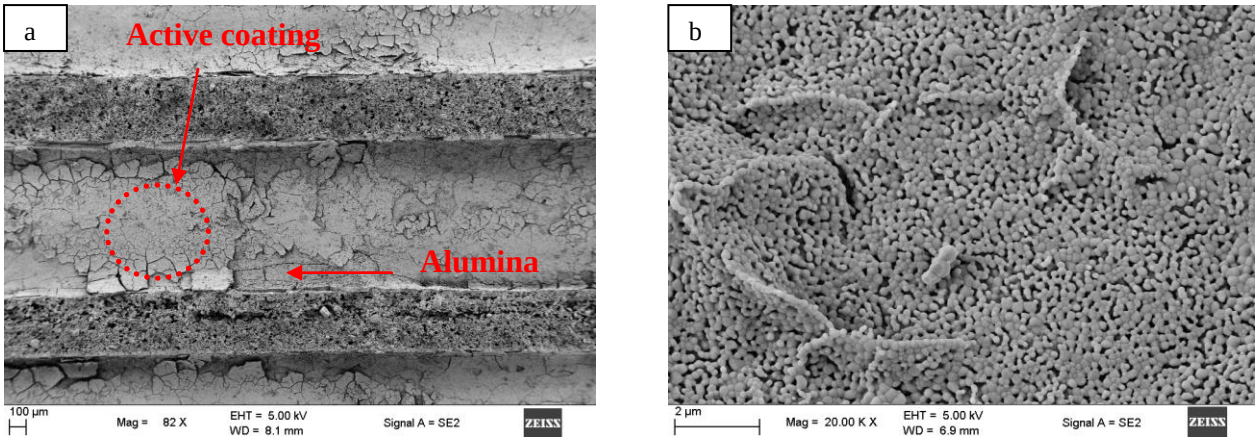

Figure 3.8: SEM images of the 10 weight % iron-molybdenum supported on gamma-alumina coated monolith, (a) coating within channels (b) 20 000 times magnification

Figure 3.5 shows the bare cordierite monolith after sectioning within the channels and also with a higher magnification within the channel. The random particle observed and circled in this image is due to a piece of cordierite from sectioning the monolith. The 5 weight % iron-molybdenum coated monolith is shown in Figure 3.6. The coating within the channels is highlighted in Figure 3.6 (a), however, also noted are areas which have not been coated. Figure 3.6 (b) depicts the molybdenum trioxide plate-like structures and the spherical-like morphology of iron molybdate, at a higher magnification. Instead of monolayer coverage over the bare monolith, agglomeration of the iron-molybdenum active layer was observed, suggesting that the coating probably does not adhere well to the cordierite structure. In

Figure 3.7, the monolith coated with 10 weight % gamma-alumina shows complete coverage of the channels within the monolith. However, this does not account for the entire monolith, as there could be a possibility of exposed bare cordierite sites. Figure 3.8 depicts the 10 weight % iron-molybdenum active layer supported on the gamma-alumina coated monolith. Figure 3.8 (a) shows that the iron-molybdenum active layer adheres to the gamma-alumina within the channels and attains better monolayer coverage, than direct coating of the iron-molybdenum catalyst shown in Figure 3.6 (a). Also, successful supporting of the iron-molybdenum active layer on the gamma-alumina is shown by the difference in morphology at higher magnifications in Figures 3.7 (b) and 3.8 (b). Figure 3.8 (b) shows that the active layer is predominantly iron molybdate due to the spherical-like morphology, whilst molybdenum trioxide plate-like structures were not observed. The excess molybdenum may be forming bonds with alumina [36, 37], which could explain the dominating iron molybdate morphology on the surface.

3.3.2 Reaction studies

In the catalytic testing work for this project, studies on the carborundum packed reactor tube (blank), bare monolith and coated monoliths were performed. The blank reactor (non-catalytic) study was completed to assess the efficacy of 24 grit carborundum in quenching the radical reactions in this reactor setup. The blank reactor study in this work refers to a carborundum packed reactor tube, plugged with glass wool at both ends.

3.3.2.1 Blank reactor study

The contribution from the carborundum packed reactor tube was investigated at a temperature range from 350 °C to 500 °C, in increments of 50 °C, using the gas flow rates mentioned in Section *3.2.5*. Previous work in the research group has shown an empty reactor tube and void space may impact significantly on conversion, in the oxidative dehydrogenation of *n*-hexane [38] and *n*-octane [14]. The authors suggested silicon carbide (carborundum) as an effective packing material to quench free radical reactions in a 316 stainless steel reactor tube. Considering, the reactor tube used for this work was 316 stainless steel and larger in dimensions to the reported reactor tube, a non-catalytic study of this carborundum packed reactor tube was completed prior to catalytic testing.

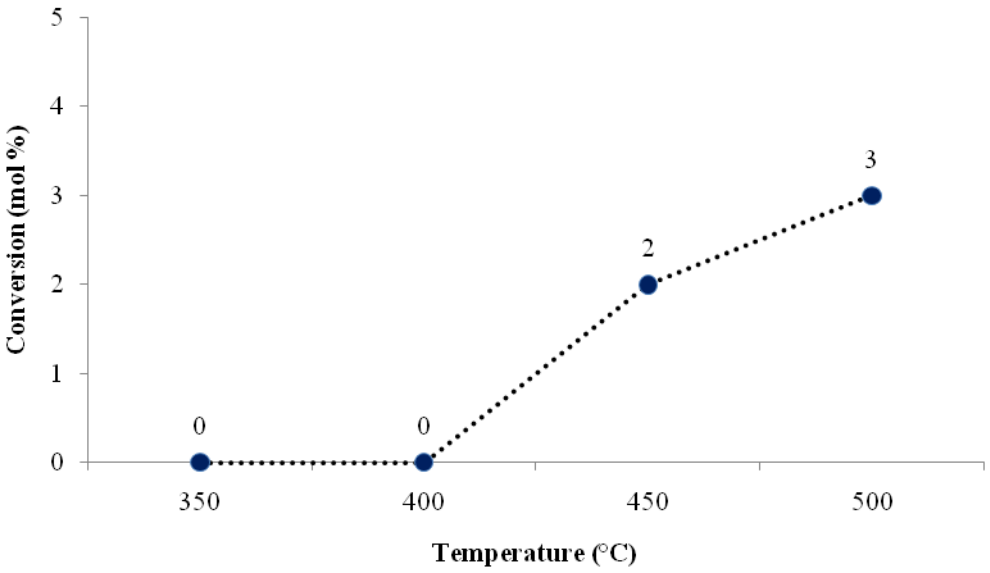

Figure 3.9: Conversion of *n*-octane in the carborundum packed reactor tube as a function of temperature at a GHSV of 1000 h^{-1} and carbon to oxygen ratio of 8:2

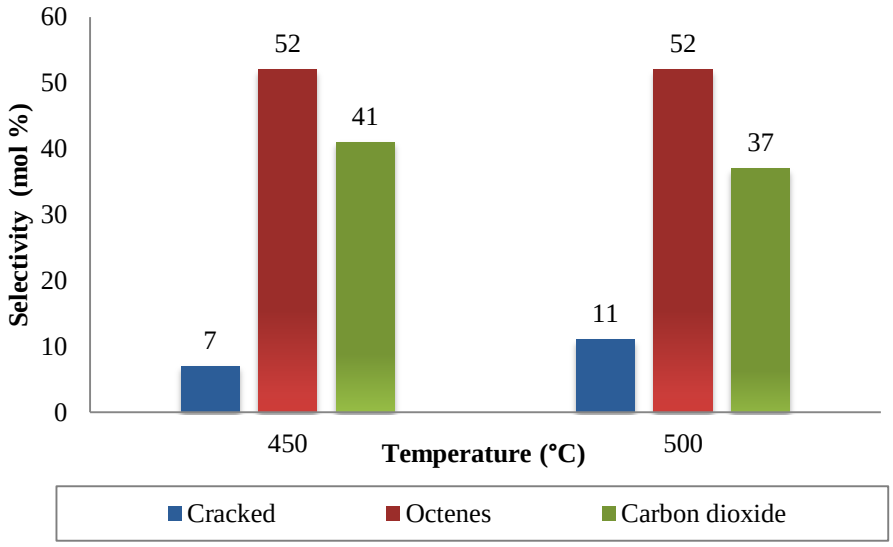

Figure 3.10: Product selectivity profile from the carborundum packed reactor tube at a GHSV of 1000 h^{-1} and carbon to oxygen ratio of 8:2

The effect of the conversion of *n*-octane as a function of temperature is shown in Figure 3.9. No conversion was observed at 350 °C and 400 °C, however, conversion increased beyond 400 °C. The conversion increased gradually from zero to 2 % at 450 °C and finally 3 % at 500 °C.

Figure 3.10 shows the selectivity to the major products formed namely cracked products, octenes and carbon dioxide. Products grouped as cracked were C_1 to C_3 alkanes and C_2 to C_6 alkenes. The octenes formed were 1-octene, trans-2-octene and cis-2-octene, trans-3-octene and trans-4-octene. The products observed may possibly be formed from the thermal energy provided by the reactor system to break C-H and C-C bonds of *n*-octane. Carbon dioxide could be formed as a result of the combustion of these products or even the direct combustion of the alkane feed. The reactor can also initiate free radicals which could be responsible for the product profile shown in Figure 3.10. Increasing the temperature from 450 °C to 500 °C resulted in a 4 % increase in the selectivity towards the formation of cracked products, whilst carbon dioxide selectivity decreased by 4 %. This would suggest that at 500 °C, as the conversion of *n*-octane increased, cracked products increased accordingly, however, they were not combusted to carbon dioxide.

It was clear from this study that carborundum was effective in filling the void spaces of the reactor tube and quenching free radical reactions at these flow rates, since a low conversion and the formation cyclic oxygenates were not observed. Also noted was the thermal conversion of *n*-octane above 400 °C at these conditions. A reaction temperature of 400 °C was therefore chosen for further catalytic experiments, to prevent any contribution from the thermal activation of *n*-octane.

3.3.2.2 Bare monolith and 5 weight % iron-molybdenum coated monolith

The bare and 5 weight % iron-molybdenum coated monoliths were tested under the experimental conditions mentioned in Section *3.2.5*. Initial testing was performed on the bare cordierite monolith, to assess the contribution from this non-coated ceramic support, in the oxidation of *n*-octane. The iron-molybdenum active layer was then applied directly to the monolith, without a secondary support such as gamma-alumina. The effect of this direct 5 weight % iron-molybdenum coating over the cordierite monolith was investigated.

In comparison to the blank reactor studies, higher conversions and diverse selectivity profiles were noted for the monolithic reactions. A 27 % conversion of *n*-octane was observed over the bare monolith, whilst a conversion of 22 % was observed for the 5 weight % coated monolith. A direct correlation between the high activitiy and surface area of the support cannot be made, since monoliths offer a low BET surface area (< 1 m^2/g) [39]. The reactor tube packed with carborundum showed no conversion under these conditions, therefore, the

reactor tube in this setup does not contribute to this activity. Instead, it may be more plausible to ascribe this high activity to the material make-up of the support. The monolith may also provide significant void spaces for further reactions, due to the 1 mm width and 25 mm length of the channels.

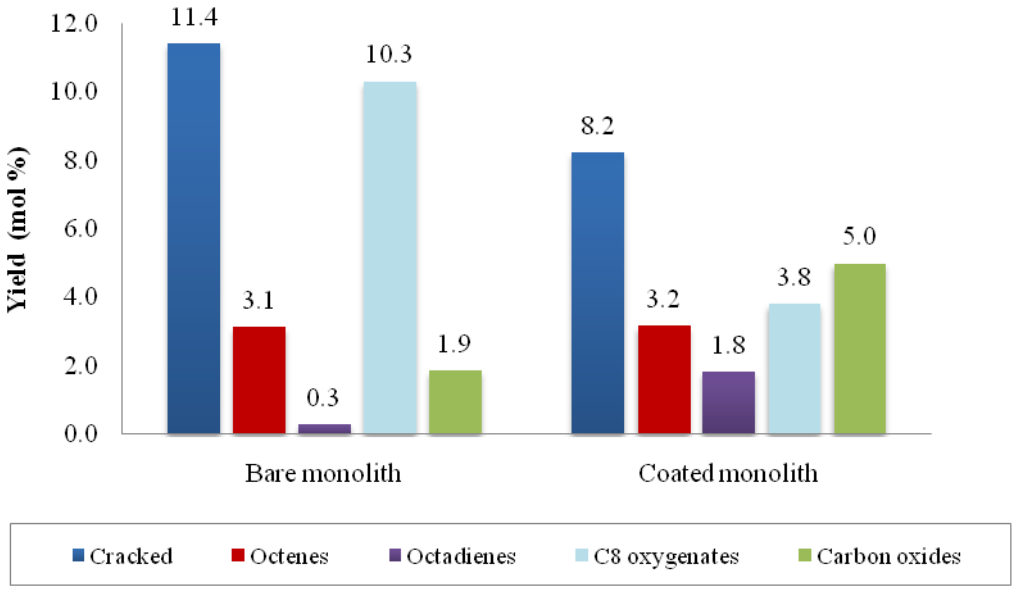

Figure 3.11: Product yield profile for bare monolith and coated monolith reactions at a GHSV of 1000 h^{-1} and carbon to oxygen ratio of 8:2

The products from the bare monolith reaction, as shown in Figure 3.11, were grouped as cracked, octenes, octadienes, C_8 oxygenates and carbon oxides. Cracked products, grouped from Figure 3.11 and shown in more detail in Table 3.2, consisted of C_1-C_7 alkanes, C_1-C_3 oxygenates and C_2-C_7 alkenes. C_8 oxygenates were separated into octadienones, cyclic ethers, octanones and octanols. Also, carbon oxides were divided into carbon monoxide and carbon dioxide.

Cracked products and C_8 oxygenates, with yields 11.4 % and 10.3 %, respectively, dominated the product profile for the bare monolith reaction. A high yield of oxygenated compounds, relative to the products formed, is usually an indication of homogeneous gas phase reactions, as shown in single gauze reactors at short contact times [9-11]. The highest yield belonging to C_8 oxygenated products, over the bare monolith, therefore strongly suggests the participation of free radicals. In support of this theory, cyclic ethers, usually formed by a free radical mechanism [40], were detected and grouped in the C_8 oxygenated products.

Amid the decrease in conversion of the reactant over the iron-molybdenum coated monolith reaction, the yield to cracked products, C_8 oxygenates and carbon oxides differed significantly, compared to octenes and octadienes, as shown in Figure 3.11. Particularly, the yield to cracked products decreased from 11.5 % to 8.3 %, C_8 oxygenates decreased from 10.3 % to 3.7 % and carbon oxides increased from 1.9 % to 5.0 %, from the bare monolith to coated monolith, respectively. However, no noteworthy change in yield was observed for octenes, whilst the yield of octadienes increased from 0.3 % to 1.8 %. The product yield profile for the iron-molybdenum coated monolith therefore suggests that the free radical mechanism is being retarded due to the coating. A more detailed breakdown of the products formed, as shown in Table 3.2, may provide for a better comparison and mechanistic interpretation.

Table 3.2: Selectivities and yields of products for bare and coated monolith reactions

	Bare monolith		5 weight % coated monolith	
Products	Selectivity (%)	Yield (%)	Selectivity (%)	Yield (%)
C_1-C_7 Alkanes	13.9	3.8	9.5	2.1
C_2-C_7 Alkenes	23.6	6.4	24.8	5.5
C_1-C_3 Oxygenates	4.8	1.3	3.1	0.7
Octenes	11.6	3.1	14.4	3.2
Octadienes	1.0	0.3	8.2	1.8
Octadienones	1.5	0.4	1.0	0.2
Cyclic ethers	31.6	8.5	15.2	3.3
Octanones	4.3	1.2	0.5	0.1
Octanols	0.8	0.2	0.6	0.1
Carbon monoxide	2.8	0.8	4.8	1.1
Carbon dioxide	4.1	1.1	17.9	3.9

The saturated hydrocarbons from the bare monolith reaction consisted largely of, methane, ethane, propane as the major components while C_4-C_7 hydrocarbons were the minor components and together contributed to the 13.9 % selectivity, as shown in Table 3.2. The unsaturated cracked hydrocarbons, formed over the bare monolith, consisted of mainly ethylene, 1-pentene and 1-hexene, totaling a selectivity of 19.5 % from the 23.6 % selectivity to C_2-C_7 alkenes. Propylene, isomers of butene and 1-heptene were produced in small quantities, contributing to the remainder 4.1 % selectivity to cracked alkenes. The high selectivity, as shown in Table 3.2 for the bare monolith, towards cracked alkanes and alkenes may be due to the acidity of the surface of the monolith. It is well known that silica and silica-alumina surfaces facilitate the cracking of alkanes [41, 42]. The higher ratio of silica in the cordierite structure ($5SiO_2$•$2Al_2O_3$•$2MgO$) compared to alumina and magnesium oxide, could therefore be responsible for the high selectivity toward cracked alkanes and alkenes. Initially, *n*-octane may undergo hydrogen abstraction via the acidic site, thus forming a carbenium ion, which after beta-scission, may directly result in an olefin or undergo a further hydride transfer step to form a saturated hydrocarbon [43]. Although, acidic cracking may explain the high selectivity to cracked products, silica [44] and magnesium oxide [45] can also activate oxygen, producing O_2^-, which usually is associated with free radical reactions. The trend of the high selectivity toward C_1-C_3 alkanes and ethylene, as well as the alpha-olefins 1-pentene and 1-hexene herein correlates with the typical reported non-catalytic mechanism of alkane cracking [43, 46], thus also suggesting that the cracking mechanism may occur through free radicals. Cracked C_1-C_3 oxygenates, such as methanol, acetone and 1-propanol could possibly be formed from the oxygen activation of the cracked alkanes, forming an alkoxy [44] and/or peroxy species [9], which are further rearranged or cleaved.

The C_8 oxygenates, formed from the bare monolith, were dominated by cyclic ethers with a 31.6 % selectivity and 8.5 % yield, as shown in Table 3.2. Cyclic ethers are usually formed in the oxidation of alkanes through a radical type mechanism [11, 13, 47]. In this reaction, five (furan) and six (pyran) membered cyclic rings were formed and identified by their characteristic mass spectra. The furans consisted of 2-butyl-tetrahydrofuran, 2,5-methyl-propyl-tetrahydrofuran, 2,5-diethyl-tetrahydrofuran and the pyrans, included 2-propyl-tetrahydropyran and 2,6-methyl-ethyl-tetrahydropyran. Isomers of 2,5-methyl-propyl-tetrahydrofuran, 2,5-diethyl-tetrahydrofuran and 2,6-methyl-ethyl-tetrahydropyran were also present in the product stream. A dioxygen cyclic ether was detected in small quantities, as

2H-pyran-2-one-tetrahydro-6-propyl. The mass spectra of the cyclic ethers formed are shown in Appendix 3.

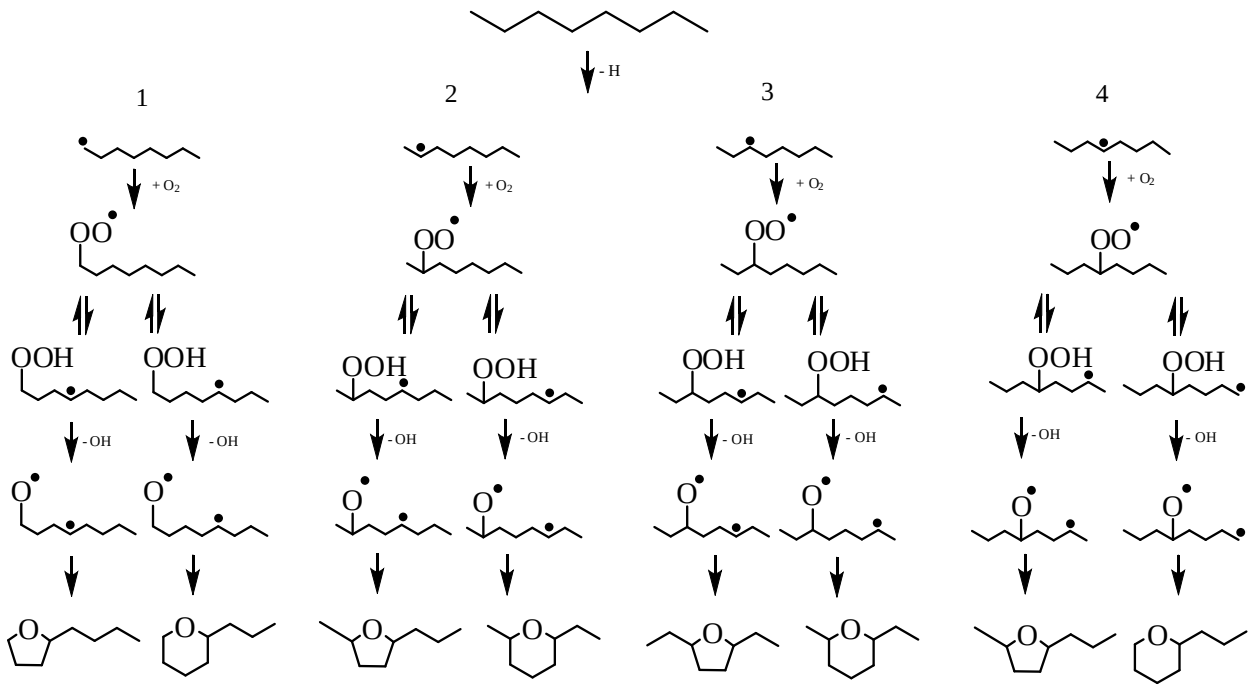

Scheme 3.1: Proposed mechanism for cyclic ether formation from the oxidation of *n*-octane

The proposed mechanistic routes for the formation of the dominant cyclic ethers are shown in Scheme 3.1. Four possible pathways may exist from the initial hydrogen abstraction, which can occur on the surface of the bare monolith. Abstraction of hydrogen from the first, second, third or fourth carbon of *n*-octane results in an alkyl radical. The alkyl radical then reacts with oxygen, possibly a non-selective oxygen species, yielding a peroxy species. This peroxy radical isomerizes, forming either, if not both, intermediates of hydroperoxy alkyl radicals. Removal of an OH produces the unstable di-radical specie which cyclizes to give the stable five and or six membered cyclic ether.

The cyclic ethers formed were dominated by 2-propyl-tetrahydropyran and 2,5-methyl-propyl-tetrahydrofuran. This indicates that perhaps route four is more favoured for cyclic ether formation, over routes one, two and three. The other C_8 oxygenated compounds formed in considerably lower selectivies and yields, included octanones, in the form of 2-octanone, 3-octanone and 4-octanone, and octanols, in the form of 3-octanol and 4-octanol. The major octanones were 3-octanone and 2-octanone, whilst 4-octanone was produced in trace quantity resulting in a total of 4.3 % selectivity. Octanone formation may be a result of decomposition

of the hydroperoxy species [48], which in the reaction over the bare monolith could occur via routes 2, 3 and 4. A low selectivity of 0.8 % to octanols was found in the product stream, possibly due to hydrolysis of the di-radical species. The hydroperoxy species can also undergo a second addition of oxygen [12], which may be the intermediate species for the formation of octadienones and the 2H-pyran-2-one-tetrahydro-6-propyl cyclic ether.

The octenes formed over the bare monolith were 1-octene, isomers of 2-octene, trans-3-octene and trans-4-octene, accumulating to the 11.6 % selectivity. The alkyl radicals, shown in Figure 12, after hydrogen abstraction, may undergo oxidative dehydrogenation to form these olefins [11]. Apart from the formation of octenes, dienes were also observed, in the form of isomers of 3,5-octadiene. The 1.0 % selectivity to diene formation may be a result of the decomposition of the hydroperoxy species [13]. This possibly occurs via the hydroperoxy species from route 3 and route 4, thus producing 3,5-octadiene and water.

Octenes, octadienes, octadienones, octanones and octanols were formed in lower selectivities and yields compared to cracked products and cyclic ethers, respectively, over the bare monolith. This could be supporting evidence that a radical mechanism occurred over the bare monolith, yielding predominantly cracked products and cyclic ethers, whilst octenes, octadienes, octadienones, octanones and octanols were products of side reactions via the proposed mechanistic routes. Also, cyclic ethers dominated the selectivity profile for C_8 oxygenates, thus suggesting that the rate of cyclic ether formation was greater than the rate of side product formation. The mechanism for carbon oxide formation is not entirely clear, however, this low selectivity and yield may be due to partial oxidation, sequential oxidation to combustion products or direct combustion at any point during the mechanism.

The product yield profile over the iron-molybdenum coated monolith, shown in Figure 3.11, differed from that of the reaction over the bare monolith. Notable differences in selectivities were also observed, as shown in Table 3.2. Overall, the selectivities to cracked products and C_8 oxygenates decreased, whilst the selectivities to octenes, octadienes and carbon oxides increased. The iron-molybdenum coating possibly stabilizes the alkyl radicals formed, allowing for the octenes to desorb from the surface faster, as opposed to further reacting with active oxygen, ultimately resulting in a greater selectivity of 14.4 % to octenes. Also, the basic nature of the iron-molybdenum active layer probably favours the decomposition of the hydroperoxy species as an alternative to removal of a hydroxide. This theory is supported by

the decrease in the selectivities to octadienones, cyclic ethers, octanones and octanols, and the increase in the selectivity to octadienes. Carbon oxides, particularly carbon dioxide, increased in selectivity and yield after active layer coating, perhaps due to molybdenum trioxide which facilitates complete combustion [49-51].

The product yield and selectivity profile for the iron-molybdenum coated monolith reaction shows that a 5 weight % percent coating does not strongly suppress the radical mechanism, since the surface of the monolith is not entirely covered with coating, as shown in Figure 3.6 (a). A higher weight % coating may prove better, however, the iron-molybdenum active layer adheres weakly to the bare monolith. Instead, coating the bare monolith with a secondary support prior to active layer coating could provide for better adherence and a higher attainable weight loading.

3.3.2.3 Gamma-alumina coated monolith and iron-molybdenum supported on gamma-alumina coated monolith

The importance of understanding the contribution made by the monolith prior to active layer coating cannot be over emphasized, as shown from the results of the reaction with the bare monolith in Section *3.3.2.2*. The monolith with a 10 weight % gamma-alumina coating was therefore tested under the reaction conditions described in Section *3.2.5*. The 10 weight % coating was chosen so as to coat as much of the monolith channels as possible, without blocking the channels, since the active layer would be coated over this. In order to understand the effect of coating the bare monolith with gamma-alumina, in the oxidation of *n*-octane, the product yield profile over the gamma-alumina coated monolith was compared to the product yield profile over the bare monolith,

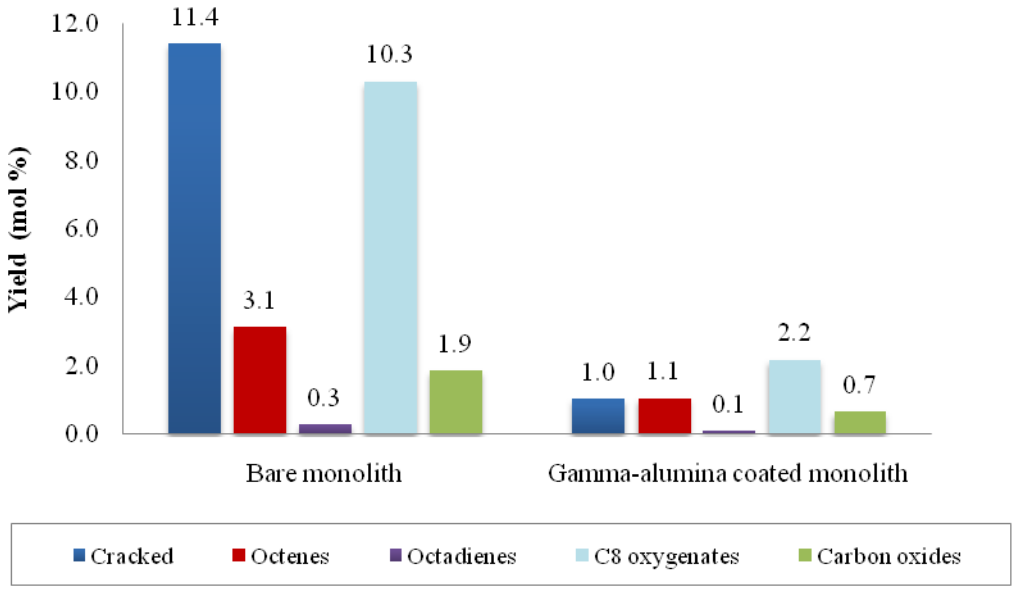

Figure 3.12: Product yield profile of bare monolith and 10 weight % gamma-alumina coated monolith at a GHSV of 1000 h^{-1} and carbon to oxygen ratio of 8:2

Coating the ceramic monolith with 10 weight % gamma-alumina resulted in a substantial decrease in the conversion of *n*-octane, from 27 % for the bare monolith to 5 % for the alumina coated monolith. The product yield profile for the alumina coated monolith, as shown in Figure 3.12, was therefore significantly different to the bare monolith. Cracked and C_8 oxygenated products decreased in yield from 11.4 % to 1.1 % and 10.3 % to 2.2 %, respectively. In comparison to cracked and C_8 oxygenated products, moderate decreases in yields were observed for octenes, octadienes and carbon oxides. Ultimately, comparing the gamma-alumina coated monolith reaction and the bare monolith reaction, similar products were observed in lesser quantity over the gamma-alumina coated monolith, whilst products such as octadienones and 2H-pyran-2-one-tetrahydro-6-propyl were not detected in the product stream.

The decrease in conversion and, hence, decrease in yields to cracked and C_8 oxygenated products may perhaps be due to the alumina covering the reactive sites of silica and magnesium oxide on the monolith. The gamma-alumina may have also neutralized the high acidic nature of the monolith surface, in turn reducing the rate of hydrogen abstraction. Although SEM imaging of the sectioned gamma-alumina coated monolith shows that the channels were coated, there could be the possibility of some small exposed sites remaining, which may be responsible for the low conversion. Alternatively, gamma-alumina may also

promote the radical mechanism, however, being less active in comparison to silica or magnesium oxide, due to its amphoteric nature. A future study of the effect of gamma-alumina washcoat loading in the oxidation of *n*-octane may thus aid in better understanding the role of gamma-alumina in homogeneous gas phase reactions over monoliths. The effect of the amount of washcoat loading on the monolith was not the primary focus of this research effort, however, it may prove useful in future work.

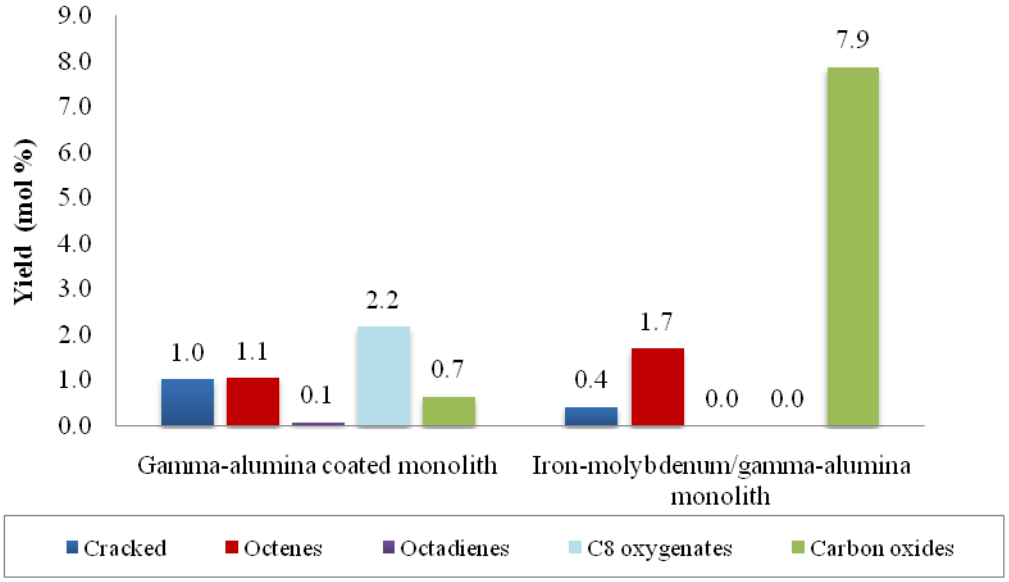

Figure 3.13: Product yield profile of the gamma-alumina coated monolith and 10 weight % iron-molybdenum supported on a gamma-alumina coated monolith at a GHSV of 1000 h^{-1} and carbon to oxygen ratio of 8:2

The product yield profile, in Figure 3.13, for the 10 weight % iron-molybdenum active layer coated onto the gamma-alumina coated monolith, was compared to the yield profile for the gamma-alumina coated monolith with no active layer coating. A higher conversion of 10 % was found for the iron-molybdenum active layer coated gamma-alumina monolith. Apart from the increase in conversion of the reactant, the product yield profile for the active layer supported on the gamma-alumina coated monolith was very different. After coating the active layer, carbon oxides dominated the product yield profile, giving a 7.9 % yield. Also, the formation of octadienes and C_8 oxygenates was suppressed. A mild decrease in cracked products was observed in the product yield profile, after active layer coating, as well as an increase in the yield to octenes.

Table 3.3: Selectivities of products from the gamma-alumina coated monolith reaction and iron-molybdenum supported on the gamma-alumina coated monolith

	Gamma-alumina coated monolith	Iron-molybdenum/gamma-alumina coated monolith
Products	Selectivity (%)	
C_1-C_7 Alkanes	8.6	2.9
C_2-C_7 Alkenes	8.9	1.3
C_1-C_3 Oxygenates	3.0	-
Octenes	21.2	17.0
Octadienes	1.6	-
Cyclic ethers	39.0	-
Octanones	4.6	-
Carbon monoxide	2.9	14.6
Carbon dioxide	10.2	64.2

Apart from the active layer supported on the gamma-alumina coated monolith not yielding cracked oxygenates, octadienes or C_8 oxygenate, as shown in Table 3.3 and Figure 3.13, the selectivities to specific products also differed. Cracked alkanes for the gamma-alumina supported active layer monolith reaction consisted of methane, ethane and propane contributing to a selectivity of 2.9 %. At the same time, 1-hexene was the only cracked alkene formed, with a selectivity of 1.3 %. Carbon oxides, collectively as carbon monoxide and carbon dioxide were produced in the highest yield. Carbon dioxide, however, dominated with a selectivity of 64.2 %, whilst carbon monoxide was produced with a selectivity of 14.6 %. Carbon monoxide and carbon dioxide are usually associated as being secondary products from the consecutive oxidation of alkenes, though, carbon dioxide is also suggested to be a combustion product from the direct oxidation of the alkane reactant [52]. Moreover, in the case of the selective oxidation of butane, Martin-Aranda *et al.* showed a greater selectivity to carbon oxides over nickel molybdate, than over alkali metal promoted nickel molybdate [53]. The interaction of butenes with the nickel molybdate was suggested, by these authors, to

occur more strongly than the promoted molybdate, thus leading to consecutive oxidation and hence a higher selectivity to carbon oxides. The high yield and selectivity to carbon oxides, in the oxidation of *n*-octane herein, could therefore be a result of the strong interaction of the octenes and iron molybdate, which seems to be the dominant morphology, as seen in Figure 3.8(b). Also, the interaction between the iron molybdate and gamma-alumina needs to be taken into consideration, since molybdenum supported on gamma-alumina has high Brønsted acidity, which may drive the products towards consecutive or deep oxidation [36].

3.4 Conclusion and perspective

The oxidation of *n*-octane over the bare cordierite monolith produced mainly cracked products and C_8 oxygenates. Cyclic ethers were produced in 31.6 % selectivity over the bare cordierite monolith at a total gas flow rate of 131.7 ml/min, with a C:O ratio of 8:2 and 11.43 % *n*-octane in the total feed. These results suggest a free radical mechanism may be dominating in this reaction. A mechanism was therefore postulated, via four possible routes of hydrogen abstraction, resulting in the respective cyclic ethers formed. Coating the active iron-molybdenum layer directly on the monolith does not allow for good adherence, however, it does reduce the production of cyclic ethers. The 10 weight % coating of gamma-alumina over the cordierite monolith has a more pronounced effect on the homogeneous gas phase mechanism, reducing the conversion from 27 % to 5 %. An iron-molybdenum active layer of 10 weight % supported over a gamma-alumina coated monolith favours deep oxidation. Overall, coating the bare cordierite monolith with gamma-alumina proves effective in retarding the free radical mechanism, however, a higher weight % coating may be required to suppress the formation of cyclic ethers. Future work on this system should involve investigating a lower weight % coating of the iron-molybdenum active layer on the gamma-alumina coated monolith. Also, higher flow rates could be explored as an attempt at reducing consecutive oxidation.

3.5 Acknowledgements

We would like to thank SASOL, the NRF and THRIP for financial support. Also, we would like to thank Mr Vishal Bharuth at the UKZN Electron Microscopy Unit, Mr Danasegran Padayachee at the UKZN Chemical Engineering Workshop and Mr Enock Checkure at the School of Chemistry and Physics.

3.6 References

[1] A. Cybulski, J.A. Moulijn, Catalysis Reviews 36 (1994) 179-270.

[2] D.A. Hickman, L.D. Schmidt, Journal of Catalysis 138 (1992) 267-282.

[3] M. Huff, L.D. Schmidt, Journal of Physical Chemistry 97 (1993) 11815-11822.

[4] D.A. Hickman, L.D. Schmidt, Science 259 (1993) 343-346.

[5] S.S. Bharadwaj, C. Yokoyama, L.D. Schmidt, Applied Catalysis A: General 140 (1996) 73-97.

[6] A. Beretta, L. Piovesan, P. Forzatti, Journal of Catalysis 184 (1999) 455-468.

[7] A. Beretta, P. Forzatti, E. Ranzi, Journal of Catalysis 184 (1999) 469-478.

[8] A.G. Dietz, A.F. Carlsson, L.D. Schmidt, Journal of Catalysis 176 (1996) 459-473.

[9] D.I. Iordanoglou, L.D. Schmidt, Journal of Catalysis 176 (1998) 503-512.

[10] D.I. Iordanoglou, A.S. Bodke, L.D. Schmidt, Journal of Catalysis 187 (1999) 400-409.

[11] R.P. O'Connor, L.D. Schmidt, Chemical Engineering Science 55 (2000) 5693-5703.

[12] F. Buda, R. Bounaceur, V. Warth, P.A. Glaude, R. Fournet, F. Battin-Leclerc, Combustion and Flame 142 (2005) 170-186.

[13] C.K. Westbrook, W.J. Pitz, O. Herbinet, H.J. Curran, E.J. Silke, Combustion and Flame 156 (2009) 181-199.

[14] H.B. Friedrich, A.S. Mahomed, Applied Catalysis A: General 347 (2008) 11-22.

[15] V.A. Sadykov, S.N. Pavlova, N.F. Saputina, I.A. Zolotarskii, N.A. Pakhomov, E.M. Moroz, V.A. Kuzmin, A.V. Kalinkin, Catalysis Today 61 (2000) 93-99.

[16] G. Karamullaoglu, T. Dogu, Chemical Engineering Communications 190 (2003) 1427-1438.

[17] N. Burriesci, F. Garbassi, M. Petrera, G. Petrini, N. Pernicone, Solid State Reactions in Fe-Mo Oxide Catalysts for Methanol Oxidation During Aging in Industrial Plants, in: B. Delmon, G.F. Froment, (Eds.), Studies in Surface Science and Catalysis, Elsevier, 1980, 115-126.

[18] M. Carbucicchio, P. Forzaiti, E. Tronconi, P.L. Villa, F. Trifiro, Deactivation of Silica Supported Fe_2O_3 -MoO_3 Catalyst for the Oxidation of Methanol, in: B. Delmon, G.F. Froment, (Eds.), Studies in Surface Science and Catalysis, Elsevier, 1980, 103-113.

[19] A.P.V. Soares, M.F. Portela, A. Kiennemann, A comparison of iron molybdate catalysts for methanol oxidation prepared by copreciptation and new sol-gel method, in: R.K. Grasselli, S.T. Oyama, A.M. Gaffney, J.E. Lyons, (Eds.), Studies in Surface Science and Catalysis, Elsevier, 1997, 807-816.

[20] A.P.V. Soares, M.F. Portela, A. Kiennemann, Catalysis Reviews 47 (2005) 125-174.

[21] K.I. Ivanov, D.Y. Dimitrov, Catalysis Today 154 (2010) 250-255.

[22] G. Jin, W. Weng, Z. Lin, N.F. Dummer, S.H. Taylor, C.J. Kiely, J.K. Bartley, G.J. Hutchings, Journal of Catalysis 296 (2012) 55-64.

[23] S. Pradhan, J.K. Bartley, D. Bethell, A.F. Carley, M. Conte, S. Golunski, M.P. House, R.L. Jenkins, R. Lloyd, G.J. Hutchings, Nature Chemistry 4 (2012) 134-139.

[24] D. Parviz, M. Kazemeini, A.M. Rashidi, K. Jafari Jozani, Journal of Nanoparticle Research 12 (2010) 1509-1521.

[25] L. Villegas, F. Masset, N. Guilhaume, Applied Catalysis A: General 320 (2007) 43-55.

[26] Y. Ding, S.-H. Yu, C. Liu, Z.-A. Zang, Chemistry – A European Journal 13 (2007) 746-753.

[27] Q. Xu, G. Jia, J. Zhang, Z. Feng, C. Li, The Journal of Physical Chemistry C 112 (2008) 9387-9393.

[28] Y.S. Yoon, N. Fujikawa, W. Ueda, Y. Moro-oka, K.W. Lee, Catalysis Today 24 (1995) 327-333.

[29] G.A. Tsigkinos, W.W. Swanson, Industrial & Engineering Chemistry Product Research and Development 17 (1978) 208-214.

[30] A.P.V. Soares, M.F. Portela, A. Kiennemann, L. Hilaire, Chemical Engineering Science 58 (2003) 1315-1322.

[31] K. Routray, W. Zhou, C.J. Kiely, W. Grünert, I.E. Wachs, Journal of Catalysis 275 (2010) 84-98.

[32] H. Tian, I.E. Wachs, L.E. Briand, The Journal of Physical Chemistry B 109 (2005) 23491-23499.

[33] P. Forzatti, P.L. Villa, N. Ferlazzo, D. Jones, Journal of Catalysis 76 (1982) 188-207.

[34] J.-L. Li, Y.-X. Zhang, C.-W. Liu, Q.-M. Zhu, Catalysis Today 51 (1999) 195-199.

[35] M.R. Sun-Kou, S. Mendioroz, J.L.G. Fierro, J.M. Palacios, A. Guerrero-Ruiz, Journal of Materials Science 30 (1995) 496-503.

[36] M.C. Abello, M.F. Gomez, L.E. Cadús, Industrial & Engineering Chemistry Research 35 (1996) 2137-2143.

[37] K. Chen, S. Xie, A.T. Bell, E. Iglesia, Journal of Catalysis 198 (2001) 232-242.

[38] H.B. Friedrich, N. Govender, M.R. Mathebula, Applied Catalysis A: General 297 (2006) 81-89.

[39] E. Soghrati, M. Kazemeini, A.M. Rashidi, K.J. Jozani, Procedia Engineering 42 (2012) 1484-1492.

[40] O. Herbinet, S. Bax, P.-A. Glaude, V. Carré, F. Battin-Leclerc, Fuel 90 (2011) 528-535.

[41] C.L. Thomas, Industrial & Engineering Chemistry 41 (1949) 2564-2573.

[42] Y.V. Kissin, Catalysis Reviews 43 (2001) 85-146.

[43] S.T. Sie, Industrial & Engineering Chemistry Research 31 (1992) 1881-1889.

[44] F. Cavani, F. Trifirò, Catalysis Today 51 (1999) 561-580.

[45] M. Iwamoto, J.H. Lunsford, The Journal of Physical Chemistry 84 (1980) 3079-3084.

[46] B.S. Greensfelder, H.H. Voge, G.M. Good, Industrial & Engineering Chemistry 41 (1949) 2573-2584.

[47] E.S.C. Kwok, J. Arey, R. Atkinson, The Journal of Physical Chemistry 100 (1996) 214-219.

[48] T.Y. Stoylkova, C.D. Chanev, H.T. Lechert, C.P. Bezouhanova, Applied Catalysis A: General 203 (2000) 121-126.

[49] J. Haber, E. Serwicka, Polyhedron 5 (1986) 107-109.

[50] K. Brückman, R. Grabowski, J. Haber, A. Mazurkiewicz, J. Słoczyński, T. Wiltowski, Journal of Catalysis 104 (1987) 71-79.

[51] J. Haber, E. Lalik, Catalysis Today 33 (1997) 119-137.

[52] L.M. Madeira, F.J. Maldonado-Hódar, M.F. Portela, F. Freire, R.M. Martin-Aranda, M. Oliveira, Applied Catalysis A: General 135 (1996) 137-153.

[53] R.M. Martin-Aranda, M.F. Portela, L.M. Madeira, F. Freire, M. Oliveira, Applied Catalysis A: General 127 (1995) 201-217.

Chapter 4

Summary and conclusion

Summarising, coated monoliths prepared included a 5 weight % iron-molybdenum active layer directly on the bare monolith, a 10 weight % gamma-alumina coated monolith and a 10 weight % iron-molybdenum active layer coating supported over a gamma-alumina coated cordierite monolith. Characterization of the iron-molybdenum powder showed the presence of iron molybdate and molybdenum trioxide, in a ratio of 2.2:1 Mo:Fe. The SEM images of sectioned pieces of the monoliths used in the catalytic testing showed that coating was achieved within the channels. The method of dip coating and growing the active phase over the monolith was therefore effective, as also was the slurry coating of gamma-alumina.

Prior to the catalytic investigation of the bare and coated monoliths, a blank reactor study was done. No conversion was observed at 350 °C and 400 °C, for the carborundum packed reactor tube, at 1000 h^{-1}. Since thermal activation of *n*-octane was observed beyond 400 °C, further reactions were performed isothermally at 400 °C to avoid any activation of the reactant due to the reactor set up.

The oxidation of *n*-octane over the bare cordierite monolith produced mainly cyclic ethers with a selectivity of 31.6 %. The formation of cyclic ethers in the oxidation of alkanes usually occurs via a radical mechanism. A proposed mechanistic route, via four possible routes of hydrogen abstraction, showed how these cyclic ethers may have formed during the reaction. Coating the bare monolith with an iron-molybdenum layer retarded the formation of cyclic ethers, however, not as effectively as gamma-alumina, which reduced conversion from 27 % to 5 %, with a 10 weight % coating of gamma-alumina. Supporting the iron-molybdenum active layer onto the gamma-alumina coated monolith did not yield any cyclic ethers, though, instead it favoured mainly deep oxidation. The high selectivity to carbon oxides may, therefore, be due to consecutive oxidation or direct oxidation of *n*-octane, or perhaps the interaction of iron molybdate and gamma-alumina, leading to a high Brønsted acidity and, hence, favouring carbon oxide formation. Overall, the bare cordierite monolith seems to be responsible for the radical mechanism and also the high selectivity to cyclic ethers. It may also be important to consider using gamma-alumina as a secondary support,

prior to active layer coating, and not coat the active layer directly onto the bare cordierite monolith.

Future work for this study could include further understanding the contribution of the gamma-alumina coating to the monolith, by performing the oxidation of *n*-octane using varying weight % coatings of gamma-alumina on the monolith. Investigating a lower weight % coating of the iron-molybdenum active layer on the gamma-alumina coated monolith may also be an option, together with exploring higher flow rates as an attempt at reducing consecutive or deep oxidation. Effort could also be directed towards testing of the powder form of the catalysts, without the presence of the monolith, however, a suitable method for fair comparison may need to be established first.

Appendix 1

XRD and ICP-OES

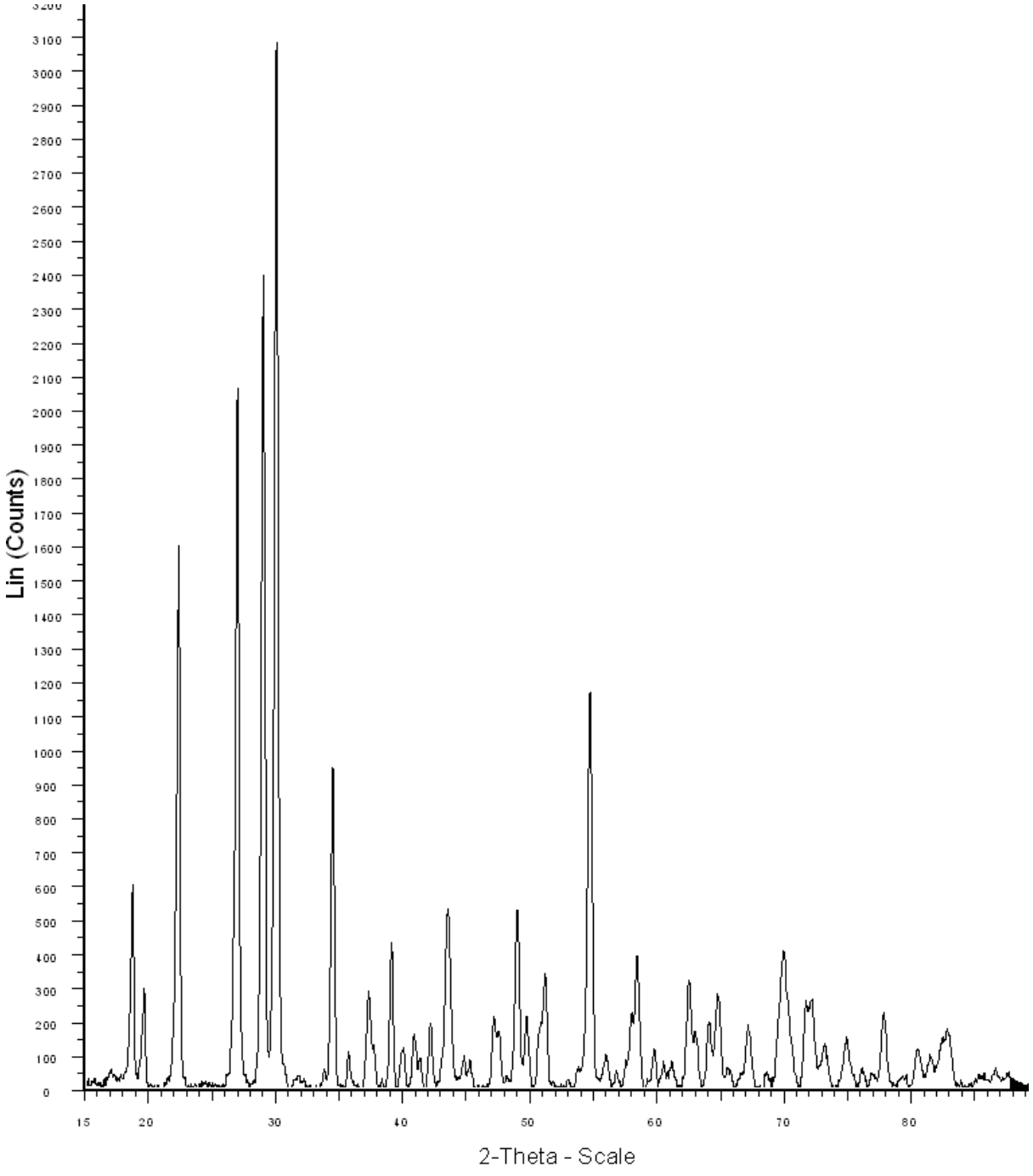

Appendix 1 Figure 1: XRD diffractogram of cordierite monolith

Preparation of standards and sample for iron molybdate:

$Fe_2(MoO_4)_3 \bullet MoO_3$

Total molar mass = 2 x 55.85 + 3 x (95.94 + 4 x 16) + 95.94 + 3 x 16

= 735.46 $g.mol^{-1}$

Fe: 2(55.85)/735.46 = 0.15

Mo: 4(95.94)/735.46 = 0.52

Dissolving approximately 0.020g in 100ml $\longrightarrow$ 0.20 $g.L^{-1}$ catalyst

Fe: 0.15 x 0.20 = 0.03 $g.L^{-1}$

Mo: 0.52 x 0.20 = 0.104$g.L^{-1}$

1$g.L^{-1}$ = 1000 ppm

0.03$g.L^{-1}$ = x

Therefore x = 30 ppm, similarly Mo = 104 ppm

1000 ppm solutions of molybdenum and iron were prepared from ammonium heptamolybdate (1.8396 g, Merck) and iron nitrate nonahydrate (7.2402 g, Merck), respectively. A working solution of 400 ppm molybdenum and 100 ppm iron was prepared by transferring 40.00 ml of molybdenum solution and 10.00 ml iron solution, respectively, into a 100 ml volumetric flask, adding 5 ml concentrated hydrochloric acid (32 %, SMM Instruments) and diluting to 100 ml with double distilled water.

Fe: $C_1V_1 = C_2V_2$ Mo: $C_1V_1 = C_2V_2$

$100 \times V_1 = 10 \times 100$ $100 \times V_1 = 40 \times 100$

V_1 = 10 ml V_1 = 40 ml

Standard solutions were prepared in 25 ml volumetric flasks, with 1 ml concentrated hydrochloric acid and diluted with double distilled water. Volumes used from the working solution are represented in table 1.

Fe: $C_1V_1 = C_2V_2$ Mo: $C_1V_1 = C_2V_2$

$100 \times V_1 = 10 \times 25$ $100 \times V_1 = 40 \times 25$

$V_1 = 2.5$ ml $V_1 = 2.5$ ml

Appendix 1 Table 1: Concentration of standards and volumes transferred from standards

Standards	1	2	3	4	5
Fe/ppm	10	20	30	40	50
Mo/ppm	40	80	120	160	200
Volume from working solution/ml	2.5	5	7.5	10	12.5

Catalyst (0.0216 g) was dissolved in concentrated hydrochloric acid and diluted to 100 ml with double distilled water.

Calculation of ratio:

Three emission lines were chosen during ICP-OES analysis. The concentration was determined using the most preferred emission line.

Mo: 111.0 $mg.L^{-1}$

Mols = (111.0 x 0.100)/95.94 = 0.1157 mmol

Fe: 28.84 $mg.L^{-1}$

Mols = (28.84 x 0.100)/55.85 = 0.05164 mmol

Mo:Fe therefore = 2.2:1

Appendix 2

Reactor setup

Figure 1: Reactor setup for reactions in this research project

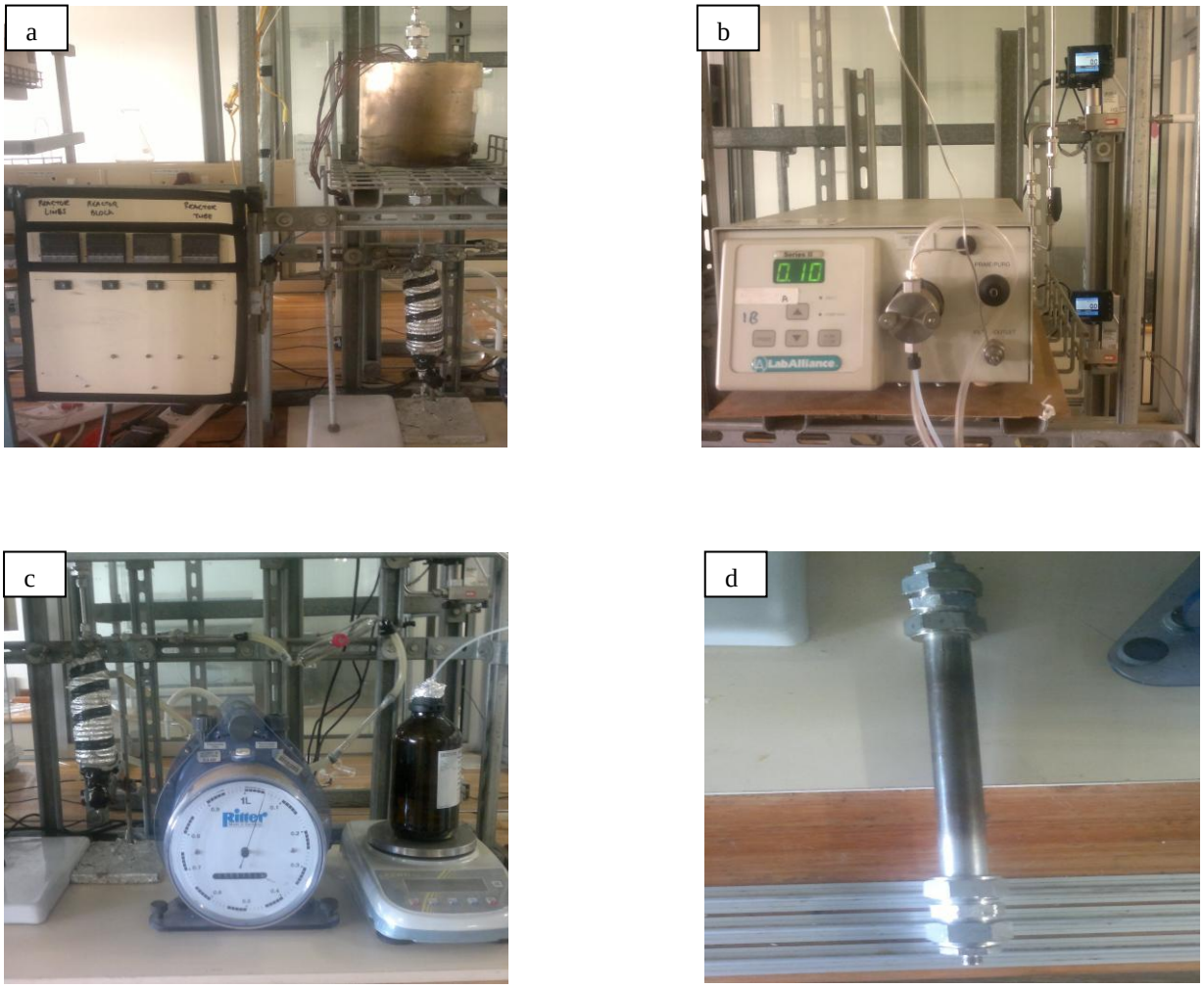

Figure 2: Closer view of reactor setup, (a) Temperature control units and reactor block (b) HPLC pump and mass flow controllers (c) catch pot, wet gas flow meter and *n*-octane (d) reactor tube

Appendix 3

Product identification and quantification

GC-FID details:

Injector temperature: 250 °C

Detector: 250 °C

Carrier gas: Hydrogen

Make up gas: Nitrogen

Ratio: 150:1

Column flow: 1.13 ml/min

Table 1: GC temperature programme

Rate/° C.minute^{-1}	Temperature/° C	Time/ minutes
	35	1
1	40	5
2	120	1
10	150	1

Total run time: 56 minutes

GC-TCD details:

Injector temperature: 250 °C

Detector: 250 °C

Carrier gas: Argon

Pressure: 120 kPa

Table 2: GC-TCD temperature programme

Rate/° C.minute^{-1}	Temperature/° C	Time/ minutes
	35	1
1	40	5
2	120	1
10	150	1

Total run time: 7 minutes

GC-MS details:

Injector temperature: 250 °C

Detector: 250 °C

Carrier gas: Helium

Column flow rate: 0.60 ml/min

Split ratio: 25

Table 3: GC-MS temperature programme

Rate/° C.minute^{-1}	Temperature/° C	Time/ minutes
	35	2
1	40	5
2	80	2
2	160	10

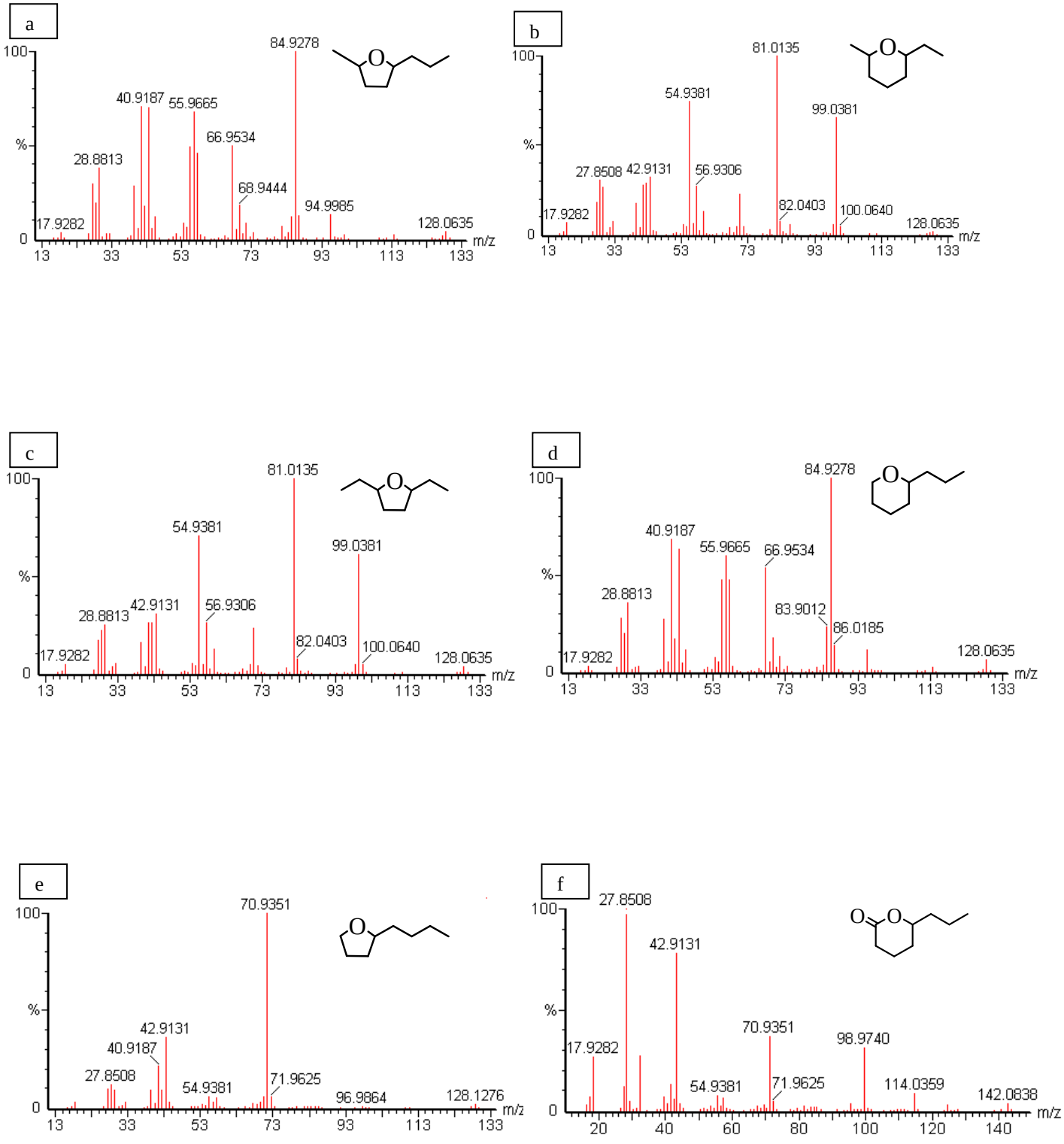

Appendix 3 Figure 1: Mass spectra of cyclic ethers, (a) 2,5-methyl-propyl-tetrahydrofuran (b) 2,6-methyl-ethyl-tetrahydropyran (c) 2,5-diethyl-tetrahydrofuran (d) 2-propyl-tetrahydropyran (e) 2-butyl-tetrahydrofuran (f) 2H-pyran-2-one-tetrahydro-6-propyl

GSHV calculation:

Flow rate of octane (ml/min)	0.10
Density of octane (g/ml)	0.703
Mass flowrate of n-Octane (g/min)	0.0703
Molar mass of octane (g/mol)	114.23
Mol flow rate of n-Octane (mol/min)	**0.0006154**
pV = nRT	
Universal gas Constant (J/K.mol)	8.314
Temperature (K)	298.15
Pressure (Pa)	101325
Volumetric flow of n-Octane (m3/min)	1.5056E-05
Volumetric flow of n-Octane (ml/min)	**15.06**
Octane : Oxygen Ratio	**1**
Carbon : Oxygen Ratio (8 : Oxygen)	2
Mol flow rate of oxygen (mol/min)	**0.0006154**
pV = nRT	
Volumetric flow of oxygen (ml/min)	**15.056**
pV=nRT	
Mol flow rate of air (O2 is 21% of air)	0.002931
Volumetric flow of nitrogen in air (ml/min)	**56.6**
Volumetric flow of air (mls/min)	**71.7**
Volume of Catalyst/Bed (ml)	7.85
Volumetric flow of nitrogen (ml/min)	45
Total Volumetric Flow of Gases (ml/min)	131.7
GHSV (1/hr)	**1007**
n-Octane : Total feed (percentage)	11.43

Example of spreadsheet:

Mass of Octane sent in to the reactor	
Mass of octane(inital)/g	1012.46
Mass of octane (final)/g	1008.36
Mass of Octane in/g	**3.93**

Moles in from balance	
Moles of Octane in	0.034404272
Moles of carbon in	**0.275234177**

Gas flowing out of reactor	
Out gas (initial)	63140.37
Out gas (final)	63147.68
Out gas flow(L)	7.31
Out gas flow(ml)	**7310**

Mass of liquid	
Total mass of liquid (weighed)/g	3.88
Mass of Organic layer/g	3.39
Mass of Aqueous layer/g	0.49
% of water in Organic	0.00
% of water in Aqeous	76.52
Actual mass of organic/g	**3.39**
Actual mass of aqeous/g	**0.12**
Mass of water	0.37

Moles of Octane in/mol	**0.2752342**
Moles of Octane out in gas/mol	0.0088683
Moles of Octane out in liquid/mol	0.1923251
Moles of Octane out/mol	**0.2011934**
Moles converted/mol	**0.074040789**
Conversion/%	**26.90**

Carbon Mole Balance	
Moles of Octane in/mol	**0.2752342**
Moles of Octane out/mol	0.2011934
Moles of gaseous product formed/mol	0.0199130
Moles of carbon oxides formed/mol	0.0049581

Moles of liquid product formed/mol	0.0464293
Total moles of Carbon out/mol	**0.2724937**
Carbon balance/%	**99**

Carbon Product Balance	
Moles of Converted/mol	**0.0740408**
Moles of Product Formed/mol	**0.0713003**
Carbon Balance/%	**96**

CO and CO_2:

Products	**Peak Area from GC**
Carbon Monoxide	811
Carbon Dioxide	993
Total	**1804**

Volume fraction	**Peak area/calibration factor**
Carbon Monoxide	6.74E-03
Carbon Dioxide	9.86E-03
Total	**1.66E-02**

Volume/ml	**Volume fraction * Flow per minute**
Carbon Monoxide	4.92E+01
Carbon Dioxide	7.20E+01
Total	**1.21E+02**

Mol carbon/mol	**pV=nRT**
Carbon Monoxide	2.01E-03
Carbon Dioxide	2.94E-03
Total	4.96E-03

Gaseous product:

Products	Peak area from GC
Methane	133192
Ethylene	152592
Ethane	
Acetaldehyde	
Propylene	63175
Propane	118693
Propionaldehyde	
1-Butene	19359
Methanol	
Butanal	
Butane	45069
Ethanol	
Acetone	
1-Pentene	117385
1-Propanol	
Pentanal	
Pentane	34246
1-Hexene	79777
Hexane	13556
Benzene	
Methyl-cyclopentane	
1-Heptene	
Heptane	
Toluene	
1,7-Octadiene	
Hexanal	
1-Octene	
Trans-4-octene	
Cis-4-octene	
Trans-3-octene	
n-octane	331078
Trans-2-octene	
Cis-2-octene	
Ethylbenzene	
Styrene	
o-xylene	
2,5-methyl-ethyl tetrahydropyran	
2,5-methyl-propyl tetrahydrofuran	
2,5-diethyl tetrahydrofuran	
2-propyl tetrahydropyran	

Furan and pyran isomers	
2-butyl tetrahydrofuran	
Cyclooctane	
4-octanone	
3-octanone	
2-octanone	
1-Octanone	
1-Octanal	
4-octanol	
3-octanol	
2-octanol	
1-Octanol	
1-Octene oxide	
Benzyl Alcohol	
2 oxygen pyran	
Octadienes	
Octadienones	
Total	**1108122**

Corrected Area	RF	Peak area/Response Factor
Methane	**0.97**	1.37E+05
Ethylene	**1.02**	1.50E+05
Ethane	**0.97**	0.00E+00
Acetaldehyde	**0.35**	0.00E+00
Propylene	**1.00**	6.32E+04
Propane	**0.98**	1.21E+05
Propionaldehyde	**0.58**	0.00E+00
1-Butene	**1.00**	1.94E+04
Methanol	**0.23**	0.00E+00
Butanal	**0.62**	0.00E+00
Butane	**1.03**	4.38E+04
Ethanol	**0.46**	0.00E+00
Acetone	**0.49**	0.00E+00
1-Pentene	**1.00**	1.17E+05
1-Propanol	**0.60**	0.00E+00
Pentanal	**0.66**	0.00E+00
Pentane	**1.04**	3.29E+04
1-Hexene	**0.99**	8.06E+04
Hexane	**1.03**	1.32E+04
Benzene	**1.12**	0.00E+00
Methyl-cyclopentane	**0.93**	0.00E+00
1-Heptene	**1.00**	0.00E+00
Heptane	**1.00**	0.00E+00
Toluene	**1.20**	0.00E+00

1,7-Octadiene	**1.03**	0.00E+00
Hexanal	**1.16**	0.00E+00
1-Octene	**1.03**	0.00E+00
Trans-4-octene	**1.03**	0.00E+00
Cis-4-octene	**1.03**	0.00E+00
Trans-3-octene	**1.03**	0.00E+00
n-octane	**0.97**	3.41E+05
Trans-2-octene	**1.02**	0.00E+00
Cis-2-octene	**1.02**	0.00E+00
Ethylbenzene	**1.03**	0.00E+00
Styrene	**1.29**	0.00E+00
o-xylene	**1.02**	0.00E+00
2,5-methyl-ethyl tetrahydropyran	**0.70**	0.00E+00
2,5-methyl-propyl tetrahydrofuran	**0.70**	0.00E+00
2,5-diethyl tetrahydrofuran	**0.70**	0.00E+00
2-propyl tetrahydropyran	**0.70**	0.00E+00
Furan and pyran isomers	**0.70**	0.00E+00
2-butyl tetrahydrofuran	**0.70**	0.00E+00
Cyclooctane	**0.90**	0.00E+00
4-octanone	**0.80**	0.00E+00
3-octanone	**0.80**	0.00E+00
2-octanone	**0.80**	0.00E+00
1-Octanone	**0.80**	0.00E+00
1-Octanal	**0.78**	0.00E+00
4-octanol	**0.85**	0.00E+00
3-octanol	**0.85**	0.00E+00
2-octanol	**0.85**	0.00E+00
1-Octanol	**0.85**	0.00E+00
1-Octene oxide	**0.70**	0.00E+00
Benzyl Alcohol	**1.16**	0.00E+00
2 oxygen pyran	**0.65**	0.00E+00
Octadienes		
Octadienones		
Total		**1.12E+06**

Volume fraction	**Molar Mass**	**Corrected Area * Constant * (Molar mass of methane/Molar mass of component)**
Methane	**16.04**	1.06E-02
Ethylene	**28.05**	6.62E-03
Ethane	**28.05**	0.00E+00
Acetaldehyde	**44.05**	0.00E+00
Propylene	**42.08**	1.86E-03

Propane	**44.10**	3.41E-03
Propionaldehyde	**58.08**	0.00E+00
1-Butene	**56.11**	4.28E-04
Methanol	**32.04**	0.00E+00
Butanal	**72.11**	0.00E+00
Butane	**58.12**	9.35E-04
Ethanol	**46.07**	0.00E+00
Acetone	**58.08**	0.00E+00
1-Pentene	**70.13**	2.08E-03
1-Propanol	**60.10**	0.00E+00
Pentanal	**86.13**	0.00E+00
Pentane	**72.15**	5.67E-04
1-Hexene	**84.16**	1.19E-03
Hexane	**86.18**	1.90E-04
Benzene	**78.11**	0.00E+00
Methyl-cyclopentane	**84.16**	0.00E+00
1-Heptene	**98.19**	0.00E+00
Heptane	**100.21**	0.00E+00
Toluene	**92.14**	0.00E+00
1,7-Octadiene	**110.20**	0.00E+00
Hexanal	**100.16**	0.00E+00
1-Octene	**112.24**	0.00E+00
Trans-4-octene	**112.24**	0.00E+00
Cis-4-octene	**112.24**	0.00E+00
Trans-3-octene	**112.24**	0.00E+00
n-octane	**114.23**	3.71E-03
Trans-2-octene	**112.24**	0.00E+00
Cis-2-octene	**112.24**	0.00E+00
Ethylbenzene	**106.17**	0.00E+00
Styrene	**104.15**	0.00E+00
o-xylene	**106.16**	0.00E+00
2,5-methyl-ethyl tetrahydropyran	**128.21**	0.00E+00
2,5-methyl-propyl tetrahydrofuran	**128.21**	0.00E+00
2,5-diethyl tetrahydrofuran	**128.21**	0.00E+00
2-propyl tetrahydropyran	**128.21**	0.00E+00
Furan and pyran isomers	**128.21**	0.00E+00
2-butyl tetrahydrofuran	**128.21**	0.00E+00
Cyclooctane	**112.21**	0.00E+00
4-octanone	**128.21**	0.00E+00
3-octanone	**128.21**	0.00E+00
2-octanone	**128.21**	0.00E+00
1-Octanone	**128.21**	0.00E+00
1-Octanal	**128.21**	0.00E+00

4-octanol	**130.23**	0.00E+00
3-octanol	**130.23**	0.00E+00
2-octanol	**130.23**	0.00E+00
1-Octanol	**130.23**	0.00E+00
1-Octene oxide	**128.21**	0.00E+00
Benzyl Alcohol	**108.14**	0.00E+00
2 oxygen pyran	**144.21**	0.00E+00
Octadienes		
Octadienones		
Total		**3.16E-02**

Volume/ml	Volume fraction * Volume flowing out
Methane	7.77E+01
Ethylene	4.84E+01
Ethane	0.00E+00
Acetaldehyde	0.00E+00
Propylene	1.36E+01
Propane	2.49E+01
Propionaldehyde	0.00E+00
1-Butene	3.13E+00
Methanol	0.00E+00
Butanal	0.00E+00
Butane	6.83E+00
Ethanol	0.00E+00
Acetone	0.00E+00
1-Pentene	1.52E+01
1-Propanol	0.00E+00
Pentanal	0.00E+00
Pentane	4.14E+00
1-Hexene	8.69E+00
Hexane	1.39E+00
Benzene	0.00E+00
Methyl-cyclopentane	0.00E+00
1-Heptene	0.00E+00
Heptane	0.00E+00
Toluene	0.00E+00
1,7-Octadiene	0.00E+00
Hexanal	0.00E+00
1-Octene	0.00E+00
Trans-4-octene	0.00E+00
Cis-4-octene	0.00E+00
Trans-3-octene	0.00E+00
n-octane	2.71E+01
Trans-2-octene	0.00E+00

Cis-2-octene	0.00E+00
Ethylbenzene	0.00E+00
Styrene	0.00E+00
o-xylene	0.00E+00
2,5-methyl-ethyl tetrahydropyran	0.00E+00
2,5-methyl-propyl tetrahydrofuran	0.00E+00
2,5-diethyl tetrahydrofuran	0.00E+00
2-propyl tetrahydropyran	0.00E+00
Furan and pyran isomers	0.00E+00
2-butyl tetrahydrofuran	0.00E+00
Cyclooctane	0.00E+00
4-octanone	0.00E+00
3-octanone	0.00E+00
2-octanone	0.00E+00
1-Octanone	0.00E+00
1-Octanal	0.00E+00
4-octanol	0.00E+00
3-octanol	0.00E+00
2-octanol	0.00E+00
1-Octanol	0.00E+00
1-Octene oxide	0.00E+00
Benzyl Alcohol	0.00E+00
2 oxygen pyran	0.00E+00
Octadienes	
Octadienones	
Total	**2.31E+02**

Mols	**pV=nRT**
Methane	3.18E-03
Ethylene	1.98E-03
Ethane	0.00E+00
Acetaldehyde	0.00E+00
Propylene	5.57E-04
Propane	1.02E-03
Propionaldehyde	0.00E+00
1-Butene	1.28E-04
Methanol	0.00E+00
Butanal	0.00E+00
Butane	2.79E-04
Ethanol	0.00E+00
Acetone	0.00E+00
1-Pentene	6.21E-04

1-Propanol	0.00E+00
Pentanal	0.00E+00
Pentane	1.69E-04
1-Hexene	3.55E-04
Hexane	5.67E-05
Benzene	0.00E+00
Methyl-cyclopentane	0.00E+00
1-Heptene	0.00E+00
Heptane	0.00E+00
Toluene	0.00E+00
1,7-Octadiene	0.00E+00
Hexanal	0.00E+00
1-Octene	0.00E+00
Trans-4-octene	0.00E+00
Cis-4-octene	0.00E+00
Trans-3-octene	0.00E+00
n-octane	1.11E-03
Trans-2-octene	0.00E+00
Cis-2-octene	0.00E+00
Ethylbenzene	0.00E+00
Styrene	0.00E+00
o-xylene	0.00E+00
2,5-methyl-ethyl tetrahydropyran	0.00E+00
2,5-methyl-propyl tetrahydrofuran	0.00E+00
2,5-diethyl tetrahydrofuran	0.00E+00
2-propyl tetrahydropyran	0.00E+00
Furan and pyran isomers	0.00E+00
2-butyl tetrahydrofuran	0.00E+00
Cyclooctane	0.00E+00
4-octanone	0.00E+00
3-octanone	0.00E+00
2-octanone	0.00E+00
1-Octanone	0.00E+00
1-Octanal	0.00E+00
4-octanol	0.00E+00
3-octanol	0.00E+00
2-octanol	0.00E+00
1-Octanol	0.00E+00
1-Octene oxide	0.00E+00
Benzyl Alcohol	0.00E+00
2 oxygen pyran	0.00E+00
Octadienes	
Octadienones	

Total	9.45E-03

Mols of carbon	Carbon Number	Carbon number * mols
Methane	1	3.18E-03
Ethylene	2	3.96E-03
Ethane	2	0.00E+00
Acetaldehyde	2	0.00E+00
Propylene	3	1.67E-03
Propane	3	3.06E-03
Propionaldehyde	3	0.00E+00
1-Butene	4	5.12E-04
Methanol	1	0.00E+00
Butanal	4	0.00E+00
Butane	4	1.12E-03
Ethanol	2	0.00E+00
Acetone	3	0.00E+00
1-Pentene	5	3.10E-03
1-Propanol	3	0.00E+00
Pentanal	5	0.00E+00
Pentane	5	8.47E-04
1-Hexene	6	2.13E-03
Hexane	6	3.40E-04
Benzene	6	0.00E+00
Methyl-cyclopentane	6	0.00E+00
1-Heptene	7	0.00E+00
Heptane	7	0.00E+00
Toluene	8	0.00E+00
1,7-Octadiene	8	0.00E+00
Hexanal	8	0.00E+00
1-Octene	8	0.00E+00
Trans-4-octene	8	0.00E+00
Cis-4-octene	8	0.00E+00
Trans-3-octene	8	0.00E+00
n-octane	8	8.87E-03
Trans-2-octene	8	0.00E+00
Cis-2-octene	8	0.00E+00
Ethylbenzene	8	0.00E+00
Styrene	8	0.00E+00
o-xylene	8	0.00E+00
2,5-methyl-ethyl tetrahydropyran	8	0.00E+00
2,5-methyl-propyl tetrahydrofuran	8	0.00E+00
2,5-diethyl	8	0.00E+00

tetrahydrofuran		
2-propyl tetrahydropyran	**8**	0.00E+00
Furan and pyran isomers	**8**	0.00E+00
2-butyl tetrahydrofuran	**8**	0.00E+00
Cyclooctane	**8**	0.00E+00
4-octanone	**8**	0.00E+00
3-octanone	**8**	0.00E+00
2-octanone	**8**	0.00E+00
1-Octanone	**8**	0.00E+00
1-Octanal	**8**	0.00E+00
4-octanol	**8**	0.00E+00
3-octanol	**8**	0.00E+00
2-octanol	**8**	0.00E+00
1-Octanol	**8**	0.00E+00
1-Octene oxide	**8**	0.00E+00
Benzyl Alcohol	**8**	0.00E+00
2 oxygen pyran	**8**	0.00E+00
Octadienes		
Octadienones		
Total		**2.88E-02**

Organic liquid:

Products in Organic Layer	Peak Area
Methane	
Ethylene	
Ethane	
Acetaldehyde	
Propylene	
Propane	
Propionaldehyde	
1-Butene	
Methanol	8517
Butanal	
Butane	
Ethanol	
Acetone	
1-Pentene	93521
1-Propanol	
Pentanal	
Pentane	18633
1-Hexene	65408
Hexane	10878
Benzene	

Methyl-cyclopentane	
1-Heptene	33567
Heptane	20350
Toluene	
1,7-Octadiene	
Hexanal	
1-Octene	66685
Trans-4-octene	51151
Cis-4-octene	
Trans-3-octene	112850
n-octane	7528111
Trans-2-octene	74199
Cis-2-octene	34194
Ethylbenzene	
Styrene	
o-xylene	
2,5-methyl-ethyl tetrahydropyran	65908
2,5-methyl-propyl tetrahydrofuran	187311
2,5-diethyl tetrahydrofuran	105157
2-propyl tetrahydropyran	243269
Furan and pyran isomers	41629
2-butyl tetrahydrofuran	63337
Cyclooctane	
4-octanone	12130
3-octanone	52255
2-octanone	48497
1-Octanone	
1-Octanal	
4-octanol	
3-octanol	9349
2-octanol	12934
1-Octanol	
1-Octene oxide	
Benzyl Alcohol	
2 oxygen pyran	11557
Octadienes	27195
Octadienones	33555
Total	**9032147.00**

Corrected Area	RF	Peak area/Response Factor
Methane	**0.97**	0
Ethylene	**1.02**	0
Ethane	**0.97**	0
Acetaldehyde	**0.35**	0
Propylene	**1.00**	0
Propane	**0.98**	0
Propionaldehyde	**0.58**	0
1-Butene	**1.00**	0
Methanol	**0.23**	37030
Butanal	**0.62**	0
Butane	**1.03**	0
Ethanol	**0.46**	0
Acetone	**0.49**	0
1-Pentene	**1.00**	93521
1-Propanol	**0.60**	0
Pentanal	**0.66**	0
Pentane	**1.04**	17916
1-Hexene	**0.99**	66069
Hexane	**1.03**	10561
Benzene	**1.12**	0
Methyl-cyclopentane	**0.93**	0
1-Heptene	**1.00**	33567
Heptane	**1.00**	20350
Toluene	**1.20**	0
1,7-Octadiene	**1.03**	0
Hexanal	**1.16**	0
1-Octene	**1.03**	64743
Trans-4-octene	**1.03**	49661
Cis-4-octene	**1.03**	0
Trans-3-octene	**1.03**	109563
n-octane	**0.97**	7760939
Trans-2-octene	**1.02**	72744
Cis-2-octene	**1.02**	33524
Ethylbenzene	**1.03**	0
Styrene	**1.29**	0
o-xylene	**1.02**	0
2,5-methyl-ethyl tetrahydropyran	**0.70**	94154
2,5-methyl-propyl tetrahydrofuran	**0.70**	267587
2,5-diethyl tetrahydrofuran	**0.70**	150224
2-propyl tetrahydropyran	**0.70**	347527
Furan and pyran isomers	**0.70**	59470
2-butyl tetrahydrofuran	**0.70**	90481

Cyclooctane	**0.90**	0
4-octanone	**0.80**	15163
3-octanone	**0.80**	65319
2-octanone	**0.80**	60621
1-Octanone	**0.80**	0
1-Octanal	**0.78**	0
4-octanol	**0.85**	0
3-octanol	**0.85**	10999
2-octanol	**0.85**	15216
1-Octanol	**0.85**	0
1-Octene oxide	**0.70**	0
Benzyl Alcohol	**1.16**	0
2 oxygen pyran	**0.60**	19262
Octadienes	**1.03**	26403
Octadienones	**0.70**	47936
Total		**9640551**

Normalised Area %	**(Corrected Area/Total Corrected Area)*100**
Methane	0.00
Ethylene	0.00
Ethane	0.00
Acetaldehyde	0.00
Propylene	0.00
Propane	0.00
Propionaldehyde	0.00
1-Butene	0.00
Methanol	0.38
Butanal	0.00
Butane	0.00
Ethanol	0.00
Acetone	0.00
1-Pentene	0.97
1-Propanol	0.00
Pentanal	0.00
Pentane	0.19
1-Hexene	0.69
Hexane	0.11
Benzene	0.00
Methyl-cyclopentane	0.00
1-Heptene	0.35
Heptane	0.21
Toluene	0.00
1,7-Octadiene	0.00

Hexanal	0.00
1-Octene	0.67
Trans-4-octene	0.52
Cis-4-octene	0.00
Trans-3-octene	1.14
n-octane	80.50
Trans-2-octene	0.75
Cis-2-octene	0.35
Ethylbenzene	0.00
Styrene	0.00
o-xylene	0.00
2,5-methyl-ethyl tetrahydropyran	0.98
2,5-methyl-propyl tetrahydrofuran	2.78
2,5-diethyl tetrahydrofuran	1.56
2-propyl tetrahydropyran	3.60
Furan and pyran isomers	0.62
2-butyl tetrahydrofuran	0.94
Cyclooctane	0.00
4-octanone	0.16
3-octanone	0.68
2-octanone	0.63
1-Octanone	0.00
1-Octanal	0.00
4-octanol	0.00
3-octanol	0.11
2-octanol	0.16
1-Octanol	0.00
1-Octene oxide	0.00
Benzyl Alcohol	0.00
2 oxygen pyran	0.20
Octadienes	0.27
Octadienones	0.50
Total	**100.00**

Mass out/g	**(Normalised Area %/100)*Actual Mass of Organic Layer**
Methane	0
Ethylene	0
Ethane	0
Acetaldehyde	0
Propylene	0
Propane	0

Propionaldehyde	0
1-Butene	0
Methanol	0.013021369
Butanal	0
Butane	0
Ethanol	0
Acetone	0
1-Pentene	0.032885693
1-Propanol	0
Pentanal	0
Pentane	0.006300098
1-Hexene	0.023232371
Hexane	0.003713724
Benzene	0
Methyl-cyclopentane	0
1-Heptene	0.011803488
Heptane	0.007155867
Toluene	0
1,7-Octadiene	0
Hexanal	0
1-Octene	0.022766107
Trans-4-octene	0.017462835
Cis-4-octene	0
Trans-3-octene	0.038526733
n-octane	2.729054003
Trans-2-octene	0.025579717
Cis-2-octene	0.011788202
Ethylbenzene	0
Styrene	0
o-xylene	0
2,5-methyl-ethyl tetrahydropyran	0.033108381
2,5-methyl-propyl tetrahydrofuran	0.094094252
2,5-diethyl tetrahydrofuran	0.052824817
2-propyl tetrahydropyran	0.122204326
Furan and pyran isomers	0.020912011
2-butyl tetrahydrofuran	0.031816859
Cyclooctane	0
4-octanone	0.005331736
3-octanone	0.022968663
2-octanone	0.021316836
1-Octanone	0
1-Octanal	0
4-octanol	0

3-octanol	0.003867623
2-octanol	0.005350715
1-Octanol	0
1-Octene oxide	0
Benzyl Alcohol	0
2 oxygen pyran	0.006773166
Octadienes	0.009284311
Octadienones	0.016856098

Total	**3.39**

Moles out/mol	**Molar mass**	**Mass/Molar mass**
Methane	**16.04**	0
Ethylene	**28.05**	0
Ethane	**28.05**	0
Acetaldehyde	**44.05**	0
Propylene	**42.08**	0
Propane	**44.10**	0
Propionaldehyde	**58.08**	0
1-Butene	**56.11**	0
Methanol	**32.04**	0.00040641
Butanal	**72.11**	0
Butane	**58.12**	0
Ethanol	**46.07**	0
Acetone	**58.08**	0
1-Pentene	**70.13**	0.000468925
1-Propanol	**60.10**	0
Pentanal	**86.13**	0
Pentane	**72.15**	8.73194E-05
1-Hexene	**84.16**	0.00027605
Hexane	**86.18**	4.30926E-05
Benzene	**78.11**	0
Methyl-cyclopentane	**84.16**	0
1-Heptene	**98.19**	0.000120211
Heptane	**100.21**	7.14087E-05
Toluene	**92.14**	0
1,7-Octadiene	**110.20**	0
Hexanal	**100.16**	0
1-Octene	**112.24**	0.000202834
Trans-4-octene	**112.24**	0.000155585
Cis-4-octene	**112.24**	0
Trans-3-octene	**112.24**	0.000343253
n-octane	**114.23**	0.023890869

Trans-2-octene	**112.24**	0.000227902
Cis-2-octene	**112.24**	0.000105027
Ethylbenzene	**106.17**	0
Styrene	**104.15**	0
o-xylene	**106.16**	0
2,5-methyl-ethyl tetrahydropyran	**128.21**	0.000258236
2,5-methyl-propyl tetrahydrofuran	**128.21**	0.000733907
2,5-diethyl tetrahydrofuran	**128.21**	0.000412018
2-propyl tetrahydropyran	**128.21**	0.000953158
Furan and pyran isomers	**128.21**	0.000163107
2-butyl tetrahydrofuran	**128.21**	0.000248162
Cyclooctane	**112.21**	0
4-octanone	**128.21**	4.1586E-05
3-octanone	**128.21**	0.000179149
2-octanone	**128.21**	0.000166265
1-Octanone	**128.21**	0
1-Octanal	**128.21**	0
4-octanol	**130.23**	0
3-octanol	**130.23**	2.96984E-05
2-octanol	**130.23**	4.10867E-05
1-Octanol	**130.23**	0
1-Octene oxide	**128.21**	0
Benzyl Alcohol	**108.14**	0
2 oxygen pyran	**144.21**	4.69674E-05
Octadienes	**110.2**	8.42496E-05
Octadienones	**128**	0.000131688
Total		**0.029888164**

Moles of carbon out/mol		**Moles*Number of carbons**
Methane	1	0
Ethylene	2	0
Ethane	2	0
Acetaldehyde	2	0
Propylene	3	0
Propane	3	0
Propionaldehyde	3	0
1-Butene	4	0
Methanol	1	0.00040641
Butanal	4	0
Butane	4	0
Ethanol	2	0

Acetone	3	0
1-Pentene	5	0.002344624
1-Propanol	3	0
Pentanal	5	0
Pentane	5	0.000436597
1-Hexene	6	0.0016563
Hexane	6	0.000258556
Benzene	6	0
Methyl-cyclopentane	6	0
1-Heptene	7	0.000841475
Heptane	7	0.000499861
Toluene	8	0
1,7-Octadiene	8	0
Hexanal	8	0
1-Octene	8	0.001622673
Trans-4-octene	8	0.001244678
Cis-4-octene	8	0
Trans-3-octene	8	0.002746025
n-octane	8	0.191126955
Trans-2-octene	8	0.001823216
Cis-2-octene	8	0.000840214
Ethylbenzene	8	0
Styrene	8	0
o-xylene	8	0
2,5-methyl-ethyl tetrahydropyran	8	0.002065884
2,5-methyl-propyl tetrahydrofuran	8	0.005871258
2,5-diethyl tetrahydrofuran	8	0.003296143
2-propyl tetrahydropyran	8	0.00762526
Furan and pyran isomers	8	0.00130486
2-butyl tetrahydrofuran	8	0.001985297
Cyclooctane	8	0
4-octanone	8	0.000332688
3-octanone	8	0.00143319
2-octanone	8	0.00133012
1-Octanone	8	0
1-Octanal	8	0
4-octanol	8	0
3-octanol	8	0.000237587
2-octanol	8	0.000328693
1-Octanol	8	0
1-Octene oxide	8	0
Benzyl Alcohol	8	0
2 oxygen pyran	8	0.000375739

Octadienes	8	0.000673997
Octadienones	8	0.001053506
Total		**0.233761807**

Aqueous liquid:

Products in aqueous layer	Peak Area
Methane	
Ethylene	
Ethane	
Acetaldehyde	
Propylene	
Propane	
Propionaldehyde	
1-Butene	
Methanol	92759
Butanal	
Butane	
Ethanol	
Acetone	5383
1-Pentene	31362
1-Propanol	44312
Pentanal	
Pentane	14658
1-Hexene	18787
Hexane	
Benzene	
Methyl-cyclopentane	
1-Heptene	
Heptane	
Toluene	
1,7-Octadiene	
Hexanal	
1-Octene	
Trans-4-octene	
Cis-4-octene	
Trans-3-octene	
n-octane	93624
Trans-2-octene	
Cis-2-octene	
Ethylbenzene	
Styrene	
o-xylene	

2,5-methyl-ethyl tetrahydropyran	
2,5-methyl-propyl tetrahydrofuran	
2,5-diethyl tetrahydrofuran	
2-propyl tetrahydropyran	
Furan and pyran isomers	
2-butyl tetrahydrofuran	
Cyclooctane	
4-octanone	
3-octanone	
2-octanone	
1-Octanone	
1-Octanal	
4-octanol	
3-octanol	
2-octanol	
1-Octanol	
1-Octene oxide	
Benzyl Alcohol	
2 oxygen pyran	
Octadienes	
Octadienones	
Total	**300885.00**

Corrected Area	Peak area/Response Factor
Methane	0
Ethylene	0
Ethane	0
Acetaldehyde	0
Propylene	0
Propane	0
Propionaldehyde	0
1-Butene	0
Methanol	403300
Butanal	0
Butane	0
Ethanol	0
Acetone	10985.71429
1-Pentene	31362
1-Propanol	73853.33333

Pentanal	0
Pentane	14094.23077
1-Hexene	18976.76768
Hexane	0
Benzene	0
Methyl-cyclopentane	0
1-Heptene	0
Heptane	0
Toluene	0
1,7-Octadiene	0
Hexanal	0
1-Octene	0
Trans-4-octene	0
Cis-4-octene	0
Trans-3-octene	0
n-octane	96519.58763
Trans-2-octene	0
Cis-2-octene	0
Ethylbenzene	0
Styrene	0
o-xylene	0
2,5-methyl-ethyl tetrahydropyran	0
2,5-methyl-propyl tetrahydrofuran	0
2,5-diethyl tetrahydrofuran	0
2-propyl tetrahydropyran	0
Furan and pyran isomers	0
2-butyl tetrahydrofuran	0
Cyclooctane	0
4-octanone	0
3-octanone	0
2-octanone	0
1-Octanone	0
1-Octanal	0
4-octanol	0
3-octanol	0
2-octanol	0
1-Octanol	0
1-Octene oxide	0
Benzyl Alcohol	0
2 oxygen pyran	0
Octadienes	0
Octadienones	0

Total	649091.6337

Normalised Area	(Corrected Area/Total Corrected Area)*100
Methane	0
Ethylene	0
Ethane	0
Acetaldehyde	0
Propylene	0
Propane	0
Propionaldehyde	0
1-Butene	0
Methanol	62.13298386
Butanal	0
Butane	0
Ethanol	0
Acetone	1.692475101
1-Pentene	4.831675278
1-Propanol	11.37795182
Pentanal	0
Pentane	2.171377667
1-Hexene	2.923588395
Hexane	0
Benzene	0
Methyl-cyclopentane	0
1-Heptene	0
Heptane	0
Toluene	0
1,7-Octadiene	0
Hexanal	0
1-Octene	0
Trans-4-octene	0
Cis-4-octene	0
Trans-3-octene	0
n-octane	14.86994788
Trans-2-octene	0
Cis-2-octene	0
Ethylbenzene	0
Styrene	0
o-xylene	0
2,5-methyl-ethyl tetrahydropyran	0
2,5-methyl-propyl tetrahydrofuran	0
2,5-diethyl tetrahydrofuran	0

2-propyl tetrahydropyran	0
Furan and pyran isomers	0
2-butyl tetrahydrofuran	0
Cyclooctane	0
4-octanone	0
3-octanone	0
2-octanone	0
1-Octanone	0
1-Octanal	0
4-octanol	0
3-octanol	0
2-octanol	0
1-Octanol	0
1-Octene oxide	0
Benzyl Alcohol	0
Octanoic acid	0
Octadienes	0
Octadienones	0
Total	**100**

Mass out/g	**(Normalised Area/100)*Actual Mass of Liquid Layer**
Methane	0
Ethylene	0
Ethane	0
Acetaldehyde	0
Propylene	0
Propane	0
Propionaldehyde	0
1-Butene	0
Methanol	0.071485241
Butanal	0
Butane	0
Ethanol	0
Acetone	0.001947226
1-Pentene	0.005558939
1-Propanol	0.013090561
Pentanal	0
Pentane	0.002498213
1-Hexene	0.003363647
Hexane	0
Benzene	0
Methyl-cyclopentane	0

1-Heptene	0
Heptane	0
Toluene	0
1,7-Octadiene	0
Hexanal	0
1-Octene	0
Trans-4-octene	0
Cis-4-octene	0
Trans-3-octene	0
n-octane	0.017108172
Trans-2-octene	0
Cis-2-octene	0
Ethylbenzene	0
Styrene	0
o-xylene	0
2,5-methyl-ethyl tetrahydropyran	0
2,5-methyl-propyl tetrahydrofuran	0
2,5-diethyl tetrahydrofuran	0
2-propyl tetrahydropyran	0
Furan and pyran isomers	0
2-butyl tetrahydrofuran	0
Cyclooctane	0
4-octanone	0
3-octanone	0
2-octanone	0
1-Octanone	0
1-Octanal	0
4-octanol	0
3-octanol	0
2-octanol	0
1-Octanol	0
1-Octene oxide	0
Benzyl Alcohol	0
2 oxygen pyran	0
Octadienes	0
Octadienones	0
Total	**0.115052**

Moles out/mol	**Mass/Molar mass**
Methane	0
Ethylene	0

Ethane	0
Acetaldehyde	0
Propylene	0
Propane	0
Propionaldehyde	0
1-Butene	0
Methanol	0.002231125
Butanal	0
Butane	0
Ethanol	0
Acetone	3.35266E-05
1-Pentene	7.92662E-05
1-Propanol	0.000217813
Pentanal	0
Pentane	3.46253E-05
1-Hexene	3.99673E-05
Hexane	0
Benzene	0
Methyl-cyclopentane	0
1-Heptene	0
Heptane	0
Toluene	0
1,7-Octadiene	0
Hexanal	0
1-Octene	0
Trans-4-octene	0
Cis-4-octene	0
Trans-3-octene	0
n-octane	0.00014977
Trans-2-octene	0
Cis-2-octene	0
Ethylbenzene	0
Styrene	0
o-xylene	0
2,5-methyl-ethyl tetrahydropyran	0
2,5-methyl-propyl tetrahydrofuran	0
2,5-diethyl tetrahydrofuran	0
2-propyl tetrahydropyran	0
Furan and pyran isomers	0
2-butyl tetrahydrofuran	0
Cyclooctane	0
4-octanone	0
3-octanone	0

2-octanone	0
1-Octanone	0
1-Octanal	0
4-octanol	0
3-octanol	0
2-octanol	0
1-Octanol	0
1-Octene oxide	0
Benzyl Alcohol	0
2 oxygen pyran	0
Octadienes	0
Octadienones	0

Total	**0.002786093**

Moles of carbon out/mol	**Moles*Number of carbons**
Methane	0
Ethylene	0
Ethane	0
Acetaldehyde	0
Propylene	0
Propane	0
Propionaldehyde	0
1-Butene	0
Methanol	0.002231125
Butanal	0
Butane	0
Ethanol	0
Acetone	0.00010058
1-Pentene	0.000396331
1-Propanol	0.000653439
Pentanal	0
Pentane	0.000173126
1-Hexene	0.000239804
Hexane	0
Benzene	0
Methyl-cyclopentane	0
1-Heptene	0
Heptane	0
Toluene	0
1,7-Octadiene	0
Hexanal	0
1-Octene	0
Trans-4-octene	0

Cis-4-octene	0
Trans-3-octene	0
n-octane	0.001198156
Trans-2-octene	0
Cis-2-octene	0
Ethylbenzene	0
Styrene	0
o-xylene	0
2,5-methyl-ethyl tetrahydropyran	0
2,5-methyl-propyl tetrahydrofuran	0
2,5-diethyl tetrahydrofuran	0
2-propyl tetrahydropyran	0
Furan and pyran isomers	0
2-butyl tetrahydrofuran	0
Cyclooctane	0
4-octanone	0
3-octanone	0
2-octanone	0
1-Octanone	0
1-Octanal	0
4-octanol	0
3-octanol	0
2-octanol	0
1-Octanol	0
1-Octene oxide	0
Benzyl Alcohol	0
2 oxygen pyran	0
Octadienes	0
Octadienones	0
Total	**0.004992561**